The Dissertation Committee for John William Steele Certifies that this is the approved version of the following dissertation:

Mechanisms of Impaired Mitochondrial One-carbon Metabolism and Drug Exposures to Valproic Acid or Dolutegravir in Neural Tube Defects

Committee:

Richard H. Finnell, Co-Supervisor

Dean R. Appling, Co-Supervisor

Seema Agarwala

John B. Wallingford

Steven S. Gross

Mechanisms of Impaired Mitochondrial One-carbon Metabolism and Drug Exposures to Valproic Acid or Dolutegravir in Neural Tube Defects

by

John William Steele

Dissertation

Presented to the Faculty of the Graduate School of

The University of Texas at Austin

in Partial Fulfillment

of the Requirements

for the Degree of

Doctor of Philosophy

The University of Texas at Austin

May 2020

Dedication

This dissertation is dedicated to my loving parents, James and Irene Steele. My work would not have been possible without their unfailing support and encouragement.

Acknowledgements

First, I must thank my mentor, Dr. Richard Finnell, who supported me even in the lowest and most challenging times of my graduate career. I would also like to thank Drs. Bogdan Wlodarczyk and Robert Cabrera, who have been my close mentors and shaped my understanding of science and my scientific approach. Dr. Linda Lin not only assisted me on most of my mouse experiments, but she has also been one of my dearest friends for the last six years. Nellie Chen performed thousands of genotyping reactions contributing to this work and has been the best undergraduate assistant for which a graduate student could ever hope. Xuanye Cao assisted with data analysis on RNA-seq experiments. Drs. Renu Pandey and Stefano Tiziani performed the LC-MS on VPA-treated embryos at Dell Pediatric Research Institute. Gabriel Tukeman assisted with the DTG cell culture experiments, and Dr. Robert Cabrera assisted with flow cytometry. Xue Gu, Jen Gilmore, Neeraj Patel, and Laura Guillen provided administrative support for my projects and made sure I always got paid. I also want to sincerely thank the following current or former members of the Finnell Lab who either assisted directly on my projects or otherwise contributed positively to my graduate experience: Sung-Eun Kim, Tian Tian, Yunping Lei, Hui Wei, Yael Pomerantz, Xiao Han, Jimi Kim, Amanda Vaughn, Manami Toriyama, and Rachel Tittle. I want to thank Sharon Bayliss, John Bayliss, and Dr. Tim George, who contributed significantly to my first publication as a graduate student, and I want to thank Baylor College of Medicine for hosting my graduate research for the last three years. Finally, I would like to thank my committee members, Drs. Dean Appling, Steven Gross, Seema Agarwala, and John Wallingford for their considerate advice and guidance.

Abstract

Mechanisms of Impaired Mitochondrial One-carbon Metabolism and Drug Exposures to Valproic Acid or Dolutegravir in Neural Tube Defects

John William Steele, Ph.D.

The University of Texas at Austin, 2020

Supervisors: Richard H. Finnell and Dean R. Appling

Neural tube defects (NTDs) are among the most severe and prevalent human congenital malformations. Their etiology is complex and multifactorial, influenced by dynamically interacting genetic and environmental factors. It is well known that maternal dietary folate status is the greatest modifying factor associated with risk for NTD-affected pregnancies, and that dietary fortification of folic acid (FA) can prevent a significant proportion of NTDs. However, many NTDs have proven to be FA-resistant, presenting a need to understand mechanisms underlying these FA-resistant defects and develop novel intervention strategies targeting this population. A class of FA-resistant NTD mouse models have been developed by inactivating genes associated with mitochondrial one-carbon metabolism (mOCM). Thus, Part One of this work sought to elucidate mechanisms by which impaired mOCM results in FA-resistant NTDs. By crossing mice heterozygous for loss of *Slc25a32*, a gene coding for the mitochondrial folate transporter, with mice heterozygous for the *Crooked Tail* (*Cd*) allele of *Lrp6*, a gene coding for a Wnt co-receptor, it was discovered that a proportion of resulting co-heterozygous offspring presented with

NTDs, suggesting a novel digenic interaction between *Lrp6* and mOCM. Further experiments demonstrated that *Lrp6* regulates expression of mOCM genes in mouse embryos, while CHO cells lacking *Slc25a32* demonstrated impaired Wnt signaling rescued by the one-carbon donor, glycine. Building on those data, it was discovered that maternal glycine supplementation could prevent NTDs in *Slc25a32* null embryos, and that glycine or serine supplementation may reduce NTDs in *Lrp6 Cd* mice. Part One experiments also demonstrated that embryonic stem cells lacking *Mthfd1l*, another mOCM gene, have proliferation defects and are sensitive to hypoxia.

Environmental exposure to certain pharmaceutical compounds also increases risk for NTDs. Part Two of this work sought to identify mechanisms of NTD pathology associated with two common pharmaceuticals, the anticonvulsant, valproic acid (VPA), and the HIV integrase inhibitor, dolutegravir (DTG). Untargeted metabolic profiling was performed on VPA-treated mouse embryos, and predictive biomarkers of VPA sensitivity were identified by comparing VPA-affected and unaffected embryos. Other experiments identified a novel, calcium-enhanced interaction between DTG, folate, and folate receptor, suggesting a plausible mechanism by which DTG may enhance NTD risk.

Table of Contents

List of Tables

List of Figures

Chapter 1: Introduction

1.1 Neural Tube Defects

1.1.1 Embryology of Neural Tube Defects

Neural tube defects (NTDs) are severe congenital defects characterized by anatomical anomalies of the fetal or infant central nervous system (CNS, brain or spinal cord). In vertebrates, the CNS arises from an embryonic structure known as the neural tube which, in amphibian and amniote vertebrate taxa, develops from a flat sheet of neuroepithelial tissue, known as the neural plate, through complex morphological tissue movements that ultimately result in bending and folding of the neuroepithelium into a closed tube (Nikolopoulou et al. 2017). These processes are collectively described as primary neurulation or neural tube closure (NTC).

The complex morphogenesis of NTC requires tissue-level coordination of several morphological and cellular events. For example, NTC first requires elongation of the neural plate along the embryo's anterior-posterior (AP) axis with simultaneous narrowing of the plate's mediolateral (ML) width. This process, known as convergent extension, is accomplished through dynamic intercalation of neural plate cells along these two axes (Wallingford, Fraser, and Harland 2002; Huebner and Wallingford 2018), and requires coordinated mediation of cell-cell interactions and cytoskeletal dynamics by the Wnt/Planar Cell Polarity signaling pathway (Wallingford 2012; Butler and Wallingford 2017). The bending and folding process that shapes the neural plate into a tube is similarly complex. A wedge forms along the midline of the neural plate through a cellular process known as apical constriction, whereby the apical surface of individual neuroepithelial cells constricts relative to the basal surface forming a point of bent tissue called the mediolateral

hinge point (MHP) (Nikolopoulou et al. 2017). This process of apical constriction is similarly observed at two points adjacent to either side of the MHP known as the dorsolateral hinge points (DLHPs) (Shum and Copp 1996). Bending at the MHP and DLHPs is thought to generate mechanical force necessary to fold the neural plate and bring the neural folds in apposition to one another allowing for subsequent fusion (Eom, Amarnath, and Agarwala 2013). It appears the non-neural surface ectoderm may also play a role in generating these mechanical forces (Nikolopoulou et al. 2019). Apical constriction itself is complex at the cellular level, mediated by cell-cell interactions (Baumholtz et al. 2017), modulation of cytoskeletal dynamics (Haigo et al. 2003; Copp and Greene 2010; Escuin et al. 2015), and coordination of cell cycle and cell polarity (Eom, Amarnath, and Agarwala 2013). Final tissue fusion of the neural folds at the dorsal midline is perhaps the most poorly understood morphogenic aspect of NTC, but clearly requires complex and coordinated cell behaviors, such as cellular extension of membrane protrusions between the apposed tissues (Pai et al. 2012; Ray and Niswander 2012; Eom, Amarnath, and Agarwala 2013; Rolo et al. 2016). Disruption of any of these morphological or cellular functions may result in failure of NTC leading to subsequent NTDs, thus illustrating the embryological intricacy underlying these defects.

Adding to this complexity, there is a fair amount of diversity among vertebrates in their respective processes for NTC. For example, apart from convergent extension, neural tube development in zebrafish does not even closely resemble any of the morphogenic mechanisms outlined in the above description of primary neurulation. In zebrafish, the neural tube forms from post-convergent extension structures known as the neural keel and neural rod, which hollow into a tube through polarized cell divisions at the midline (Araya et al. 2016). In amphibians, NTC is nearly simultaneous along the entire AP axis of the embryo (Nikolopoulou et al. 2017), while primary neurulation in avian models occurs in a

continuous, bidirectional, zipper-like fashion along the AP axis from two separate initiation sites (Van Straaten et al. 1996). In mice, NTC is initiated at three separate locations along the AP axis: closure 1 occurring at the hindbrain/cervical boundary, closure 2 at the forebrain/midbrain boundary, and closure 3 initiating at the most rostral tip of the forebrain (Shum and Copp 1996; Greene and Copp 2009). NTC in humans is highly controversial given an inability to study human embryos using the same tools as other animal models. Some argue for a single closure site model of human primary neurulation (de Bakker et al. 2017), while others favor evidence suggesting at least two or more sites of closure initiation (Van Allen et al. 1993; Nakatsu, Uwabe, and Shiota 2000; O'Rahilly and Muller 2002; Greene and Copp 2009).

There is also a great deal of diversity in the presentation of NTDs depending on the severity and location of the defect along the AP axis. In humans, anterior NTDs (referring to the brain) are classified as anencephaly and are usually fatal prenatally or shortly after birth (Wallingford et al. 2013). In mice, anterior NTDs are referred to as exencephaly. Posterior NTDs (referring to the spine) are called spina bifida (Wallingford et al. 2013). This condition is survivable, but usually requires prenatal or postnatal surgical correction; but even then, spina bifida patients generally suffer lifelong complications associated with irreversible neurological damage, including bladder dysfunction, ambulatory problems, and cognitive impairment (McComb 1997; Young et al. 2013). Damage caused by the spina bifida lesion may also result in secondary conditions, such as hydrocephalus (whereby impaired drainage of cerebral spinal fluid results in accumulation of fluid in the brain ventricles increasing intracranial pressure) and Chiari-type II malformations (whereby the caudal cerebellum is pulled posteriorly through the foramen magnum, disrupting normal cerebellar development) (McComb 1997; McDowell et al. 2018; Steele et al. 2020). It is also important to note that there are various forms of spina bifida as well (Centers for

Disease 2016). Myelomeningocele is the most severe form, characterized by protrusion and exposure of the spinal cord in an exposed cyst (McComb 1997). In the case of meningoceles, only the meninges of the spinal cord are exposed (McComb 1997), while in spina bifida occulta (the least severe form) there is an opening in the spine with no exposed neural tissue. Spina bifida occulta often goes unnoticed and undiagnosed (Centers for Disease 2016). It should also be noted that there is much debate about whether less severe subsets of spina bifida are the result of failed NTC or unrelated dysplasia of vertebrae in the spine (Greene and Copp 2014). The rarest, most severe, and fatal form of NTD, craniorachischisis, is characterized by failed NTC along the entire AP axis (Wallingford et al. 2013; Greene and Copp 2014). Several other birth defects of the CNS are often classified as NTDs, despite being cephalic disorders that likely do not occur through failed primary neurulation (Wallingford et al. 2013; Greene and Copp 2014). Examples include encephaloceles, iniencephaly, and hydranencephaly. Ultimately, the complexity of the cellular and molecular processes orchestrating NTC, the diverse embryology of neural tube development among various animal models, and the diversity of the various classifications of these defects illustrate the challenges of studying the underlying mechanisms of NTDs.

1.1.2 Etiology of Neural Tube Defects

NTDs are estimated to affect approximately 18.6 per 10,000 live births globally (Blencowe et al. 2018). Their etiology is complex and multifactorial, influenced by interacting genetic and environmental factors (Wallingford et al. 2013). Associated genetic factors alone are quite numerous, with over 300 genetic NTD mouse models having been identified thus far (Wilde, Petersen, and Niswander 2014). These NTD associated genes span a wide range of biological functions and pathways, including one-carbon metabolism, Wnt signaling, planar cell polarity, DNA repair, energy metabolism, retinoid metabolism,

cytoskeletal function, cell-cell junctions, and oxidative stress, among many others (Wallingford et al. 2013). In the last decade, NTD research funding has heavily emphasized genomic association studies of small-scale cohorts with some success in identifying associated human variants. However, the rare and diverse nature of these defects makes it difficult to obtain sample sizes that are large enough to elicit sufficient statistical power for proper risk assessment of identified variants (Steele, Kim, and Finnell 2020). Often, these smaller-scale studies are limited to identifying candidate genes and variants without conventional validation. The complex genetic architecture underlying NTDs is best described by the omnigenic model of inheritance (Boyle, Li, and Pritchard 2017), whereby several "core" variants interact with all other variants across the genome to elicit complex traits. This concept is best illustrated by a recent study demonstrating that accumulation of singleton loss-of-function variants beyond a threshold level is determinative of NTD risk, likely more so than any one variant in any particular gene (Chen et al. 2018). Thus deepening our understanding of the genetic factors underlying NTDs requires an understanding of how candidate variants interact in a global genomic landscape (Steele, Kim, and Finnell 2020).

This complex genetic etiology is further complicated when one factors in genomic interactions with environmental risk factors. Many environmental risk factors for NTDs have been identified, including maternal nutritional status (Wallingford et al. 2013), antiepileptic drug exposure (Wlodarczyk et al. 2012), as well as maternal diabetes and obesity (Wallingford et al. 2013). The challenge lies in understanding how these environmental risk factors interact with underlying genetic susceptibility predisposing to NTDs. A classic example of this concept is illustrated in mouse models of hyperthermia-induced NTDs which demonstrate that some mouse strains are more sensitive to heat-induced defects than others (Finnell et al. 1986; Finnell et al. 2000). More recently, using

mouse models of maternal diabetes, it was demonstrated that the teratogenic potential of maternal hyperglycemia is exacerbated in *Mthfr* and *Folr1* mutant mouse strains, demonstrating a genetic interaction between folate metabolism and diabetes (Lopez-Escobar et al. 2019). Clearly, NTD etiology is derived from interacting genetic and environmental influences, and elucidating these complex gene-environment interactions is key to developing targeted prevention strategies rooted in a precision medicine approach (Steele, Kim, and Finnell 2020).

1.1.3 Prevention of Neural Tube Defects

As mentioned, many NTD cases are fatal; but even treatable NTDs, such as spina bifida, generally result in permanent damage and lifelong disability. Thus, public health research has emphasized prevention by identifying the underlying genetic and environmental risk factors. Deploying intervention strategies during the periconceptional period is critical since NTC occurs relatively early in development, between days 19 and 30 of gestation for humans, often before the mother is even aware of the pregnancy. By 1998, it was well established that low maternal folate status was a significant modifier contributing to NTD birth outcomes, so the Food and Drug Administration (FDA) instituted mandatory folic acid (FA) fortification of the US food supply resulting in a nationally decreased prevalence of affected pregnancies by 36% ('Prevention of neural tube defects: results of the Medical Research Council Vitamin Study. MRC Vitamin Study Research Group' 1991; 'Folic acid to prevent neural tube defects' 1991; Williams et al. 2002; Williams et al. 2015). More than two decades later; however, FA remains the only effective weapon in the arsenal of NTD prevention; yet it has not come close to eliminating the public health burden of these debilitating defects. Despite knowing the protective properties of FA, many countries do not impose mandatory FA fortification; and as a result,

an estimated 230,000 children are born each year with folate-preventable defects (Kancherla et al. 2018). In addition, a significant proportion of NTDs are not preventable by FA fortification, with these FA-resistant NTDs occurring at an apparent baseline rate of 5 per 10,000 live births (Heseker et al. 2009). As such, there remains a critical need to understand the mechanisms underlying FA-resistant NTDs and to develop novel intervention strategies targeting this population.

Several alternative preventions have been proposed. Inositol, for example, has been advocated as a potential intervention for NTDs associated with maternal diabetes, after finding that myo-inositol supplementation reduced the proportion of NTD-affected offspring in a diabetic rat model from 20.4% to 9.5% (Reece et al. 1997). A small randomized pilot study was conducted in the United Kingdom comparing high risk mothers who had a previous NTD-affected pregnancy supplemented with FA or co-supplemented with FA and inositol. Three NTD recurrences were observed in the FA supplemented cohort, while no recurrences were observed in the co-supplemented cohort (Greene et al. 2016). The authors are thus pursuing a larger randomized trial to confirm the efficacy of inositol supplementation for preventing FA-resistant NTDs (Greene, Leung, and Copp 2017). Supplementation with the nucleotide precursors, thymidine, adenine, and guanosine monophosphate (GMP) were found to reduce occurrences of spina bifida, but not exencephaly, in the *Curly tail* mouse model of FA-resistant defects (Leung et al. 2013). Formate, a product of mitochondrial one-carbon metabolism that contributes carbon units to thymidine and purine synthesis, has also been demonstrated to rescue NTDs in several FA-resistant mouse strains lacking genes necessary for mitochondrial one-carbon metabolism (Momb et al. 2013; Momb and Appling 2014; Pai et al. 2015; Kim et al. 2018; Santos et al. 2020). Most recently, quercetin, a flavonoid compound extracted from plants, has been demonstrated to reduce NTDs in models of diabetic embryopathy, and it is

believed to function through amelioration of oxidative stress (Cao et al. 2016; Khaksary Mahabady et al. 2016; Tan et al. 2018). Notably, these proposed alternate interventions all seem to prevent NTDs in specific genetic or environmental contexts, emphasizing that a precision medicine paradigm may be necessary to develop future prevention strategies by targeting appropriate supplements to the appropriate patient based on genetics or environmental risk factors.

1.2 One-carbon Metabolism

One-carbon metabolism (OCM) is a subset of enzymatic, single-carbon transfer reactions mediated by the vitamin coenzyme, folate (vitamin B9). OCM has many relevant links to human health and disease, including cancer, birth defects, cardiovascular health, and cognition (Ducker and Rabinowitz 2017). One-carbon (1-C) units from serine, glycine, and other carbon donors are shuttled through the pathway and partitioned to various functions, such as *de novo* nucleotide synthesis, essential for DNA replication and RNA transcription, and the methylation cycle which contributes to epigenetic methylation of DNA and post-translational modifications of protein. Additionally, some reactions driving OCM promote turnover of the reducing equivalents $NADP^+$ and NAD^+, synthesize ATP, and connect centrally to other metabolic pathways, such as amino acid metabolism, energy metabolism, transsulfuration/glutathione synthesis, and choline metabolism (Ducker and Rabinowitz 2017). Therefore, OCM influences critical cellular functions such as proliferation, gene expression, regulation of protein function, protein synthesis, and general maintenance of metabolic homeostasis and cellular redox balance. The protective influence of FA against NTDs, the identification of OCM mutant mouse models displaying NTD phenotypes, and the discovery of human OCM gene variants in NTD cases demonstrates the importance of this pathway in NTC (Wallingford et al. 2013; Steele, Kim, and Finnell

2020). That said, given the variety of biological functions connected to OCM, we lack a sufficient understanding of the complicated underlying mechanisms through which OCM contributes to NTC and by which FA elicits its protective effects (Wallingford et al. 2013). Furthermore, the identification of FA-resistant mouse models with functional impairment of OCM illustrate the necessity to better understand the role OCM plays in NTD pathology and prevention (Momb and Appling 2014).

1.2.1 Folate

Folate, or vitamin B9, is an essential vitamin that works as a coenzyme for OCM reactions by serving as a carrier for 1-C units and facilitating partitioning of those units to various functions. A variety of molecular folate species exist characterized by their varying oxidation states. Folic acid (FA), for example, the inexpensive synthetic form usually used for dietary supplementation or fortification, is an oxidized species that must be biologically reduced to tetrahydrofolate (THF) to be utilized for OCM. This reduction occurs through the dihydrofolate reductase enzyme (DHFR) in two steps. First, FA is reduced to dihydrofolate (DHF), a naturally occurring folate species within cells generated as a product of thymidine synthesis by oxidizing 1-C loaded THFs. DHFR also reduces DHF back to THF; thus, the natural role of DHFR is to regenerate cellular THF pools consumed during thymidine synthesis. Importantly, while plants are capable of photosynthesizing folates, animals cannot, and therefore must obtain them from their diet (Ducker and Rabinowitz 2017).

THF's molecular structure consists of a pteridine ring linked to para-aminobenzoic acid (Figure 1.1). The N5 nitrogen on the pteridine ring and the N10 nitrogen on the para-aminobenzoate moiety are each capable of hosting a 1-C unit individually (i.e. 5-formyl-THF, 5-methyl-THF, 10-formyl-THF) or together bridged through a single carbon (i.e.

5,10-methylene-THF and 5,10-methenyl-THF). Cellular folates are also typically poly-glutamated (Figure 1.1), which is essential for cellular retention of folates (McBurney and Whitmore 1974; Taylor and Hanna 1977; Kim et al. 1996). This "poly-glutamated tail" is synthesized by the enzyme folylpolyglutamate synthetase (FPGS) (Shane 1989). Interestingly, FPGS has differentially spliced cytosolic and mitochondrial isoforms and poly-glutamated folates are not transported across the mitochondrial membrane, suggesting poly-glutamination may also play a role in the sub-cellular compartmentalization of folates (Lawrence, Hackett, and Moran 2011; Lawrence et al. 2014).

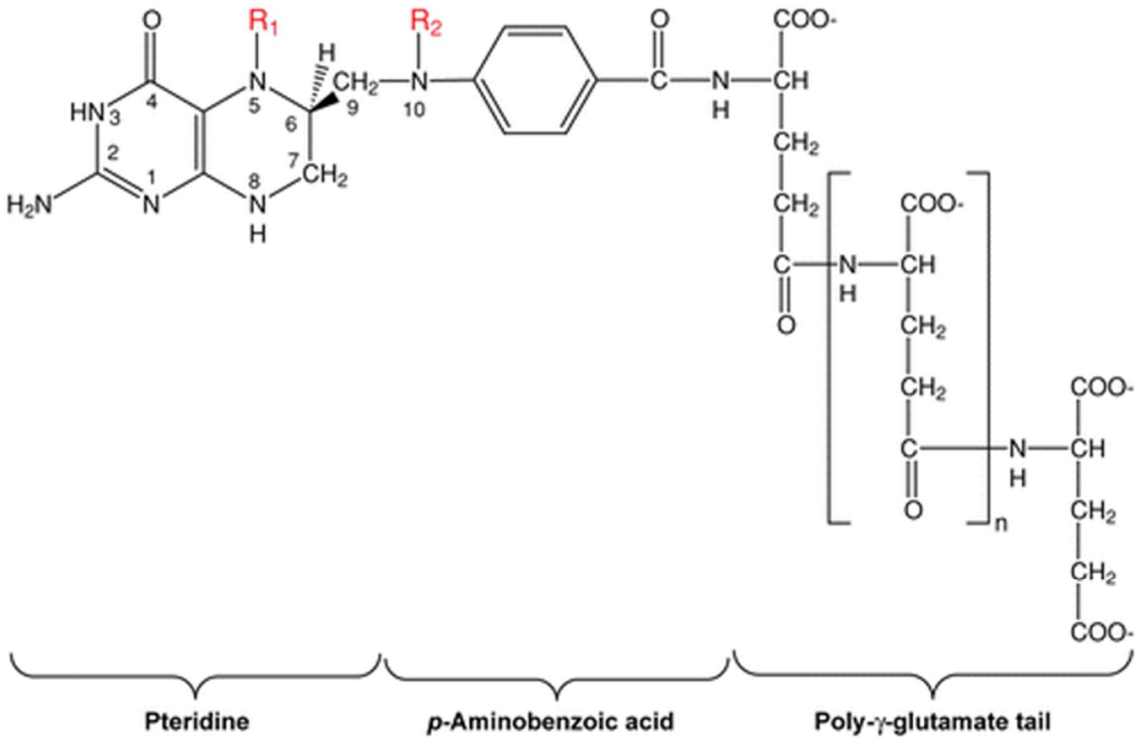

Tibbetts AS, Appling DR. 2010.
Annu. Rev. Nutr. 30:57–81

Figure 1.1 Molecular Structure of Tetrahydrofolate (THF)

THF is composed of a pteridine ring, a para-aminobenzoic acid moiety, and a poly-glutamate tail. Carbon units can be carried on the N5 nitrogen (R1), on the N10 nitrogen (R2), or both in various oxidation states.

(Figure from Tibbetts and Appling (2010)).

1.2.2 Folate Transport

Folates are transported into cells via various folate transporters (Figure 1.2). Parts of this section on folate transport have been previously published in a review for which the dissertation author contributed in the journal *Biochimie*, *"One-carbon metabolism and folate transporter genes: do they factor prominently in the genetic etiology of neural tube defects?"* (Steele, Kim, and Finnell 2020). The previously published material will be denoted with quotes and additional indentation.

1.2.2.1 Folate Receptors

> "Folate Receptors (FRs) are cysteine rich glycosylphosphatidylinositol-anchored proteins that have a high binding affinity to folate and mediate the uptake of folate to cells via endocytosis-mediated internalization of receptor-folate complexes (Chen et al. 2013). Folate is then released to the cytoplasm of cells from the acidified endosome followed by FR-mediated endocytosis with the help of the proton-coupled folate transporter (PCFT) (Zhao et al. 2009). It has also been proposed that FR1 may act as a nuclear transcription factor that regulates expression of pluripotency factors (Boshnjaku et al. 2012; Mohanty et al. 2016). The expression of folate receptors is limited to the placenta, the neural tube, and the kidney during embryonic development, and the expression of FR1 is limited to the epithelial cells of the choroid plexus, lung, and renal tubular cells in adults. Three separate genes (FR1, 2, and 3) encode folate receptors in humans, whereas there are only two genes (*Folr1* and *Folr2*) in the mouse. *Folr1* deficiency in mice is associated with cranial neural tube defects along with heart defects, facial malformations, and early embryonic lethality by embryonic day E10, whereas *Folr2* depletion in the mouse results in no significant phenotypic malformations

(Piedrahita et al. 1999). The *Folr1* nullizygous phenotypes can be rescued with maternal folate supplementation in the form of folinic acid (Piedrahita et al. 1999). A higher concentration of FR autoantibodies in maternal serum has been suggested to be a risk factor in human NTDs (Rothenberg et al. 2004) and a recent report implies the existence of a genetic association between FRs and myelomeningocele with the discovery of twelve novel variants in human cases (Findley et al. 2017). Folate deficiency due to a brain specific loss-of-function mutation of *FOLR1* in humans is associated with cerebral folate transport defects that cause brain malformations and several neurological disorders including epilepsy, which can be partly reversed by folinic acid treatment (Steinfeld et al. 2009)."

1.2.2.2 Reduced Folate Carrier (SLC19A1)

"Reduced Folate Carrier 1 (RFC1) is an anion antiporter mediating the intake of reduced folates at a neutral pH, such as 5-methyltetrahydrofolate (5-methyl-THF) or 5-formyltetrahydrofolate (5-formyl-THF); however, with relatively low affinity for folic acid (Yang, Sirotnak, and Dembo 1984). *RFC1* is ubiquitously expressed during early development and is expressed in human tissues including the brush border of the small and large intestine, the basolateral membrane of renal tubular epithelium, hepatocytes, choroid plexus, and retinal pigment epithelium. Thus, it has been considered a primary folate transporter in cells. *Rfc1* gene inactivation in mice is embryonic lethal before E6.5 (Gelineau-van Waes et al. 2008). Maternal folic acid supplementation of heterozygous dams with low dosage extended embryo survival until E9.5-E10.5, although they presented with severe neural tube defects, while high-dose folic acid supplementation rescued *Rfc1* null embryos until term (E18.5) (Gelineau-van Waes et al. 2008). A common

human polymorphism of *RFC1* (A80G) is associated with several diseases including neural tube defects (De Marco et al. 2003), and recently eight rare variants of *RFC1*, including one pathogenic variant, were found in myelomeningocele patients (Findley et al. 2017). These findings suggest a close association between RFC genes and neural tube closure defects in both the human and mouse."

1.2.2.3 Proton Coupled Folate Transporter (SLC46A1)

"PCFT is an electrogenic folate transporter that is highly expressed in the duodenum and jejunum in humans (Qiu et al. 2006). It has the highest affinity for folate at pH5.5, and also has a high affinity for 5-methyl-THF and 5-formyl-THF under low pH conditions. PCFT mediates the folate absorption in the brush-border membrane of the small intestine, which has a low pH microenvironment. It is also a critical folate transporter in the central nervous system, as it mediates the folate absorption from blood to cerebrospinal fluid in the choroid plexus. Additionally, it has been reported that PCFT releases folates from acidic endosomes in cultured cells, suggesting a supportive role of PCFT in FR1 dependent folate transport (Zhao et al. 2009). Loss-of-function mutations in the *PCFT* gene in humans is associated with hereditary folate malabsorption (HFM) syndrome (Qiu et al. 2006), which causes systemic cerebral folate deficiency (CFD). This condition responds well to therapeutic intervention with chronic high dose folinic acid. *Pcft* null mutant mice show a lack of folate uptake in the intestines and low folate concentration and subsequent increased homocysteine levels in serum and several organs. Therefore, the *Pcft* knockout mouse may serve as a murine HFM model. Parental folate supplementation was shown to rescue folate deficiency-induced anemia in *Pcft*

mutant mice and increased the survival length of *Pcft* KO [knockout] mice (Salojin et al. 2011)."

1.2.2.4 Mitochondrial Folate Transporter (SLC25A32)

Folates enter the mitochondria through the mitochondrial folate transporter (MFT), coded for by the gene *SLC25A32* (Figure 1.2). MFT is localized to the impermeable mitochondrial inner membrane. The gene was identified from a mutant Chinese Hamster Ovary (CHO) cell line isolated from a mutagenesis screen for glycine-requiring mutants, which established four complementation cell lines demonstrating glycine-auxotrophy: glyA, glyB, glyC, and glyD (Kao, Chasin, and Puck 1969). Many of these mutants were later associated with serine catabolism; for example, the glyA mutation was identified in a gene encoding serine hydroxymethyl transferase (SHMT) activity (Simic et al. 2002). In addition to glycine auxotrophy, glyB cells lacked mitochondrial folate accumulation (Taylor and Hanna 1982). Retroviral transduction of a human placental cDNA library into glyB CHO cells discovered *SLC25A32* to restore glycine prototrophy and mitochondrial folate uptake (Titus 2000). Transfection of wildtype hamster *Slc25a32* cDNA in glyB mutant cells accomplished the same (McCarthy et al. 2004; Perchiniak et al. 2007). These observations make it clear that *Slc25a32* codes for a transporter that shuttles folates into mitochondria. Since folate is a required coenzyme for catabolism of serine into glycine by mitochondrial serine hydroxymethyl transferase (SHMT2), a plausible mechanism is evident for glycine deficiency resulting from impairment of MFT. Evidence also indicates that MFT may be the only transporter through which folates enter mitochondria, since the mitochondrial folate pool is reduced by approximately 98% in glyB compared to wildtype CHO cells (Titus and Moran 2000; McCarthy et al. 2004).

Knockout of *Slc25a32* in mice is embryo-lethal by E12.5 accompanied by 100% penetrant NTD phenotypes (Kim et al. 2018). NTDs in this model are predominantly anterior and are FA-resistant; however, approximately 78% could be rescued with maternal formate supplementation (Kim et al. 2018). Modeling suggests that THF transport by MFT is dependent on π-cation interactions with residue Trp142, since site-specific mutagenesis of Trp142 in CHO cells rendered MFT unable to facilitate mitochondrial folate uptake (Lawrence, Hackett, and Moran 2011). One human NTD case has been identified with two heterozygous loss-of-function variants in *SLC25A32*, both with predicted disruption of the Trp142 residue (Kim et al. 2018). MFT also appears capable of shuttling FAD^+/NAD^+-like substrates as well (Spaan et al. 2005), and human variants have been associated with riboflavin-responsive exercise intolerance (Schiff et al. 2016). Finally, *SLC25A32* is amplified in a range of human cancers, associated with both tumor proliferation and reduced patient survival, making MFT a proposed druggable target for cancer therapy (Santoro et al. 2020).

1.2.3 Compartmentalization of One-carbon Metabolism

OCM is physically compartmentalized in cells between the cytosol and mitochondria, with both compartments having their own distinct set of enzymes capable of performing 1-C transfer reactions (Tibbetts and Appling 2010) (Figure 1.2). Work done with *S. cerevisiae* in the 1990s supports that compartmentalization directs the conventional flow of 1-C units through OCM, with mitochondrial reactions typically proceeding in the oxidative direction, whereby 1-C units are loaded onto THF via catabolism of serine and glycine. Sarcosine or dimethylglycine derived from choline metabolism may also contribute 1-C units. The donated 1-C units are then oxidized to single-carbon formate ions, which are exported to the cytosolic compartment (Barlowe and Appling 1988;

Pasternack, Laude, and Appling 1992; Garcia-Martinez and Appling 1993; Yang and MacKenzie 1993; Pasternack, Laude, and Appling 1994; Pasternack et al. 1996; Appling et al. 1997; Kastanos, Woldman, and Appling 1997). Cytosolic OCM reactions then proceed in the reductive direction for partitioning of 1-C units to purine synthesis, thymidylate synthesis, or methionine synthesis (Tibbetts and Appling 2010). While these 1-C transformation reactions are reversible, an electrochemical potential between mitochondrial NADH and cytosolic NADPH thermodynamically favors flux of 1-C units from mitochondria to cytosol in the form of formate, since cytosolic 5,10-methylene-THF dehydrogenase (MTHFD) activity utilizes NADPH as a reductive cofactor, while mitochondrial MTHFD uses both NADH and NADPH (Yang and MacKenzie 1993; West, Horne, and Appling 1996; Shin et al. 2014; Ducker and Rabinowitz 2017; Shin, Momb, and Appling 2017). It is theorized that eukaryotes evolved this compartmentalized strategy to uncouple the redox activity of OCM's oxidation reactions from glycolytic energy metabolism, which is NADH-sensitive, thus promoting cellular "robustness" (Ducker and Rabinowitz 2017). It should also be noted that a third compartmentalization of OCM occurs in the nucleus (Tibbetts and Appling 2010). MTHFD1, DHFR, SHMT1 (serine hydroxy methyltransferase 1), a splice variant of SHMT2 (SHMT2α), and TYMS (thymidylate synthase) are all capable of nuclear localization (Anderson, Woeller, and Stover 2007; Woeller et al. 2007; Anderson and Stover 2009; Field et al. 2014). It appears that nuclear compartmentalization supports the specialized purpose of enhanced and localized thymidylate synthesis for DNA replication during S-phase of the cell cycle (McFarlane 2011; Field et al. 2014).

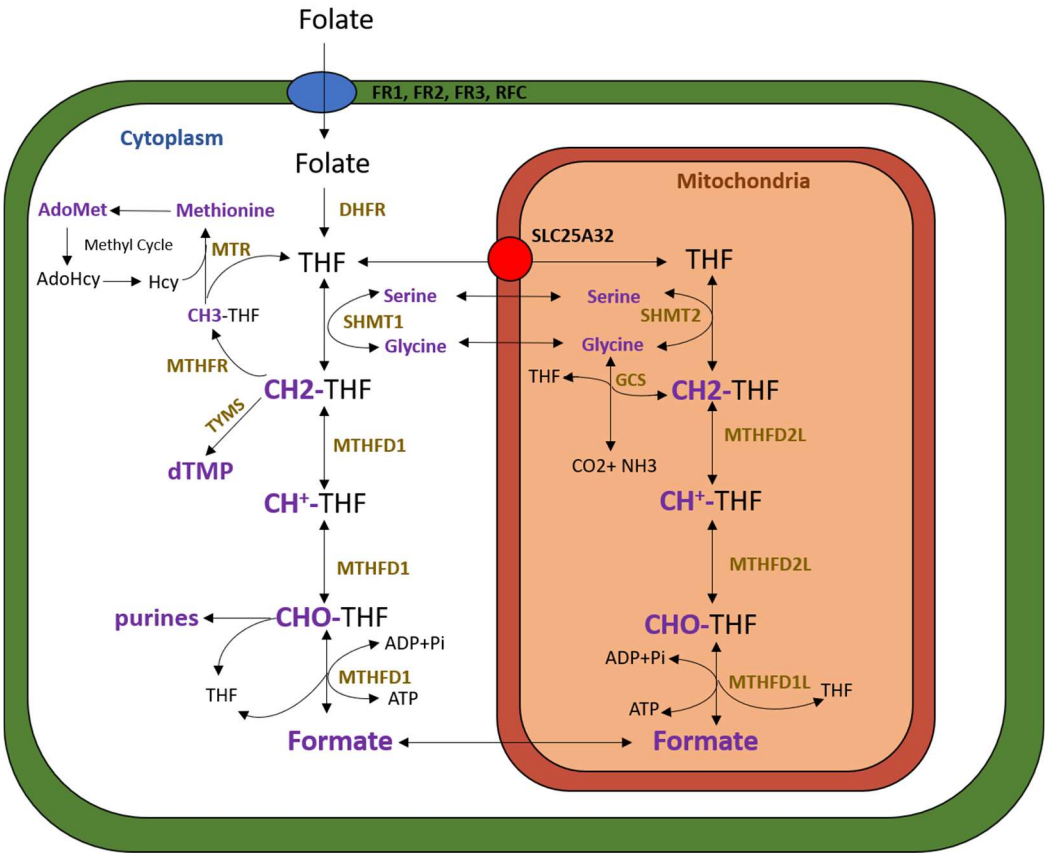

Figure 1.2 Overview of One-carbon Metabolism

"Transport of folates into the cytosol and mitochondria are depicted by the blue and red circles, respectively. Compartmentalization of one-carbon metabolism between the cytosol and mitochondria is demonstrated, with key enzymes participating in one-carbon reactions displayed in gold font. The glycine cleavage system (GCS) includes the enzymes AMT and GLDC. Carbon units, carbon donors, and carbon acceptors are displayed in purple font. CH3-THF = 5-methyl-THF, CH2-THF = 5,10-methylene-THF, CH^+-THF = 5,10-methenyl- THF, CHO-THF = 10-formyl-THF, AdoMet = S-adenosylmethionine, Hcy = homocysteine. **This figure was modified from our collaborators' in Momb et al. 2013*."

(Figure from Steele, Kim, and Finnell (2020))

Portions of the following three sections on mitochondrial OCM, cytosolic OCM, and the methionine cycle have been previously published in a review for which the dissertation author contributed in the journal *Biochimie*, *"One-carbon metabolism and folate transporter genes: do they factor prominently in the genetic etiology of neural tube defects?"* (Steele, Kim, and Finnell 2020). The previously published material will be denoted with quotes and additional indentation.

1.2.3.1 Mitochondrial One-carbon Metabolism

> "Conventionally, it is understood that the majority of carbon units enter the cycle in the mitochondrial compartment, and through folate-mediated one-carbon transfers, are increasingly oxidized to produce the single-carbon ion, formate (Tibbetts and Appling 2010). The mitochondria-derived formate is then exported to the cytosol where it serves as the predominant carbon pool for cytosolic OCM (Tibbetts and Appling 2010). The specific role of mitochondrial OCM is of interest to identifying NTD risk and prevention, since mouse knockout models of certain mitochondrial OCM genes result in defects that are not folate responsive and are instead rescued by formate supplementation. As mentioned earlier, while folic acid is the primary line of defense in NTD prevention, a baseline rate of 5 per 10,000 live births have proven to be unresponsive to folate (Heseker et al. 2009). Therefore, variants of mitochondrial OCM genes may contribute to these unpreventable cases, thus increasing NTD risk regardless of maternal folate status."
>
> "In the mitochondria, THF can be loaded with carbon units donated from serine via the activity of SHMT2 (the mitochondrial serine hydroxymethyltransferase), from glycine via the glycine cleavage system, and dimethylglycine or sarcosine by DMGDH (dimethylglycine dehydrogenase) and

SARDH (sarcosine dehydrogenase) respectively. While few variants in *SHMT2* and *DMGDH* have been identified in human patients, at least three *SARDH* polymorphisms (rs573904, rs2797840, and rs2873817) have been identified as nominally associated with NTD risk (Franke et al. 2009; Piao et al. 2016)."

Knockout of *Shmt2* in mice results in embryonic lethality, growth retardation, and impaired mitochondrial respiration, but does not cause NTDs (Tani et al. 2018). Serine catabolism by SHMT2 transfers one 1-C unit to THF, forming 5,10-methylene-THF and glycine as products (Figure 1.2).

Glycine itself can contribute 1-C units to mitochondrial OCM via the glycine cleavage system (GCS) (Figure1.2). The GCS consists of four coupled enzymes attached to the mitochondrial inner membrane: the P-protein (glycine decarboxylase, GLDC), which decarboxylates the two-carbon glycine disposing of one carbon in the form of CO_2; the T-protein (amino-methyl transferase, AMT), which transfers the remaining carbon to THF, forming 5,10-methylene-THF and an ammonium ion; and the L and H proteins which participate in an oxidation-reduction reaction essential for the H-protein's function (Kikuchi et al. 2008). Knockout of *Gldc* or *Amt* in mouse embryos results in NTDs (Narisawa et al. 2012; Pai et al. 2015). Notably, maternal formate supplementation reduces the occurrence of these defects and hydrocephalus in *Gldc* mutant mice (Pai et al. 2015; Leung et al. 2017; Santos et al. 2020).

"Furthermore, variants in *AMT* and *GLDC* that may contribute to human NTD risk have been identified in several studies (Narisawa et al. 2012; Pai et al. 2015; Shah et al. 2016)."

Dimethylglycine and sarcosine are both metabolites of choline/betaine metabolism and can contribute 1-C units to mitochondrial OCM via the activities of dimethylglycine dehydrogenase (DMGDH) and sarcosine dehydrogenase (SARDH) respectively. In the

absence of THF, DMGDH and SARDH still function, but produce formaldehyde as a byproduct of the demethylation of their respective substrates (Wittwer and Wagner 1980). This formaldehyde may serve as an alternative source for mitochondrial formate, since it can be oxidized to formate through the activity of mitochondrial aldehyde dehydrogenase (ALDH2) (Morrow et al. 2015; Dorokhov et al. 2015). This may explain why mitochondria lacking MTHFD1L are still capable of producing formate (Bryant et al. 2018).

> "After carbon units are loaded onto THF, they are oxidized to formate by the actions of mitochondrial enzymes MTHFD2/2L (methylene tetrahydrofolate dehydrogenase2/2L) and MTHFD1L. MTHFD2 and MTHFD2L are bifunctional, performing both dehydrogenation of 5,10-methylene-THF to 5,10-methyneyl-THF and subsequent hydrolysis of that product to 10-formyl-THF. While mitochondrial 10-formyl-THF may have multiple fates, including synthesis of formyl-methionine for mitochondrial gene translation, MTHFD1L specifically converts the formyl group to a free formate ion, regenerating THF in the process. While no variants in *MTHFD2* or *MTHFD2L* have been associated with NTD risk, a common insertion/deletion polymorphism in *MTHFD1L* (rs3832406) was found to be loosely associated with NTDs in a human study (Parle-McDermott et al. 2009). Furthermore, knockout of this gene in mice results in NTD phenotypes similar to null *Slc25a32* phenotypes, with *Mthfd1l* knockouts being similarly unresponsive to folate supplementation and rescuable by formate (Momb et al. 2013)."

While MTHFD2 and 2L share redundant functionality, they are expressed at different stages of development. *Mthfd2* is expressed only in embryos, while *Mthfd2l* expression turns on between E8.5 and E10.5 in mouse embryos, remains high through the remainder of gestation, and is also expressed in adult tissues (Bolusani et al. 2011; Bryant 2017). While these enzymes were originally thought to be solely NAD^+-dependent, it was

recently demonstrated that both MTHFD2L and MTHFD2 favor NAD^+ and $NADP^+$ under physiologically relevant conditions, although this has not been confirmed *in vivo* (Shin et al. 2014; Ducker and Rabinowitz 2017; Shin, Momb, and Appling 2017). Shin, Momb, and Appling (2017) propose that MTHFD2 is co-expressed with MTHFD2L during early embryogenesis to drive higher rates of mitochondrial 1-C flux to meet increased demand for 1-C units in rapidly proliferating cells.

MTHFD1L and the various fates for mitochondrial 10-formyl-THF will be discussed more thoroughly in Chapter 3.

1.2.3.2 Cytosolic One-carbon Metabolism

> "Once carbon units are exported to the cytosol in the form of mitochondrially-derived formate, they re-enter the folate cycle through the activity of MTHFD1. MTHFD1 is trifunctional, performing all three reactions carried out by the combined efforts of MTHFD2/2L and MTHFD1L in mitochondria, although typically in the reverse direction given a favorable flux of carbon units entering the cytosol as formate. A meta-analysis of nine studies spanning 4,300 NTD cases suggested that one particular polymorphism of *MTHFD1* (rs2236225) increased the likelihood of neural tube defects by 15-30% (Jiang et al. 2014)."
>
> "Cytosolic 10-formyl-THF may contribute its carbon unit to purine synthesis via enzymes coded for by the genes *GART* and *ATIC*, both functioning at different steps in purine metabolism. The *GART* polymorphism, rs2070388, was determined to have an increased odds ratio of 1.89-1.96 in NTD cases compared to controls in an Irish study (Pangilinan et al. 2012)."

Cytosolic 10-formyl-THF not utilized for purine metabolism may be oxidized by aldehyde dehydrogenase 1-like (ALDH1L1) to CO_2, regenerating THF in the process.

Alternatively, 10-formyl-THF could be further reduced to 5,10-methylene-THF by MTHFD1 (Figure 1.2).

> "Cytosolic 5,10-methylene-THF could contribute carbon units to thymidine synthesis via thymidylate synthase (TYMS), to glycine and serine metabolism via the cytosolic serine hydroxymethyltransferase (SHMT1), or it could be reduced to 5-methyl-THF by the enzyme MTHFR (methylene tetrahydrofolate reductase) to feed carbon units into the methionine cycle. When examining single nucleotide polymorphisms associated with NTD risk under conditions of low maternal folate status, *SHMT1* variant, rs12939757, was associated with increased NTD risk in the infant (Etheredge et al. 2012). Interestingly, that same study found some maternal variants of *TYMS* and *MTHFR,* as well one infant variant of *TYMS* to be slightly protective against NTDs (Etheredge et al. 2012). That study also observed three variants of *MTHFD1* (rs2236224, rs2236225, and rs11627387) to increase NTD risk (Etheredge et al. 2012). Of all OCM genes associated with human NTD risk, *MTHFR* mutant C677T is probably the most well-studied variant, being associated with a two to four-fold increase in NTD risk (Yaliwal and Desai 2012). Other *MTHFR* variants, such as the A1298C mutant, have also been identified to slightly increase NTD risk (Yaliwal and Desai 2012)."

1.2.3.3 The Methionine Cycle

> "Carbon units from 5-methyl-THF can be used to synthesize methionine from homocysteine through the methionine synthase enzyme (coded for by *MTR*) in conjunction with its cofactor, vitamin B12. Methionine synthase reductase (coded by *MTRR*) is also required to activate the methionine synthase enzyme. A maternal study demonstrated enhanced risk for mothers harboring the rs1808349

MTRR variant, as well *MTHFD1* rs2236225, *MTHFR* rs1801133, and *RFC1* rs1051226 (Cai et al. 2019). While studies have yielded conflicting results on the association of certain *MTR* variants on NTD risk, one meta-analysis looking at the common A66G mutant did not find increased NTD risk across 8 studies (Zhang et al. 2013)."

"While methionine can be utilized in many aspects of amino acid metabolism, in the methionine cycle it is converted to S-adenosylmethionine (SAM) by methionine adenosyl transferase 1a (MAT1A). Carbon units from SAM are then unloaded by various methyl transferases for methylation of various substrates, including DNA, lipids, and proteins. The product of these demethylations of SAM is S-adenosylhomocysteine [SAH], which is converted back to homocysteine to regenerate methionine. Alternatively, homocysteine can be utilized for cysteine metabolism via the transsulfuration pathway to produce the critical antioxidant, glutathione. Increased homocysteine levels are a common risk factor for NTDs (Steegers-Theunissen et al. 1994), likely because elevated homocysteine is a biomarker for impaired OCM."

1.3 Pharmaceutical Exposures and Neural Tube Defects

Epilepsy is a neurological disorder characterized by spontaneous, recurrent seizures. Most epileptics require medication with an antiepileptic drug (AED, also known as an anticonvulsant) in order to reduce the frequency and severity of their seizures. AEDs are also used in the treatment of a wide range of other conditions (Wlodarczyk et al. 2012). Between 7.6 and 12.7 million women in the United States have epilepsy with close to 25,000 epileptic pregnancies each year (Meador et al. 2008); but managing epilepsy during pregnancy can be challenging given maternal physiologic changes that can alter

pharmacodynamics and effectiveness of AED medications (Wlodarczyk et al. 2012). Moreover, it is firmly established that *in utero* AED exposure greatly enhances risk for adverse birth outcomes, with one study reporting major congenital malformations in 6.1% of AED treated epileptic pregnancies compared to 2.8% of epileptic pregnancies that went untreated (Tomson and Battino 2009). Common congenital anomalies observed from AED exposures include congenital heart defects, hypospadias, facial clefts, growth retardation, microcephaly, and NTDs (Wlodarczyk et al. 2012). Common AEDs include carbamazepine, phenytoin, phenobarbital, lamotrigine, levetiracetam, topiramate, gabapentin, vigabatrin, and valproic acid. The mechanisms of these various drugs as well as animal and human epidemiological studies assessing their teratogenic are thoroughly reviewed in Wlodarczyk et al. (2012). For the purposes of this dissertation, only valproic acid will be discussed further.

Valproic acid (VPA), marketed as Depakene and Depakote among others, is used widely as an anticonvulsant, a mood stabilizer, a prophylactic, and is used in some cases for treatment of schizophrenia (Wlodarczyk et al. 2012). It was first approved for medical use in 1978 as an AED and has been effective against several types of seizures (Scott 1993; Marson 2015). VPA's molecular interactions will be discussed more thoroughly in Chapter 4, but in general it is believed to prevent seizures by inhibiting sustained repetitive firing of neurons after depolarization by increasing recovery of voltage-activated sodium channels (Pugsley et al. 1999). The teratogenic effects of VPA are clear, with several animal studies demonstrating dose-dependent induction of developmental anomalies, including NTDs (Petrere et al. 1986; Finnell et al. 1988; Hendrickx et al. 1988; Binkerd et al. 1988; Massa et al. 2005). In humans, several epidemiological surveys have been performed (Wlodarczyk et al. 2012); in the Neurodevelopmental Effects of Antiepileptic Drugs (NEAD) study, a prospective dose-dependent study on the effects of VPA and other

AEDs, it was determined that adverse pregnancy outcomes were observed in 20.3% of VPA treated pregnancies (Meador et al. 2006), and in general, it appears VPA is associated with a 10 to 20 fold increased risk for having an NTD-affected pregnancy (Wlodarczyk et al. 2012). The mechanisms through which VPA causes birth defects are not understood. It has been proposed that VPA may elicit congenital malformations through its roles as a histone-deacetylase (HDAC) inhibitor, thus interfering with the embryo's epigenetic programming (Tremolizzo et al. 2005; Lloyd 2013). But other mechanisms have also been proposed, including oxidative stress and interference with folate transport or OCM (Alonso-Aperte et al. 1999; Frey et al. 2006; Khan et al. 2011; Lloyd 2013; Fathe, Palacios, and Finnell 2014; Semmler et al. 2017). Moreover, there is undoubtedly an underlying genetic component predisposing to AED risk. Studies in mice demonstrate that VPA sensitivity is strain-dependent, and that this sensitivity can be mapped to a specific genetic locus in Swiss-Vancouver (SWV) mice (Finnell et al. 1988; Finnell et al. 1997; Beck 1999; Finnell et al. 2000; Beck 2001; Lundberg et al. 2004). Since, VPA and other AEDs are still prescribed to women of childbearing potential and discontinuing AED use during pregnancy may also result in adverse outcomes with respect the mother's epilepsy treatment, there is a critical need to elucidate the mechanisms of VPA-induced teratology, understand the underlying genetics predisposing to susceptibility, and develop alternative AEDs with lower teratogenic potential.

Finally, AEDs are not the only class of pharmaceuticals associated with NTDs or other adverse pregnancy outcomes. Many acne medications contain tretinoin, which is a form of retinol (vitamin A). Retinoid metabolism plays an important role in embryonic development, as retinoic acid acts as a morphogen patterning the AP axis of the embryo and regulating body axis elongation (Rhinn and Dolle 2012). There is evidence to suggest exposure to tretinoin during pregnancy is associated with increased risk for NTDs ('Birth

defects due to topical adapalene and tretinoin' 1998; Lipson, Collins, and Webster 1993). More recently, the antiretroviral integrase inhibitor, dolutegravir (DTG), a clinically preferred antiretroviral therapy against HIV, was reported to potentially increase NTD risk after four NTD-affected infants were born in 2018 to mothers taking DTG in Botswana (Zash, Makhema, and Shapiro 2018). Subsequently, the World Health Organization issued guidelines that DTG be avoided by women of childbearing potential (WHO 2018). As of yet, it is unclear how DTG, and potentially other retroviral drugs of the same class, contribute to NTD risk, but Chapter 5 will present work demonstrating mechanisms of interactions between DTG and FOLR1 (FR1) as published in Cabrera et al. (2019).

PART ONE: MECHANISMS OF IMPAIRED MITOCHONDRIAL ONE-CARBON METABOLISM IN NEURAL TUBE DEFECTS

Chapter 2: Mechanistic Interactions between *Lrp6* and Mitochondrial One-carbon Metabolism in Murine Neural Tube Defects

2.1 INTRODUCTION

LRP6 (low-density lipoprotein receptor-related protein 6) is a Wnt pathway co-receptor (Brown et al. 1998). Four rare missense variants of *LRP6* were identified from 192 spina bifida cases in a California cohort (Lei et al. 2015), while seven more missense mutations were discovered from 343 NTD cases in a Chinese study (Shi et al. 2018) and 285 NTD cases in Italy (Allache et al. 2014). Thus, *LRP6* variants may contribute to some proportion of the population burden of these birth defects (perhaps 1-2%). Furthermore, several *Lrp6* mutant mouse models have been developed displaying exencephaly, occasional spina bifida, or other congenital anomalies (Carter et al. 1999; Pinson et al. 2000; Kokubu et al. 2004; Carter et al. 2005; Gray and Ross 2009; Gray et al. 2010; Allache et al. 2014). LRP6 demonstrates a dual role in mediating both canonical and non-canonical Wnt signaling (planar cell polarity) by promoting canonical Wnt activity and repressing non-canonical Wnt activity (Schweizer and Varmus 2003; Tamai et al. 2004; Gray et al. 2013). The *Crooked Tail* (*Cd*) *Lrp6* mutant, which harbors a point mutation (G494D) and was originally reported to be a canonical Wnt hypermorph (Carter et al. 2005), actually appears to be hypomorphic with respect to canonical Wnt activity since the *Cd* protein product fails to interact with its chaperon, MESDC2, and thus cannot localize to the plasma membrane (Lei et al. 2015). However, the allele is a hypermorph with respect to non-canonical Wnt activity, and it is possible that both mechanisms contribute to NTDs independently in *Cd* homozygous embryos (Gray et al. 2013).

Curiously, *Lrp6* mouse models consistently suggest an interesting interaction with folate and OCM. *Lrp6* null embryos are FA-resistant, even to the point of FA supplementation resulting in increased embryonic mortality with enhanced NTD rate in the

viable embryos (Gray and Ross 2009; Gray et al. 2010). In contrast, the *Crooked Tai*l (*Cd*) *Lrp6* mutant is FA-responsive, displaying a dose-dependent rescue of NTD phenotypes with FA supplementation (Carter et al. 1999; Carter et al. 2005). Collaborative work between the laboratories of Richard Finnell and Elizabeth Ross have found that genetic impairment of folate transport, through heterozygous knockout of *Folr1*, in conjunction with heterozygosity of the *Cd* allele results in a 41% frequency of exencephaly (Fathe 2014), while NTDs in *Cd* heterozygotes alone are a rare occurrence (Figure 2.1). It was recently discovered that LRP2 mediates folate uptake and endocytosis of the folate receptor through direct molecular interaction (Kur et al. 2014); however, no evidence has been discovered to suggest that LRP6 similarly interacts with FOLR1. Metabolic analysis of $Lrp6^{cd/cd}$ adult livers compared to those of wildtype mice on high and low-folate diets demonstrated that $Lrp6^{cd/cd}$ dams share a common metabolic profile with the wildtype dams on low-folate diets, suggesting a defect in OCM or folate metabolism (Ernest et al. 2006). Furthermore, metabolic analysis of $Lrp6^{-/-}$ embryos demonstrated decreased levels of methionine, homocysteine, and glutathione, which further supports that LRP6 may act as a critical modifier of OCM (Hansler et al. 2014). That said, the precise mechanisms through which this Wnt pathway co-receptor interacts with folate and OCM remains unknown.

The experiments presented in Chapter 2 test the hypothesis that LRP6 specifically interacts with mitochondrial OCM. By crossing $Lrp6^{+/cd}$ and $Slc25a32^{+/gt}$ dams, it was discovered that a certain proportion of co-heterozygous offspring display exencephaly. Subsequent experiments sought to elucidate the mechanistic interactions between *Lrp6* and mitochondrial OCM, and to investigate the efficacy of the 1-C supplements, glycine or serine, as intervention strategies to rescue NTDs in *Lrp6* or *Slc25a32* mutant mice.

A.

Folr$^{+/+}$; *Lrp6*$^{+/+}$ | *Folr*$^{+/-}$; *Lrp6*$^{+/+}$ | *Folr*$^{+/+}$; *Lrp6*$^{+/cd}$ | *Folr*$^{+/-}$; *Lrp6*$^{+/cd}$ Exencephaly | *Folr*$^{+/-}$; *Lrp6*$^{+/cd}$ Exencephaly

B.

***Lrp6*$^{+/cd}$ X *Folr1*$^{+/-}$**

	***Lrp6*$^{+/+}$; *Folr1*$^{+/+}$**	***Lrp6*$^{+/cd}$; *Folr1*$^{+/+}$**	***Lrp6*$^{+/+}$; *Folr1*$^{+/-}$**	***Lrp6*$^{+/cd}$; *Folr1*$^{+/-}$**
Total Embryos	**18**	**21**	**20**	**32**
Exencephaly Embryos	**0**	**0**	**0**	**13**
NTD Rate	**0%**	**0%**	**0%**	**41%**
Significance				**p<0.0001***

Figure 2.1 Digenic Interaction Between *Lrp6 Cd* and *Folr1* Causes Exencephaly in Mouse Embryos

A) E14.5-E15.5 mouse embryos resulting from crosses between *Lrp6*$^{+/cd}$ and *Folr1*$^{+/-}$ mice. The genotypes are displayed below the images and two examples of *Cd/Folr1* co-heterozygotes with exencephaly are shown on the far right.

B) Table displaying proportion of exencephaly-affected embryos from each genotype. A 41% NTD rate was observed in *Lrp6*$^{+/cd}$*; Folr1*$^{+/-}$ embryos.

*Statistical significance was determined using Fisher's Exact Test, α=0.05.

The data in panel B were published in Fathe (2014).

2.2 Materials and Methods

2.2.1 Mouse Work

2.2.1.1 General

Lrp6 Cd (Carter et al. 1999) and *Slc25a32 gt* (Kim et al. 2018) mice were housed in Baylor College of Medicine's (BCM) Neurosensory mouse facility on 12 hour light/dark cycles with standard chow and maintained according to protocols approved by the Institutional Animal Care and Use Committee (IACUC) at BCM. For experiments requiring timed mating, copulation was confirmed by morning checks for vaginal plugs, and pregnancy was confirmed by comparing dam weight on the date the plug was observed to weight measured on the date of sacrifice. Euthanasia was performed with CO_2 asphyxiation followed by cervical dislocation.

2.2.1.2 Genotyping

Genotyping for the *Lrp6 Cd* and *Slc25a32 gt* alleles was conducted using tail snips (adults) or yolk sacs (embryos) digested in DirectPCR Tail Buffer (Viagen, 101-T) with proteinase K (Viagen, 501-PK), shaking overnight at 55ºC. The proteinase K was quenched post-digestion at 95ºC for 10 minutes, and the crude DNA extracts were centrifuged at 13,000 rcf for 30 seconds. DNA was amplified by polymerase chain reaction (PCR) using LongAmp *Taq* 2X Master Mix (NEB, M0287) (*Lrp6 Cd*) or One *Taq* Quick-Load 2X Master Mix with Standard Buffer (NEB, M0486) (*Slc25a32*) in 25µL reactions. Primers used for *Lrp6 Cd* PCR were as follows: F – 5'-TGACAAGCCATCAAGCAGAG-3', R – 5'-GCTCAGAGGCTATGTGAACCA-3'. For *Lrp6 Cd*, the amplified PCR product was then digested for 2 hours at 37ºC with *Blp1* restriction enzyme (NEB, R0585). Primers used for *Slc25a32* PCR were as follows: F – 5'-AGTGTGTGAGCCGGTGCTTT-3', R (wildtype allele) – 5'-TGGGTCCTGTGGAAAGGCTA-3', R (*gt* allele) – 5'-

CCAATAAACCCTCTTGCAGTTGC-3'. The genotypes were then determined by agarose gel electrophoresis.

2.2.1.3 Glycine, Serine, and Formate Supplementation Experiments

To determine the ability of glycine to rescue NTD phenotypes in *Slc25a32*$^{gt/gt}$ embryos, heterozygous mating pairs were set up and pregnant dams were provided 2500mg/kg/d glycine *ad libitum* in drinking water continuously until euthanized (E12.5-E13.5). To determine the ability of glycine, serine, or formate to rescue NTD phenotypes in *Lrp6 Cd* embryos, heterozygous mating pairs were set up and plugged dams were provided 2500mg/kg/d glycine, 1250mg/kg/d L-serine, or 2500mg/kg/d calcium formate *ad libitum* in drinking water until sacrifice (E12.5-E13.5). The dosages were calculated based on the assumption that a 25g mouse consumes 5mL of water per day (Roscoe B. Jackson Memorial Laboratory and Green 1966).

2.2.2 Isolation and Culture of Mouse Embryonic Fibroblasts

Mouse embryonic fibroblasts (MEFs) were obtained from E13.5 embryos collected from *Lrp6*$^{+/cd}$ x *Lrp6*$^{+/cd}$ heterozygous crosses or *Lrp6*$^{+/cd}$ x *Slc25a32*$^{+/gt}$ mating pairs. After euthanasia, the mice were sprayed with 70% ethanol and the uterus was removed, washed with 70% ethanol, then washed with sterile PBS. Embryos were washed once with sterile PBS and collected in 15mL conical tubes containing a volume of 0.25% Trypsin-EDTA sufficient to cover the embryo. The yolk sacs were reserved for genotyping. The embryos were then subjected to three 10-minute incubations at 37ºC in 0.25% Trypsin-EDTA with vigorous homogenization through a Pasteur pipette between each incubation. The final homogenization was performed using a 1000µL micropipette tip. The homogenized suspension was centrifuged for 5 minutes at 200 rcf; the Trypsin-EDTA was then aspirated,

and the cell pellet was washed once with MEF cell culture media: DMEM (Gibco, 11965118), 10% FBS, 1% Penicillin-streptomycin or Anti-Anti (Gibco, 15240112). MEFs from individual embryos were then plated into gelatin-coated (EMD Millipore, ES-006-B) 10cm cell culture dishes and cultured at 5% CO_2, 37ºC. MEFs were cryopreserved after two passages and utilized for experiments no later than passage five. Canonical Wnt signaling was measured via TCF/LEF Luciferase assays as described in section 2.2.4.

2.2.3 CHO and glyB Cell Culture

CHO-K1 and glyB mutant CHO cells were provided by Dr. Richard Moran (Virginia Commonwealth University, Richmond, VA) and maintained in MEM-alpha media (Gibco, 12561056), supplemented with 10% FBS and 1% Penicillin-streptomycin. For experiments, the media was changed to a custom MEM-alpha formulation lacking glycine to elicit glycine-auxotrophy in glyB. Autonomous canonical Wnt signaling was measured via TCF/LEF Luciferase assays as described in section 2.2.4 and qPCR to measure *Lrp6* and *Wnt* gene expression was performed as described in section 2.2.6. Supplementation experiments to rescue observed defects in autonomous Wnt signaling were performed by addition of 100μM palmitic acid, 0.1mM glycine, 0.4mM glycine, or 1.6mM glycine to the custom MEM media.

2.2.4 TCF/LEF Luciferase Assay

Canonical Wnt activity was measured using a Dual-Luciferase Reporter Assay (Promega, E1910/E1960). MEFs or CHO-K1 and glyB cells were plated on day one in 24 well plates and incubated for 24 hours in a CO_2 incubator in their respective media. For CHO and glyB experiments, the non-customized MEM formulation was used at this stage of the experiment. Each treatment for each cell line was repeated in at least three replicate

wells. On day two, cells were transfected with 200ng of TCF/LEF LUC plasmid vector (expressing *Firefly* luciferase driven by TCF/LEF promotor) and 50ng of pRL-SV40 control vector (expressing *Renilla* luciferase driven by a constitutive SV40 promoter) for 4 hours in 500µL Opti-MEM (Gibco, 31985070) at 5% CO_2, 37ºC. Firefly luciferase negative controls were transfected with pRL-SV40 only. The transfection media was aspirated, cells were washed once with PBS, and provided complete growth media for overnight recovery. On day three, cells were provided experimental growth media. For *Lrp6 Cd* MEF experiments described in Section 2.3.1 and Figure 2.2., this included experimental media consisting of either unconditioned MEF media, or Wnt3a conditioned media derived from ATCC L-Wnt-3A (ATCC CRL-2647) cultures. For experiments utilizing MEFs derived from $Lrp6^{+/cd}$ x $Slc25a32^{+/gt}$ crosses described in Section 2.3.7 and Figure 2.11, this consisted of either untreated MEF media or MEF media supplemented with 100ng/µL Wnt3a (recombinant mouse protein). For CHO-K1 and glyB experiments described in sections 2.3.6 and 2.3.7 and Figures 2.10, 2.13, and 2.14, this consisted of the customized MEM-alpha formulation without supplementation or supplemented as described in Section 2.2.3. Cells were incubated in their respective experimental growth media for 16-18 hours at 5% CO_2, 37ºC. After which, the media was aspirated, the cells were washed once with PBS, covered with 100µL of passive lysis buffer (Promega, E1910/E1960), and rocked at room temperature for 15 minutes. Cell lysates were transferred to microcentrifuge tubes and centrifuged at 12,000 rcf for 1 minute at 4ºC. 10µL of lysate from each sample was then transferred to a well of an opaque-bottom 96-well plate and luminescence was measured using a plate reader luminometer after addition of 50µL beetle luciferin substrate mix (LARII, Promega), followed by a second reading after addition of 50µL coelenterazine substrate mix (Stop & Glo, Promega). The ratio of *Firefly*

luciferase luminescence was divided by the ratio of *Renilla* luminescence for normalization.

2.2.5 Quantification of Serum Folate

Serum was collected from wildtype and heterozygous *Lrp6 Cd* (n=7 $Lrp6^{+/+}$, n=5 $Lrp6^{+/cd}$) and *Slc25a32 gt* dams (n=5 $Slc25a32^{+/+}$, n=5 $Slc25a32^{+/gt}$) that were approximately three to four months of age. Whole blood was collected from facial vein bleeds using a 5mm lancet. The morphotic elements were quickly removed before coagulation by centrifugation at 7,000 rcf for 30 seconds. The resulting serum was stored at -80ºC until quantification.

Serum folate levels were quantified using a competitive binding enzyme-linked immunosorbent assay (ELISA) as previously described in Cabrera et al. (2008) and Fathe, Palacios, and Finnell (2014). 25ng/µL folate binding protein (FBP) was plated in 1µL volumes onto 96 well plates and incubated overnight at 4ºC. The wells were washed three times with TBS-T (Tris buffered saline with 0.05% Tween-20, pH 8.0) to remove excess FBP. Serial dilutions of known concentrations of folic acid (0 ng/mL to 6 ng/mL) were used to generate a competitive standard curve. Serum samples were diluted 1:39 in TBS-T containing 1% w/vol ascorbic acid (pH 3.0) and incubated at 95ºC for 10 minutes to release bound folate. The samples were centrifuged for 7 minutes at 14,000 rcf and the supernatant was reserved and brought to neutral pH with NaOH. The folic acid serial standards and diluted, neutralized serum samples were supplemented 1:9 with an HRP labelled FA (FA-HRP, Cal Bioreagents, C057). The FBP coated wells were incubated for 1 hour at room temperature with the standards and diluted serum samples in duplicate or triplicate wells for each standard or sample. The plates were then washed 3 times with TBS-T and once with TBS. 50 µL of HRP substrate (Super Signal ELISA Femto, Thermo Fisher, 37074)

was added to each well and the plates were immediately imaged using Quansys Biosciences' Q-Views Imager and Software. Median pixel intensity for each well was exported to Microsoft Excel and the standard curve was plotted logarithmically. The folate concentrations in the diluted serum samples were interpolated from the logarithmic standard curve, multiplied by the dilution factor (40), and averaged between replicate wells to obtain the total serum folate (ng/mL) in each sample.

2.2.6 RNA Extraction, qPCR, and RNA-seq

2.2.6.1 RNA Extraction and Purification from Embryos and CHO Cells

Total mRNA was extracted from E9.5 embryos collected from *Lrp6*$^{+/cd}$ x *Lrp6*$^{+/cd}$ heterozygous crosses or *Lrp6*$^{+/cd}$ x *Slc25a32*$^{+/gt}$ mating pairs. The embryos were dissected in PBS and placed in 100µL Tri-Reagent (Zymo, R2050), while the yolk sacs were reserved for genotyping. RNA was purified from the crude extracts using the Direct-zol RNA Miniprep Kit (Zymo, R2051) as per the manufacturer's instructions. Total mRNA was extracted and purified from CHO-K1 and glyB cells using the RNeasy Minikit (Qiagen, 74104) as per the manufacturer's instructions. The homogenization step was performed using a syringe with a 20-gauge needle. The CHO-K1 and glyB RNA was extracted from confluent wells of a six well plate after 24 hours incubation in the custom, glycine-deficient MEM-alpha media described in Section 2.2.3. RNA quality and quantity were confirmed by a NanoDrop spectrophotometer, and all RNA was stored at -80ºC until subsequent RNA-seq or cDNA synthesis.

2.2.6.2 cDNA Synthesis and qPCR

RNA from E9.5 *Lrp6 Cd* embryos (n=4 from each genotype) or from CHO-K1 or glyB cells (n=3 from each cell line) was reverse transcribed to cDNA using the High-

Capacity cDNA Reverse Transcription Kit (Applied Biosystems, 4368814) as per the manufacturer's instructions. cDNA quality and quantity were confirmed by a NanoDrop spectrophotometer. Quantitative PCR (qPCR) was performed using SYBR Green PCR Master Mix in 10uL reactions using designed primers at 20nM each on an ABI Quantstudio Flex 7 thermocycler. Relative expression was determined using the comparative CT method. Genes targeted for qPCR in *Lrp6 Cd* embryos were as follows: *Slc25a32, Shmt2, Gldc, Amt, Mthfd2l, Mthfd1l, Aldh1l2, Mtfmt, Mthfd1, Aldh1l1, Shmt1, Mthfr, Mtr, Dhfr, Bhmt, Folr1, Gapdh, Actb, Polm, Rpl13a*, and *Hprt*. The primers used to amplify these genes are listed in Appendix I. *Gapdh, Actb, Polm, Rpl13a*, and *Hprt* were used as housekeeping genes. Genes targeted for qPCR in CHO-K1 and glyB were as follows: *Lrp6, Wnt1, Wnt2, Wnt2b, Wnt3, Wnt3a, Wnt4, Wnt5a, Wnt5b, Wnt6, Wnt7a, Wnt7b, Wnt8a, Wnt8b, Wnt9a, Wnt9b, Wnt10a, Wnt10b, Wnt11, Wnt16, Gapdh, Actb, Polm, Rpl13a*, and *Hprt*. The primers used to amplify these genes are listed in Appendix I.

2.2.6.3 RNA-seq

RNA from E9.5 embryos collected from $Lrp6^{+/cd}$ x $Slc25a32^{+/gt}$ crosses (n=4 per genotype, except for $Lrp6^{+/cd}$; $Slc25a32^{+/gt}$ embryos where n=8, 4 with open neural tubes and 4 with closed neural tubes) were sequenced by a contractor, NovoGene (Beijing). RNA-seq data analysis was performed using kallisto and DEseq2 (Bray et al. 2016). Gene set enrichment analysis (GSEA) was performed using javaGSEA2-3.0 (Subramanian et al. 2005).

2.2.7 Statistics

Significant changes in NTD rate for all mouse embryo data sets were determined by Fisher's Exact Test (α=0.05). p-values for Hardy-Weinberg Equilibrium (p-HWE) were

determined by a Chi-square Test for goodness of fit. All other data were analyzed in Graphpad Prism (La Jolla) using unpaired t tests or one-way ANOVA with Dunnett's multiple comparisons tests (α=0.05). All error bars represent mean +/- standard error of the mean (SEM).

2.3 RESULTS

2.3.1 Canonical Wnt Signaling is Impaired in *Lrp6 Cd* MEFs

Since there is disagreement in the literature as to whether *Lrp6 Cd* is a canonical Wnt hypermorph (Carter et al. 2005; Shi et al. 2018) or is a model of impaired canonical Wnt signaling (Gray et al. 2013; Lei et al. 2015), it was first necessary to answer this question more definitively. Thus, a TCF/LEF luciferase assay was performed in *Lrp6 Cd* MEFs to measure canonical Wnt activity in response to the ligand, Wnt3a. The results confirm that the *Cd* allele impairs canonical Wnt/β-catenin activation of the TCF/LEF promotor. In *Cd* heterozygous MEFs, Wnt activity decreased by approximately half compared to wildtype, while in *Cd* homozygotes, canonical Wnt signaling was entirely ablated (Figure 2.2). These results are consistent with observations that the *Cd* protein product fails to localize to the cell membrane, and thus, cannot participate as a Wnt co-receptor (Lei et al. 2015). This is also consistent with western blot experiments demonstrating decreased active β-catenin and qPCR experiments demonstrating decreased *Axin2* expression in *Cd* homozygous mouse embryos (Gray et al. 2013).

2.3.2 Digenic Interaction between *Lrp6 Cd* and *Slc25a32* Causes NTDs in Mice

Heterozygous crosses were performed between $Lrp6^{+/cd}$ sires and $Slc25a32^{+/gt}$ dams. Reciprocal crosses were also conducted (23 total litters). Exencephaly was observed in 14 of 52 co-heterozygous embryos (26.92%), compared to 3 out of 49 *Cd* heterozygotes

(6.12%), with zero exencephaly cases in *Slc25a32* heterozygotes (Figure 2.3). Other than exencephaly, no other malformations were observed. Since *Slc25a32* codes for a folate transporter and it is already known that *Lrp6 Cd* is folate responsive, it was considered that maternal genotype may influence exencephaly risk in $Lrp6^{+/cd}$ and co-heterozygous embryos. However, there were no significant differences in NTD rate between co-heterozygous embryos in $Lrp6^{+/cd}$ dams and $Slc25a32^{+/gt}$ dams (p=0.7312, Fisher's Exact Test) (Table 2.1). Furthermore, NTD rates were higher in co-heterozygotes than in any other genotype regardless of maternal genetics, confirming that the NTD risk is compounded by embryonic co-heterozygosity. A lower proportion of co-heterozygous embryos were observed when the dam was $Lrp6^{+/cd}$, but this result was not significant (pHWE=0.1844) and there was no observed difference in resorption rate (p=0.8151).

2.3.3 Serum Folate Levels in *Lrp6Cd* and *Slc25a32* Dams

To further evaluate possible maternal influence contributing to increased NTD risk in $Lrp6^{+/cd}$; $Slc25a32^{+/gt}$ embryos, total serum folate was measured in $Lrp6^{+/cd}$ and $Slc25a32^{+/gt}$ dams. Serum folate levels in $Slc25a32^{+/gt}$ dams were comparable to that of wildtype dams (Figure 2.4). However, there was an approximately 30% reduction in serum folate for $Lrp6^{+/cd}$ dams compared to their wildtype counterparts (Figure 2.4). Since the NTD rate was not significantly lower in co-heterozygotes from $Lrp6^{+/cd}$ dams, this observed reduction in maternal folate status does not appear to have influenced NTD risk associated with $Lrp6^{+/cd}/Slc25a32^{+/gt}$ co-heterozygosity; although, it may offer an explanation as to why less co-heterozygous embryos were collected from $Lrp6^{+/cd}$ dams if it enhances risk for early embryonic lethality. Further experimentation would be needed to answer this question. Regardless, these data further support a role for *Lrp6* in regulating folate transport or folate-dependent metabolism.

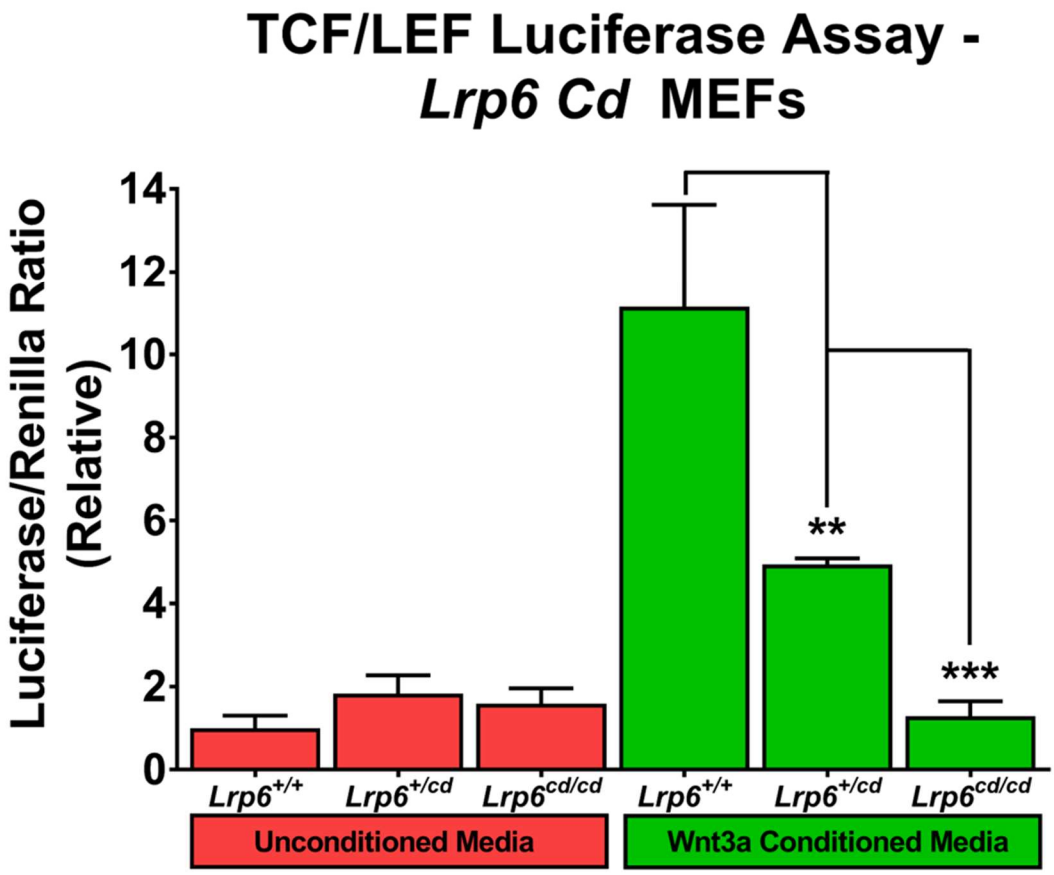

Figure 2.2 *Lrp6 Cd* Impairs Canonical Wnt Signaling in Mouse Embryonic Fibroblasts

Relative luciferase/*renilla* ratios from a TCF/LEF luciferase reporter assay in $Lrp6^{+/+}$, $Lrp6^{+/cd}$, and $Lrp6^{cd/cd}$ MEFs. No canonical Wnt activity was observed in response to unconditioned media (red), but a *Cd*-dependent inhibition of Wnt signaling was observed in response to Wnt3a conditioned media (green).

*Statistical significance was determined using unpaired t tests, $\alpha=0.05$. **, $p<0.01$. ***, $p<0.001$.

A.

Lrp6$^{+/+}$; *Slc25a32*$^{+/+}$ | *Lrp6*$^{+/cd}$; *Slc25a32*$^{+/+}$ | *Lrp6*$^{+/+}$; *Slc25a32*$^{+/gt}$ | *Lrp6*$^{+/cd}$; *Slc25a32*$^{+/gt}$ | *Lrp6*$^{+/cd}$; *Slc25a32*$^{+/gt}$ Exencephaly

B.

***Lrp6*$^{+/cd}$ (♀ or ♂) X *Slc25a32*$^{+/gt}$ (♀ or ♂)**

	***Lrp6*$^{+/+}$; *Slc25a32*$^{+/+}$**	***Lrp6*$^{+/cd}$; *Slc25a32*$^{+/+}$**	***Lrp6*$^{+/+}$; *Slc25a32*$^{+/-}$**	***Lrp6*$^{+/cd}$; *Slc25a32*$^{+/-}$**
Total Embryos	**58**	**49**	**55**	**52**
Exencephaly Embryos	**0**	**3**	**0**	**14**
NTD Rate	**0%**	**6.12%**	**0%**	**26.92%**
Significance		**p=0.0928**		**p<0.0001***

23 Total Litters, 214 Total Embryos, 20 Resorptions

Figure 2.3 Digenic Interaction Between *Lrp6 Cd* and *Slc25a32* Causes Exencephaly in Mouse Embryos

A) E13.5 mouse embryos resulting from crosses between *Lrp6*$^{+/cd}$ and *Slc25a32*$^{+/gt}$ mice. The genotypes are displayed below the images and an example of a *Cd*/*Slc25a32* co-heterozygote with exencephaly is shown on the far right.

B) Table displaying proportion of exencephaly-affected embryos from each genotype. A 26.92% NTD rate was observed in *Lrp6*$^{+/cd}$*; Slc25a32*$^{+/gt}$ embryos.

*Statistical significance was determined using Fisher's Exact Test, α=0.05.

Table 2.1 Rate of Exencephaly in Reciprocal Crosses of *Lrp6*$^{+/cd}$ and *Slc25a32*$^{+/gt}$ Mice

A) Proportion of exencephaly-affected embryos from each genotype in *Lrp6*$^{+/cd}$ dams. A 20% NTD rate was observed in *Lrp6*$^{+/cd}$*; Slc25a32*$^{+/gt}$ embryos.

B) Proportion of exencephaly-affected embryos from each genotype in *Slc25a32*$^{+/gt}$ dams. A 29.73% NTD rate was observed in *Lrp6*$^{+/cd}$*; Slc25a32*$^{+/gt}$ embryos. The difference between NTD rate observed in *Lrp6*$^{+/cd}$ dams and *Slc25a32*$^{+/gt}$ dams was not significant (p=0.7312).

*Statistical significance was determined using Fisher's Exact Test, α=0.05.

A. ***Lrp6*$^{+/cd}$ (♀) X *Slc25a32*$^{+/gt}$ (♂)**

	***Lrp6*$^{+/+}$; *Slc25a32*$^{+/+}$**	***Lrp6*$^{+/cd}$; *Slc25a32*$^{+/+}$**	***Lrp6*$^{+/+}$; *Slc25a32*$^{+/-}$**	***Lrp6*$^{+/cd}$; *Slc25a32*$^{+/-}$**
Total Embryos	**29**	**27**	**25**	**15**
Exencephaly Embryos	**0**	**1**	**0**	**3**
NTD Rate	**0%**	**3.70%**	**0%**	**20.00%**
Significance		**p=0.4821**		**p=0.0115***

11 Total Litters, 96 Total Embryos, 8 Resorptions

B. ***Slc25a32*$^{+/gt}$ (♀) X *Lrp6*$^{+/cd}$ (♂)**

	***Lrp6*$^{+/+}$; *Slc25a32*$^{+/+}$**	***Lrp6*$^{+/cd}$; *Slc25a32*$^{+/+}$**	***Lrp6*$^{+/+}$; *Slc25a32*$^{+/-}$**	***Lrp6*$^{+/cd}$; *Slc25a32*$^{+/-}$**
Total Embryos	**29**	**22**	**30**	**37**
Exencephaly Embryos	**0**	**2**	**0**	**11**
NTD Rate	**0%**	**9.09%**	**0%**	**29.73%**
Significance		**p=0.1812**		**p<0.0001***

12 Total Litters, 118 Total Embryos, 12 Resorptions

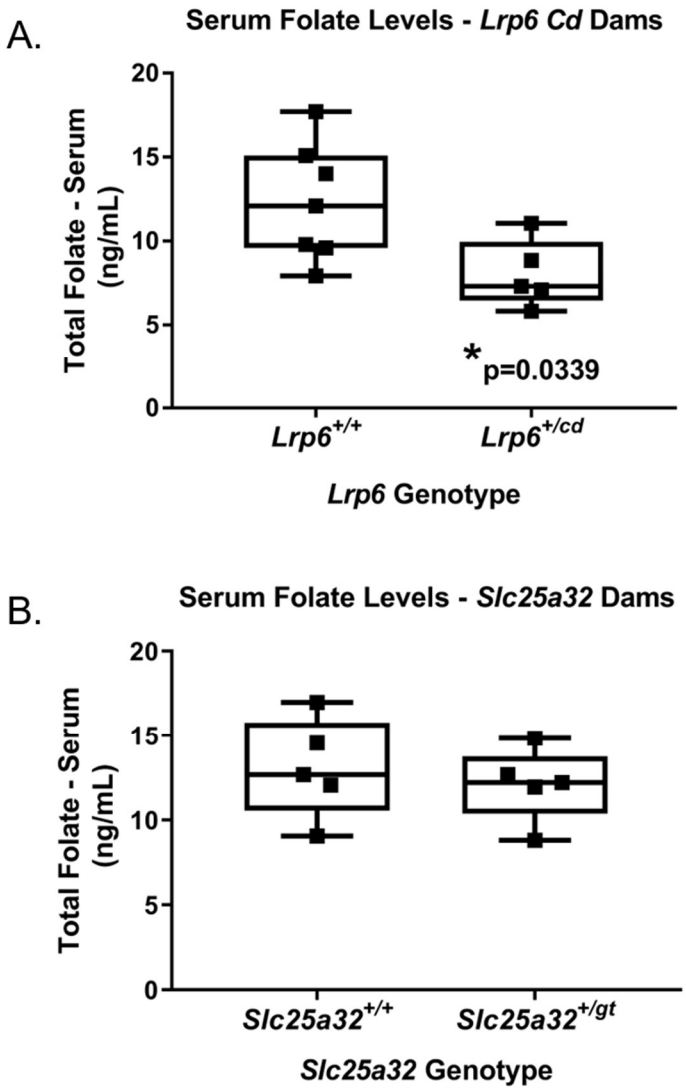

Figure 2.4 Serum Folate Status of *Lrp6*$^{+/cd}$ and *Slc25a32*$^{+/gt}$ Dams

A) Serum folate status in *Lrp6 Cd* dams.

B) Serum folate status in *Slc25a32 gt* dams.

*Statistical significance determined by unpaired student's t test, α=0.05.

2.3.4 *Lrp6 Cd* Impairs Mitochondrial OCM Gene Expression

It was hypothesized that *Lrp6 Cd* may interact with *Slc25a32* by impairing OCM gene expression. To test this hypothesis, qPCR was performed in E9.5 embryos from *Cd* heterozygous crosses comparing relative expression of OCM genes in $Lrp6^{+/+}$, $Lrp6^{+/cd}$, and $Lrp6^{cd/cd}$ embryos. 16 genes from OCM were measured, including *Folr1*, *Slc25a32*, and genes encoding cytosolic and mitochondrial OCM enzymes. Only three genes were observed to have significantly impaired expression associated with the *Cd* allele when normalized to multiple housekeeping genes: *Slc25a32*, *Shmt2*, and *Gldc* (Figure 2.5). Notably, each of these genes participate specifically in mitochondrial OCM, either by facilitating folate transport (*Slc25a32*) or catabolizing serine and glycine (*Shmt2* and *Gldc*). *Slc25a32* demonstrated an approximately 30% reduction in expression associated with *Cd* heterozygosity and an approximately 50% reduction associated with *Cd* homozygosity (Figure 2.5A), while *Gldc* and *Shmt2* exhibited similar *Cd*-dependent changes in gene expression (Figure 2.5B and 2.5C).

2.3.5 Gene Expression Analysis in $Lrp6^{+/cd}$; $Slc25a32^{+/gt}$ Embryos

RNA-seq analysis in E9.5 embryos from $Lrp6^{+/cd}$ x $Slc25a32^{+/gt}$ crosses confirmed reduced expression of *Slc25a32* in *Cd* heterozygotes. More interestingly, there appeared to be a compounded loss in expression in co-heterozygotes, perhaps an initial reduction associated with loss of one functional genomic copy of *Slc25a32* and an additional reduction associated with *Cd* heterozygosity (Figure 2.6). Thus, increased NTD rate in co-heterozygotes may be the result of *Slc25a32* expression dropping below a critical threshold for functionality. *Slc25a32* was the fifth most downregulated gene out of significantly dysregulated genes in our RNA-seq dataset (Table 2.3). Tables 2.2 and 2.3 show the top 20 upregulated and downregulated genes, respectively, in co-heterozygous embryos. It

should be noted that there did not appear to be any difference in expression of *Slc25a32* between co-heterozygotes with open and closed neural tubes (p=0.4369).

When comparing expression of other genes between *Lrp6*$^{+/cd}$*; Slc25a32*$^{+/gt}$ co-heterozygotes and wildtype embryos, there was no significant differential gene expression when the data were corrected for false discovery rate (FDR). This is likely because the analysis compares gene expression in heterozygotes, and there still appears to be haplo-sufficient functionality for both *Lrp6* and *Slc25a32* since most heterozygotes and co-heterozygotes still display normal development. Thus, for gene set enrichment analysis, significant p-values of unpaired t tests were used to identify differentially expressed genes, of which there were 149 between wildtype and co-heterozygous embryos. These genes were over-representative of pathways associated with embryonic development and neural development, including pattern specification, cell fate specification and commitment, anterior/posterior patterning, and neuronal differentiation. Other pathways over-represented in the differentially expressed gene set include cell-cell junctions, including adherens, and actin cytoskeleton (Figure 2.7). These data would suggest that increased NTD risk in co-heterozygous embryos is ultimately derived from disruption of the cellular and tissue-level morphogenic processes underlying NTC. When examining gene/pathway interactions underlying the patterning and cell fate processes effected in co-heterozygotes (Figure 2.8), several interesting genes were upregulated, including *Acvr1c* (codes for a Nodal co-receptor), *Engrailed1 (En1)*, *Pou5f1* (encodes Oct4), *Tdgf1* (teratocarcinoma-derived growthfactor 1), and *Ar* (androgen receptor). Tdgf1 is associated with forebrain defects in humans (de la Cruz et al. 2002), while En1 has been shown to interact with and regulate Wnt/β-catenin activity during development, including in midbrain neurons (Adamska et al. 2004; Bachar-Dahan et al. 2006; Alves dos Santos and Smidt 2011). Downregulated genes included transcription factors associated with neurogenesis, and

notably, *Dnaic2*. Mutations in this gene have been associated with primary cilia dyskinesia (Pennarun et al. 2000; Loges et al. 2008). Given the role of primary cilia in planar cell polarity, convergent extension, and NTDs (Wallingford 2012, 2006), this gene represents a potential candidate for further study in other NTD models of impaired mitochondrial OCM.

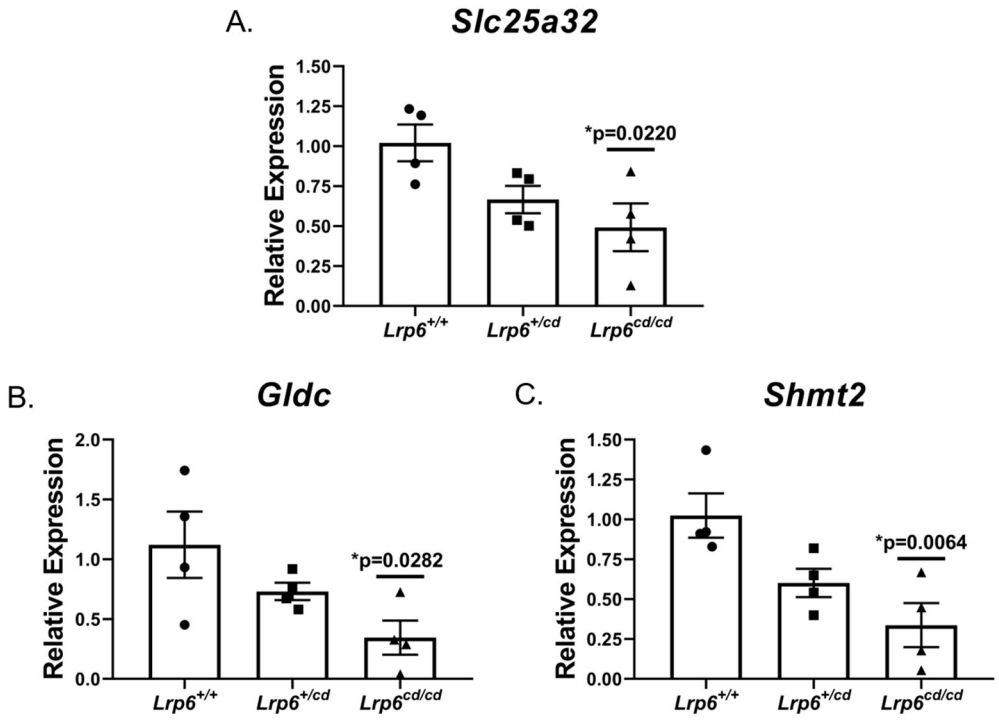

Figure 2.5 Differential Expression of Mitochondrial One-carbon Metabolism Genes in *Lrp6 Cd* Embryos

Results of qPCR showing decreased expression of *Slc25a32* (A), *Gldc* (B), and *Shmt2* (C) associated with *Lrp6 Cd* in E9.5 embryos.

*Statistical analysis was performed using one-way ANOVA with Dunnett's multiple comparisons tests (α=0.05).

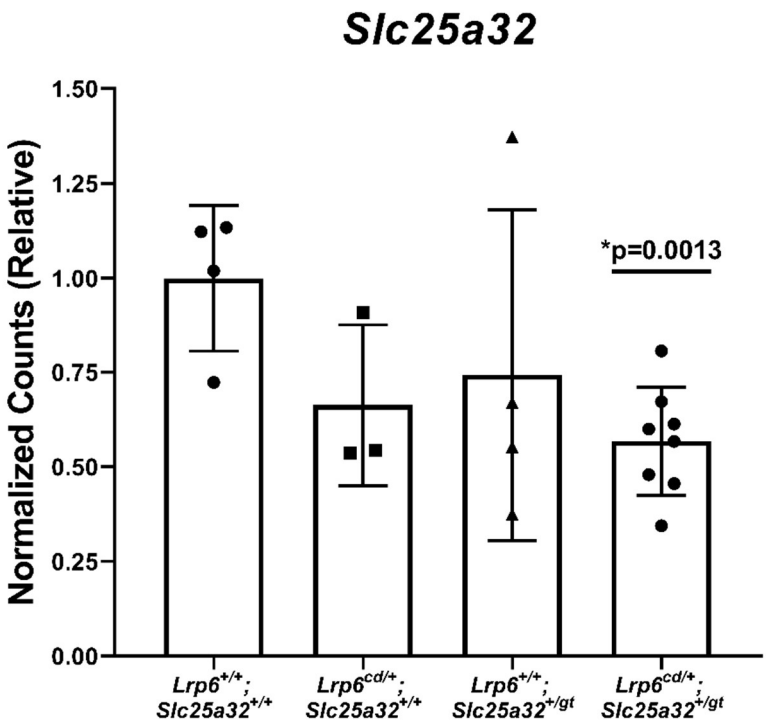

Figure 2.6 *Slc25a32* gene expression in *Lrp6 Cd/Slc25a32* Co-heterozygous Embryos

Relative normalized counts for *Slc25a32* from RNA-seq data in E9.5 embryos from $Lrp6^{+/cd}$ x $Slc25a32^{+/gt}$ crosses.

*Statistical analysis was performed using one-way ANOVA with Dunnett's multiple comparisons tests (α=0.05).

Table 2.2 Most Significantly Upregulated Genes in *Lrp6 Cd/Slc25a32* Co-heterozygous Embryos

Table listing the top 20 most upregulated genes ($p<0.05$, unpaired t test) in E9.5 *Lrp6 Cd/Slc25a32* co-heterozygous embryos compared to wildtype embryos.

Rank	Gene	FC	$\log_2$(FC)	p value
1	*Foxa2*	2.08297	1.058642	0.045809
2	*Muc1*	2.059492	1.042288	0.0068
3	*Cdh22*	1.994137	0.995765	0.02504
4	*Ptchd2*	1.942395	0.957837	0.010552
5	*Fat3*	1.9329	0.950767	0.032508
6	*Pak6*	1.776725	0.82922	0.004818
7	*Taf4a*	1.758602	0.814429	0.021336
8	*Fgf15*	1.738707	0.798015	0.023123
9	*Maneal*	1.696905	0.762906	0.02638
10	*Fgf1*	1.690379	0.757347	0.033607
11	*H2-T24*	1.667363	0.737568	0.045736
12	*Ksr2*	1.651302	0.723604	0.004968
13	*Nrcam*	1.638027	0.711959	0.048565
14	*Slco5a1*	1.625666	0.701031	0.048449
15	*Ccdc177*	1.625392	0.700788	0.041573
16	*Fgf14*	1.609294	0.686428	0.0141
17	*Fut9*	1.567346	0.648324	0.043016
18	*Pappa*	1.558355	0.640024	0.049162
19	*Astn1*	1.531194	0.614657	0.036583
20	*Fam69c*	1.519873	0.603951	0.011111

FC = fold change

Table 2.3 Most Significantly Downregulated Genes in *Lrp6 Cd/Slc25a32* Co-heterozygous Embryos

Table listing the top 20 most downregulated genes ($p<0.05$, unpaired t test) in E9.5 *Lrp6 Cd/Slc25a32* co-heterozygous embryos compared to wildtype embryos.

Rank	Gene	FC	$\log_2$(FC)	p value
1	*Nol3*	0.542019	-0.88358	0.00388
2	*Csn3*	0.555637	-0.84779	0.016555
3	*Tomt*	0.572176	-0.80547	0.011916
4	*Cpa1*	0.576623	-0.7943	0.01021
5	*Slc25a32*	0.59679	-0.7447	0.013848
6	*Tnni2*	0.600166	-0.73657	0.001456
7	*Nr4a1*	0.627348	-0.67266	0.030244
8	*Wif1*	0.648332	-0.6252	0.042747
9	*Nmi*	0.659824	-0.59985	0.019679
10	*Vstm5*	0.66008	-0.59929	0.005143
11	*Eaf2*	0.67728	-0.56218	0.030031
12	*Tns2*	0.684248	-0.54741	0.03393
13	*Tnfsf12*	0.691433	-0.53234	0.032114
14	*Rasd1*	0.6949	-0.52512	0.046668
15	*Nudt17*	0.70148	-0.51153	0.034555
16	*Tmem204*	0.712931	-0.48816	0.049712
17	*Tmem200b*	0.714049	-0.4859	0.021364
18	*Scn1b*	0.719708	-0.47452	0.02813
19	*Gja4*	0.722644	-0.46864	0.037141
20	*Fcgbp*	0.728235	-0.45752	0.003867

FC = fold change

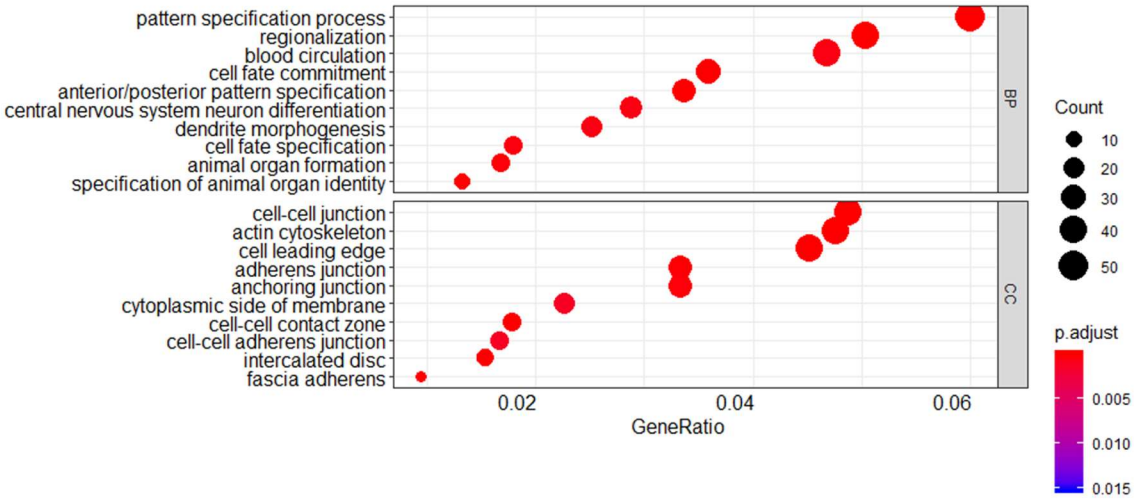

Figure 2.7 Gene Set Enrichment Analysis for Differentially Expressed Genes in *Lrp6 Cd/Slc25a32* Co-heterozygous Embryos

Gene set enrichment analysis showing top 10 classifications in the biological process gene set (BP) and cellular component gene set (CC) between $Lrp6^{+/+}$; $Slc25a32^{+/+}$ and $Lrp6^{+/cd}$; $Slc25a32^{+/gt}$ embryos at E9.5. The chart represents the number of dysregulated genes and gene ratio for each ontological category ($p < 0.05$).

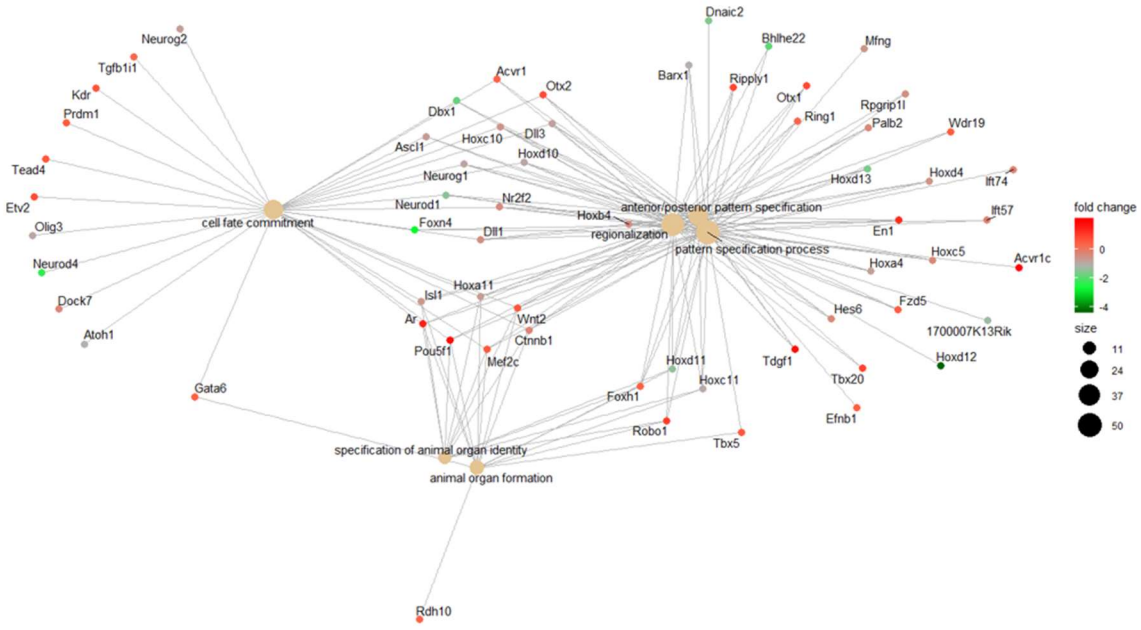

Figure 2.8 Biological Process Gene/Pathway Interaction Plot for Differentially Expressed Genes in *Lrp6 Cd/Slc25a32* Co-heterozygous Embryos

Gene pathway interaction plot showing fold changes in gene expression between $Lrp6^{+/+}$; $Slc25a32^{+/+}$ and $Lrp6^{+/cd}$; $Slc25a32^{+/gt}$ embryos at E9.5 in the biological process gene set.

2.3.6 Loss of *Slc25a32* Impairs Canonical Wnt Signaling in glyB Cells

It was also hypothesized that impairment of mitochondrial OCM could similarly disrupt *Lrp6*'s canonical Wnt activities. To address this hypothesis, canonical Wnt signaling was measured in CHO-K1 and glyb cells using TCF/LEF luciferase assays. It was discovered that CHO cells exhibit innate autonomous Wnt signaling, thus there was no need to stimulate with exogenous Wnts in the media. Autonomous Wnt signaling was reduced by approximately 70% in glyB mutants compared to wildtype CHO-K1 (Figure 2.9) suggesting mitochondrial folate transport and mitochondrial OCM may be important for Wnt signaling.

The next set of experiments were designed to determine the functional level at which *Slc25a32* may regulate canonical Wnt signaling. First, qPCR was performed to compare expression of *Wnt* genes and *Lrp6* in CHO and glyB mutants. No significant changes in expression were observed in any of the genes tested (Figure 2.10). Expression of *Wnt1, Wnt2, Wnt2b, Wnt3*, and *Wnt3a* were either expressing below the limit of detection or not at all. Thus, it appears *Slc25a32* may not be essential for *Wnt* gene expression. The next hypothesis was that *Slc25a32* may be required for Wnt/β-catenin signal transduction. This experiment was conducted using MEFs derived from crosses between $Lrp6^{+/cd}$ and $Slc25a32^{+/gt}$ mice, which do not exhibit autonomous Wnt signaling. Canonical Wnt stimulation was observed upon addition of 100ng/μL Wnt3a. A 50-60% reduction in canonical Wnt activity was detected in $Lrp6^{+/cd}$ and $Lrp6^{+/cd}$; $Slc25a32^{+/gt}$ MEFs, but no reduction was observed in $Slc25a32^{+/gt}$ MEFs (Figure 2.11). If anything, losing one copy of *Slc25a32* may have slightly enhanced Wnt signal transduction, although not significantly. These results suggest that impairment of Wnt signal transduction in $Lrp6^{+/cd}$; $Slc25a32^{+/gt}$ MEFs is elicited solely as a result of the *Cd* genotype and is not influenced by *Slc25a32*.

Finally, Wnts must undergo post-translational palmitoylation before they can be secreted (Takada et al. 2017; Parchure, Vyas, and Mayor 2018). Since palmitate synthesis requires acetyl-CoA derived from the mitochondrial citric acid cycle, it was hypothesized that impaired palmitate synthesis in glyB stemming from defective mitochondrial metabolism may impair Wnt secretion and thus Wnt signaling. This hypothesis was tested by supplementing CHO and glyB cells with 100μM palmitic acid. Palmitate supplementation did appear to enhance canonical Wnt signaling in wildtype CHO, however, glyB cells remained unresponsive (Figure 2.12). This result supports that Wnt secretion may be impaired in glyB, but not as a result of palmitate deficiency. It is possible that other processes, such as palmitoylation itself by the palmitoleoyltransferase, PORCN, may be impaired, although further experimentation would be needed to confirm this hypothesis.

2.3.7 Glycine Restores Canonical Wnt Signaling in glyB Cells

Since glyB cells are glycine auxotrophs, and glycine is known to rescue proliferation defects observed in glyB (McCarthy et al. 2004), it was hypothesized that glycine may also rescue autonomous Wnt signaling defects in glyB. A glycine dose response assay was set up to test this hypothesis. While concentrations of glycine normally found in cell culture media (0.4mM) had no effect, four-fold excess glycine (1.6mM) was sufficient to restore the autonomous Wnt defects observed in glyB mutants back to levels observed in wildtype CHO (Figure 2.13).

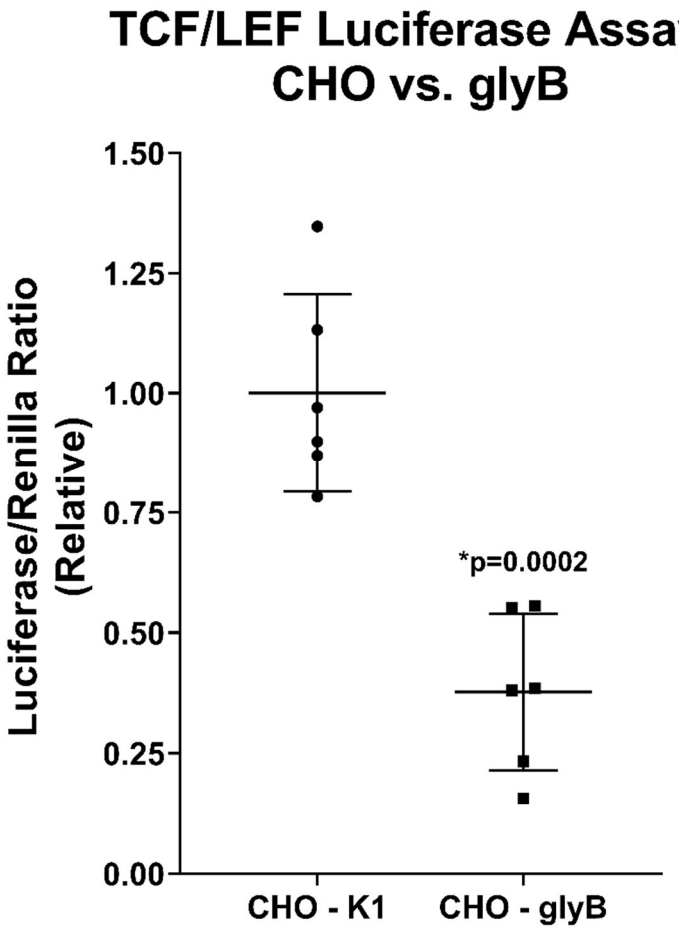

Figure 2.9 Impairment of Autonomous Canonical Wnt Signaling in glyB Mutant CHO Cells

Relative luciferase/*renilla* ratios from a TCF/LEF luciferase reporter assay in CHO-K1 and glyB mutant CHO cells.

*Statistical significance was determined using unpaired t tests, α=0.05.

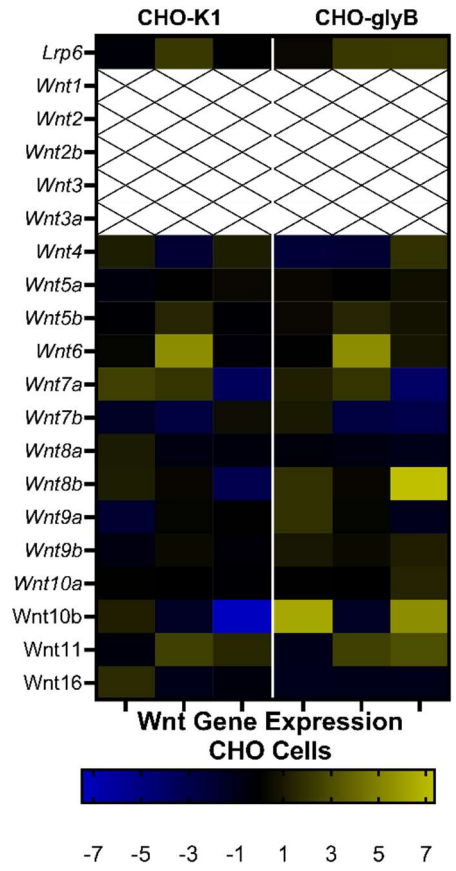

Figure 2.10 Expression of Wnt Genes in glyB Mutant CHO Cells

Heat map showing relative gene expression of *Lrp6* and *Wnt* genes in CHO-K1 and glyB cells. Each square represents the relative, comparative CT value for separate biological replicates. No significant changes in gene expression were observed.

*Statistical significance was determined using unpaired t tests, α=0.05.

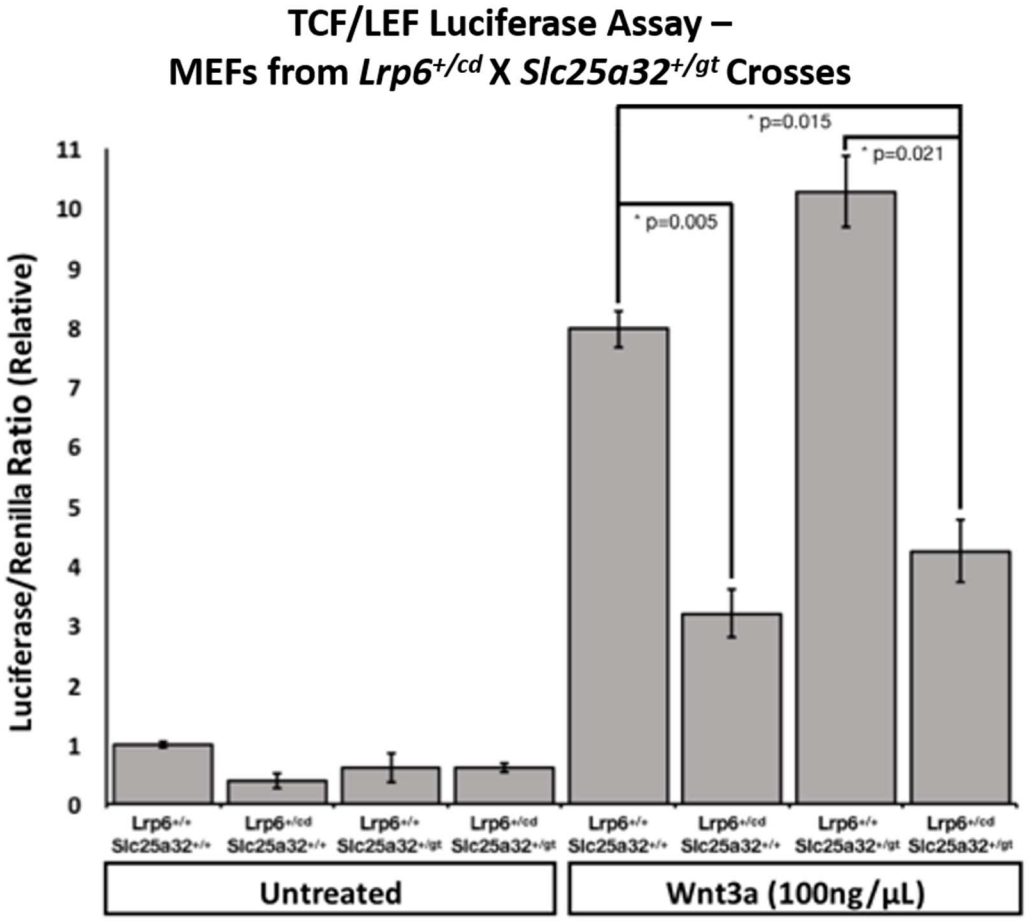

Figure 2.11 *Slc25a32* Genotype Does Not Influence Canonical Wnt Signal Transduction in Mouse Embryonic Fibroblasts

Relative luciferase/renilla ratios from a TCF/LEF luciferase reporter assay using MEFs obtained from $Lrp6^{+/cd}$ x $Slc25a32^{+/gt}$ crosses after incubation with 100ng/µL Wnt3a for 18 hours. Changes in canonical Wnt activity were observed in $Lrp6^{+/cd}$ and $Lrp6^{+/cd}$; $Slc25a32^{+/gt}$ MEFs, but no reduction was observed in $Slc25a32^{+/gt}$ MEFs.

*Statistical significance was determined using unpaired t tests, α=0.05.

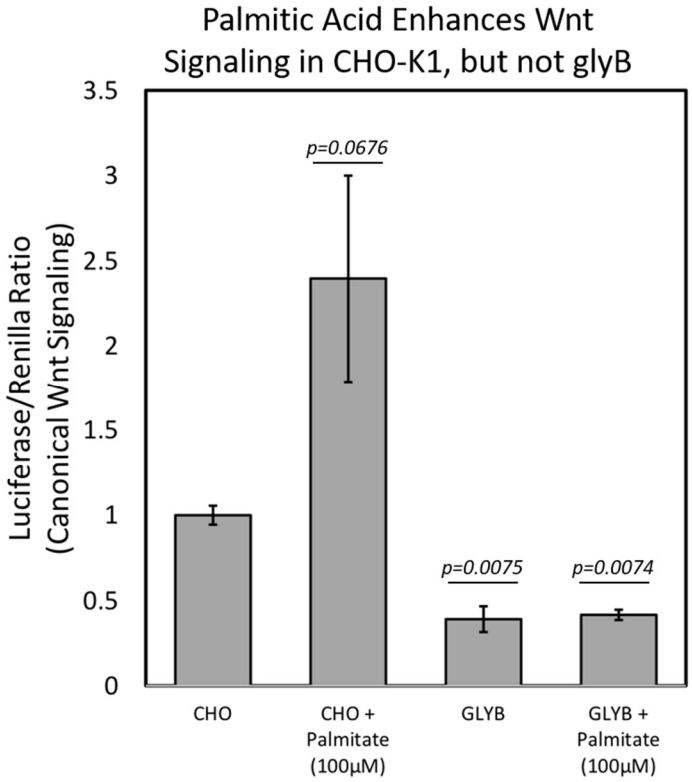

Figure 2.12 Palmitic Acid Enhances Autonomous Wnt Signaling in CHO-K1, but not glyB

Relative luciferase/*renilla* ratios from a TCF/LEF luciferase reporter assay in CHO-K1 and glyB mutants after incubation with 100µM palmitic acid for 18 hours. Changes in canonical Wnt activity were observed in palmitate-treated CHO-K1, but not in palmitate-treated glyB.

*Statistical significance was determined using unpaired t tests, α=0.05.

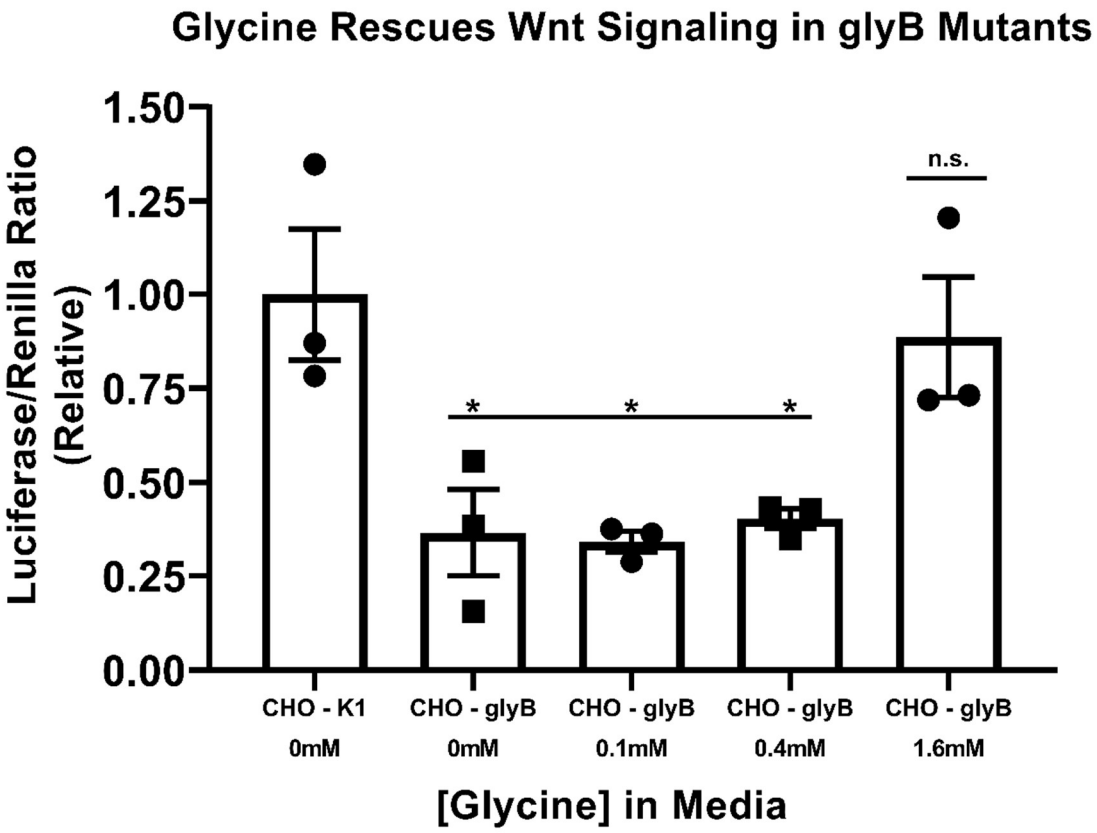

Figure 2.13 Glycine Rescues Wnt Signaling in glyB Mutant CHO Cells

Relative luciferase/*renilla* ratios from a TCF/LEF luciferase reporter assay in CHO-K1 and glyB mutants after incubation with serial dilutions of glycine supplemented media (0.1mM, 0.4mM, and 1.6mM). 1.6mM glycine restored autonomous canonical Wnt activity in glyB mutant CHO cells.

*Statistical significance was determined using unpaired t tests, α=0.05.

2.3.8 Glycine Rescues NTDs in Mouse Embryos Lacking *Slc25a32*

It was previously shown that *Slc25a32*$^{gt/gt}$ embryos exhibit 100% penetrant NTDs (Figure 2.14B), which could be rescued with maternal calcium formate supplementation (Kim et al. 2018). Since glycine rescued auxotrophy and Wnt signaling in glyB cells, which are essentially *Slc25a32* knockouts, it was hypothesized that glycine could similarly rescue NTDs in *Slc25a32* knockout mouse embryos. To test this hypothesis, heterozygous *Slc25a32* mating pairs were set up and pregnant dams were provided 2500mg/kg/d glycine throughout gestation. Of 11 *Slc25a32*$^{gt/gt}$ embryos at E13.5, only two exhibited NTDs (18.18%) (Figure 2.14C). One of those two embryos was severely underdeveloped and displayed craniorachischises. The other had a mostly closed neural tube, except in the midbrain/forebrain where the entire anterior of the embryo was deformed and the neural tube was open (Figure 2.14A). This embryo also had a facial cleft. The distribution of genotypes among the glycine supplemented offspring did not follow typical Hardy-Weinberg equilibrium (p-HWE=0.0098), with genotype distribution skewed towards wildtype embryos (*Slc25a32*$^{+/+}$=29 (39%), *Slc25a32*$^{+/gt}$ =34 (46%), *Slc25a32*$^{gt/gt}$ =11 (15%)). There was also a high rate of resorption (18.68%). This would suggest that while glycine does appear to rescue NTDs in viable *Slc25a32*$^{gt/gt}$ embryos, it may also decrease knockout embryo viability. This phenomenon will be reviewed more thoroughly in the discussion (Section 2.4).

2.3.9 Preliminary: Glycine and Serine Prevent NTDs Associated with *Lrp6 Cd*

Based on the foregoing results, it appears *Lrp6* interacts with mitochondrial OCM, and that this interaction is important for proper NTC. As such, it was hypothesized that, in addition to the previously demonstrated ability of folic acid to reduce NTD rates in *Lrp6 Cd* embryos (Carter et al. 1999), maternal supplementation of 1-C supplements, such as

formate, may also prevent NTDs in *Cd* mice. To test this hypothesis, heterozygous *Cd* mating pairs were set up and pregnant dams were provided 2500mg/kg/d calcium formate, 2500mg/kg/d glycine, or 1250 mg/kg/d L-serine throughout gestation. The serine dosage was half that of formate and glycine because serine provides two 1-C units to mitochondrial OCM, while formate and glycine only provide one. Formate, glycine, and serine did not reduce the occurrence of exencephaly in $Lrp6^{cd/cd}$ embryos, as approximately 50% of *Cd* homozygotes presented with exencephaly in un-supplemented and all supplemented litters (Figure 2.15A). However, in our colony, we do observe a proportion of heterozygous *Cd* embryos that present with exencephaly (approximately 20%), as long as the mice are maintained on their DBA/2; A/J background. Preliminarily, it was observed that the proportion of *Cd* heterozygotes presenting exencephaly phenotypes decreased in glycine and serine supplemented litters to only 5.88% and 6.38%, respectively. However, formate supplementation was unable to produce the same results (Figure 2.15B). It is important to emphasize that these data are preliminary, as a large enough sample size has not yet been collected to make appropriate statistical inferences. If confirmed, these data would suggest that glycine and serine may serve as alternate intervention strategies for human NTDs associated with deleterious, heterozygous *LRP6* variants, and further support a mechanism involving impaired mitochondrial OCM in NTDs associated with *Lrp6* mutants.

A.

B. ***Slc25a32$^{+/gt}$ X Slc25a32$^{+/gt}$ (Un-supplemented,*** *Kim et al. 2018, PNAS*)

	Slc25a32$^{+/+}$	*Slc25a32$^{+/gt}$*	*Slc25a32$^{gt/gt}$*	
Total Embryos	**76**	**135**	**60**	**p-HWE=1.00**
Embryos with NTD	**0**	**0**	**60**	
NTD Rate	**0%**	**0%**	**100%**	

35 Total Litters, 271 Total Embryos, 31 Resorptions

C. ***Slc25a32$^{+/gt}$ X Slc25a32$^{+/gt}$ (Glycine: 2500mg/kg/d)***

	Slc25a32$^{+/+}$	*Slc25a32$^{+/gt}$*	*Slc25a32$^{gt/gt}$*	
Total Embryos	**29**	**34**	**11**	**p-HWE=0.0098***
Embryos with NTD	**0**	**0**	**2**	
NTD Rate	**0%**	**0%**	**18.18%**	

11 Total Litters, 74 Total Embryos, 17 Resorptions

Figure 2.14 Maternal Glycine Supplementation Rescues Neural Tube Defects in *Slc25a32$^{gt/gt}$* Embryos

A) Images of E13.5 *Slc25a32$^{gt/gt}$* embryos from glycine supplemented dams. The embryo on the left exhibited an open cranial neural tube and a facial cleft. The embryos on the right appeared developmentally normal.

B) Table illustrating normal mendelian distribution and 100% penetrant NTDs in un-supplemented *Slc25a32$^{gt/gt}$* embryos. *Data previously published in Kim et al. (2018).

C) Table illustrating decreased prevalence of NTDs in glycine supplemented (2500mg/kg/d) *Slc25a32$^{gt/gt}$* embryos. The genotypes did not follow a mendelian distribution. *p-HWE was calculated using a Chi-square goodness of fit test (α=0.05).

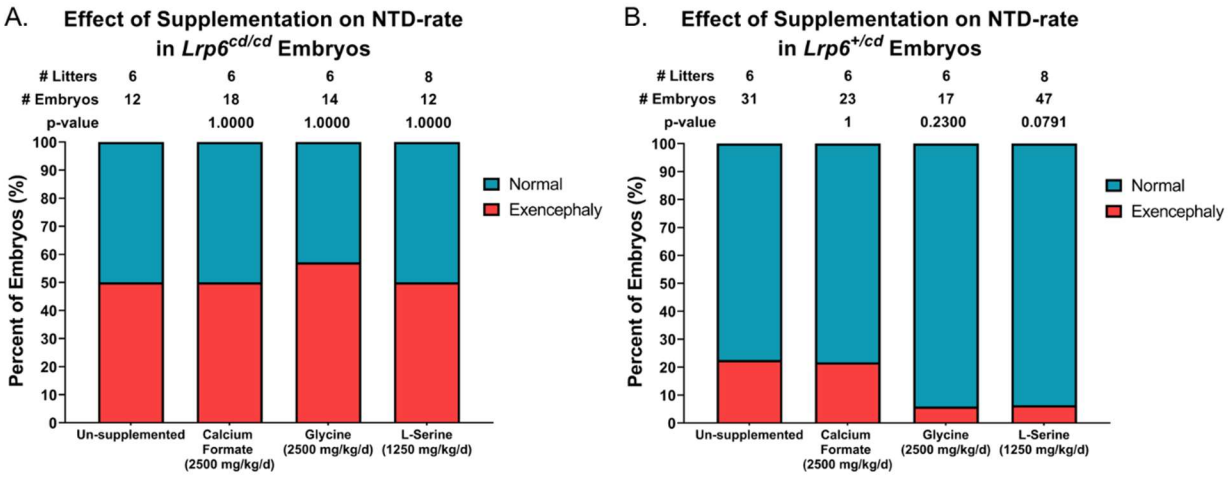

Figure 2.15 Preliminary Data: Effect of Supplementation with One-carbon Donors on NTD-rate in *Lrp6 Cd* Embryos

A) Effect of maternal calcium formate (2500mg/kg/d), glycine (2500mg/kg/d), and L-serine (1250mg/kg/d) supplementation on NTD rate in $Lrp6^{cd/cd}$ embryos.

B) Effect of maternal calcium formate (2500mg/kg/d), glycine (2500mg/kg/d), and L-serine (1250mg/kg/d) supplementation on NTD rate in $Lrp6^{+/cd}$ embryos. The occurrence of exencephaly decreased in glycine and serine supplemented dams (5.88% and 6.38%, respectively).

*Statistical significance was calculated using Fisher's Exact Test (α=0.05). *Note: These data are preliminary, and a larger sample size is needed to make appropriate statistical inferences.*

2.4 DISCUSSION

The work presented here demonstrates mechanistic interactions between *Lrp6* and mitochondrial OCM in mouse NTDs. Heterozygous crosses between *Lrp6 Cd* and *Slc25a32 gt* mice strains demonstrated that co-heterozygous embryos were at increased risk for developing exencephaly. It was further shown that these defects arose as a result of the embryonic genotype and did not depend on maternal genotype, strain background, or serum folate status. The approach of investigating digenic interactions using this co-heterozygous mouse model represents a practical strategy for dealing with the complex genetic architecture underlying NTDs. Traditionally, NTD-associated genes are studied using single-gene mouse knockout models, of which hundreds have been identified (Harris and Juriloff 2007, 2010). However, actual human NTD cases are complex, and it is unlikely that patients would be homozygous for a deleterious variant, and even less likely that such a condition could be considered a preventable birth defect. Variants contributing to preventable human NTDs are generally heterozygous and their risk is determined by interaction with other genetic variants and environmental factors. That said, mouse models that replicate this reality of the human condition are exceedingly rare, although not unheard of. For example, it was found that digenic heterozygosity for deleterious planar cell polarity pathway mutants are found in human NTD cases, and is replicable in mouse models (Wang et al. 2018). Therefore, utilization of such a model that more accurately reflects human NTD pathology is a rare opportunity allowing for an innovative approach. It remains to be seen whether these *Lrp6 Cd/Slc25a32 gt* co-heterozygotes represent a FA-resistant NTD model, but since *Lrp6 Cd* dams were shown to have a lower serum folate status but did not present with increased NTD rate, it is inherently plausible.

When exploring the mechanisms underlying this interaction, it was discovered that *Lrp6 Cd* impairs mitochondrial OCM gene expression at the levels of mitochondrial folate

transport, serine catabolism, and glycine catabolism in embryos. It was further discovered that in co-heterozygous embryos *Slc25a32* expression was reduced even further compared to both *Lrp6 Cd* heterozygotes and *Slc25a32* heterozygotes. These data suggest that mitochondria in *Cd* mutant embryos may have both a lower total folate level and a reduced capacity to perform 1-C transfer reactions necessary to load 1-C units onto THF. Further experiments are required to confirm that these observed reductions in gene expression translate to impaired OCM. Future experiments will measure total folate and distribution of folate species within the mitochondrial folate pool comparing wildtype, *Lrp6 Cd* heterozygous, and *Cd/Slc25a32* co-heterozygotes. In addition, measuring formate production in isolated mitochondria and heavy isotope labelled 1-C tracing from serine and glycine in embryos will inform as to whether there is reduced production of mitochondria-derived 1-C units and reduced incorporation of these units into purine synthesis, pyrimidine synthesis, and the methionine cycle consistent with this hypothesis.

This work also explored an alternative hypothesis as to the mechanisms underlying these interactions: that mitochondrial OCM may conversely regulate canonical Wnt signaling. The link between OCM and Wnt signaling has been known for a while, but little progress has been made in mechanistically linking these two pathways. Gray et al. (2010) showed that FA supplementation enhanced Wnt signaling in NIH-3T3 cells up to 4μg/mL, but that FA attenuated Wnt signaling at higher concentrations (above 10μg/mL). However, the design of this experiment only looked at Wnt transduction from exogenous Wnt3a and used supraphysiological concentrations of FA. It was also recently shown that impairing OCM through methionine deprivation or methotrexate, a DHFR inhibitor, resulted in impaired Wnt signaling in HEK-293T (Albrecht, Bui, and De Robertis 2019); however, this result was also obtained using exogenous Wnt3a. Our experiments in *Slc25a32*$^{+/gt}$ MEFs did not indicate a reduction in response to exogenous Wnts resulting from a single

copy loss of *Slc25a32*; however, it may be the case that a single copy of *Slc25a32* is haplo-sufficient for OCM's Wnt-modulating properties. Even so, that previously published work and our findings that glyB mutant CHO cells, which are mitochondrial folate transporter mutants, have reduced capacity to generate autonomous Wnt signaling, shows consistent support for the hypothesis that impaired OCM may disrupt Wnt signaling, indicating a possible mechanism through which impaired OCM may cause NTDs. Future experiments are needed to determine whether the observed impairment of Wnt signaling in glyB cells translates to *Slc25a32* knockout mouse embryos. Perhaps the most interesting discovery in this particular line of experimentation was that glycine could rescue the autonomous Wnt defects observed in glyB. What role does mitochondrial-derived glycine play in Wnt signaling? Glycine is an amino acid, and thus essential for protein synthesis, but it plays important roles in many other biochemical processes, including purine and glutathione synthesis. Ducker et al. (2016) found that glycine was required to support growth of mitochondrial OCM knockout cells lacking *MTHFD2* and *SHMT2*, but that glycine's essential function was not to provide 1-C units since these cell lines could not be rescued with formate supplementation. Similarly, we found that formate was not capable of rescuing autonomous Wnt defects in glyB mutants (data not shown), suggesting mitochondrial glycine's contribution to Wnt activity is not as a 1-C donor. Ducker et al. (2016) proposed that mitochondrial glycine supports cellular redox homeostasis through glutathione synthesis based on metabolic analysis of glycine-deprived *SHMT2* knockout cells and the observation that glutathione or N-acetylcysteine supplementation rescued growth deficiencies in *SHMT2* knockouts similarly to glycine. There is a lot of literature linking oxidative stress and Wnt signaling, with some literature suggesting that oxidative stress suppresses canonical Wnt activity, while in other models, oxidative stress appears to

enhance canonical Wnt signaling (Ebrahimi et al. 2018; Zhang, Tannous, and Zheng 2019). Thus, further experimentation may be needed to test this hypothesis in glyB cells.

Notably, the experiments presented in this chapter demonstrated that maternal glycine supplementation could rescue NTDs in *Slc25a32* knockout embryos similarly to formate as previously described by Kim et al. (2018). These results would suggest that 1-C units are not the only product of mitochondrial OCM required for NTC. Indeed, it seems difficult to imagine a mechanism by which glycine could provide 1-C units for purine and pyrimidine synthesis under conditions of total ablation of mitochondrial folate, since glycine contributes its 1-C unit to OCM via folate-dependent mitochondrial glycine cleavage. While it is possible there is still a certain level of folate in the mitochondria to serve as a glycine cleavage cofactor, there is no evidence to support that folates enter mitochondria by any other mechanism than MFT. Ducker et al. (2016) demonstrated that, in cell culture at least, ablation of mitochondrial OCM is compensated for via reversal of cytosolic 1-C flux, i.e. cytosolic OCM flows in the oxidative direction providing 1-C units from catabolized serine for purine and pyrimidine synthesis. While there is no evidence that this mechanism is applicable in embryos, excess glycine would certainly counteract cytosolic serine catabolism by stoichiometrically favoring serine synthesis via SHMT1. This may explain why we did not observe a typical mendelian distribution of knockout *Slc25a32* genotypes upon maternal glycine supplementation, as it is possible that excess glycine may be embryotoxic under conditions of impaired mitochondrial OCM. Glycine supplementation of *Slc25a32* knockout cells was shown to elicit cytostatis by opposing *de novo* purine and thymidine synthesis (Steven Gross, Weill-Cornell Medical College, personal communication). Moreover, cancer cells appear to consume serine in preference to glycine for maximal proliferation, and excess glycine or depleted serine results in impaired flux of glycine to purine synthesis, thus depleting cellular nucleotide pools and

inhibiting proliferation (Labuschagne et al. 2014). Notably, exogenous formate counteracts glycine-induced inhibition of cancer proliferation (Labuschagne et al. 2014). While these results would suggest glycine as a potential anti-cancer therapeutic, they also indicate that glycine as an intervention strategy for FA-resistant NTDs may be problematic. Either way, the discovery that glycine rescues NTDs in the viable *Slc25a32* knockout embryos reveals novel insights into the mechanisms of mitochondrial OCM in neural tube development. Further experimentation is needed to elucidate the reasons as to why glycine is essential for NTC, whether it be important for canonical Wnt signaling, as a 1-C donor as certainly demonstrated in glycine cleavage mutants (Pai et al. 2015; Leung et al. 2017), or by other mechanisms such as direct incorporation into purine synthesis, glutathione metabolism, or as an amino acid for protein synthesis. The arguments presented herein pose one further question: would co-supplementation of glycine and formate, or glycine and serine, in *Slc25a32* knockout embryos prove to be a more effective intervention strategy than formate or glycine alone? Further experiments are needed to answer this question.

Finally, the preliminary data suggesting glycine or serine supplementation may reduce occurrence of NTDs approximately three to four-fold in *Cd* heterozygous embryos supports a role for *Lrp6* in mitochondrial OCM. Interestingly, formate did not elicit the same effect. While providing exogenous formate as a source of 1-C units may rescue proliferation defects and NTDs associated with total ablation of mitochondrial formate production, it may be counterproductive under conditions of only moderately impaired mitochondrial OCM flux, such as we hypothesize in *Lrp6 Cd* heterozygotes. The gene expression data presented in Figures 2.6 and 2.7 support that mitochondrial folate transport, mitochondrial serine catabolism, mitochondrial glycine synthesis, and mitochondrial glycine catabolism would be impaired in *Lrp6 Cd* heterozygotes. Logically, providing excess folate, serine, or glycine would more directly rescue these deficiencies than excess

formate. Furthermore, Ducker et al. (2016) demonstrated that formate supplementation was antagonistic in *SHMT2* knockout HEK-293T cells. Thus, serine and glycine may be more suitable intervention strategies for rescuing NTDs associated with *Lrp6*-induced impairment of mitochondrial OCM.

It is important to note that we were surprised to observe *Cd* heterozygotes with exencephaly, as this was not reported in any of the previously published literature on *Lrp6 Cd*. We were initially concerned, since previous experiments crossed this line to *Folr1* and *Slc25a32* knockout lines, that a breeding mistake had somehow introduced a *Folr1* or *Slc25a32* knockout allele into our colony. However, after genotyping several litters, we were able to rule out this possibility. Thus, it is possible the *Lrp6 Cd* mouse strain has undergone some amount of genetic drift in the 21 years since this line was first generated (Carter et al. 1999). Interestingly, the approximately 20% occurrence of NTDs in *Cd* heterozygous embryos seems to depend on the genetic background. This strain was originally identified in a mixed DBA/2; A/J background (Carter et al. 1999), and to the best of our knowledge, no other genetic strain has been introduced into our *Cd* colony. We noticed that when *Lrp6 Cd* is crossed to the C57/BL6 background, the background hosting the *Slc25a32* knockout, the observed rate of NTDs in *Cd* heterozygous embryos drops to around 6.12% (Figure 2.3); and when *Lrp6 Cd* is crossed to the LM/BC background, the background hosting the *Folr1* knockout, we do not observe any NTDs in *Cd* heterozygous embryos (Figure 2.1). Thus, the NTD risk associated with *Cd* heterozygosity is clearly influenced by genetic modifiers in the host strain.

Ultimately, the data presented in this chapter support a mechanism of interaction between *Lrp6* and mitochondrial OCM. Understanding the biology and biochemistry underlying this interaction may support the efficacy of alternative intervention strategies

such as dietary fortification of glycine or serine for the prevention of human NTDs associated with *LRP6* variants or other models of impaired mitochondrial OCM.

Chapter 3: Characterization of Murine Embryonic Stem Cells Lacking *Mthfd1l*

3.1 INTRODUCTION

10-formyl-tetrahydrofolate (10-formyl-THF) is the most oxidized folate species harboring a 1-C unit, and is synthesized in mitochondria from 5,10-methylene-THF via a two-step process by the bifunctional enzymatic activities of MTHFD2 or MTHFD2L, two members of the methylene tetrahydrofolate dehydrogenase (MTHFD) family (Tibbetts and Appling 2010; Shin et al. 2014). 10-formyl-THF can be utilized for one of three fates in mitochondria (Figure 3.1). First, the formyl group may be transferred to methionyl-tRNA formyltransferase to produce N-formylmethionyl-tRNA, which is the essential initiator tRNA in mitochondrial protein translation (Minton et al. 2018; Morscher et al. 2018). Alternatively, 1-C units from 10-formyl-THF could be completely oxidized to CO_2 by aldehyde dehydrogenase 1-like 2 (ALDH1L2) simultaneously producing NADPH (Krupenko et al. 2010; Strickland et al. 2011); in this case, the 1-C units are no longer available for subsequent OCM. Finally, the formyl group could be converted to free formate by the monofunctional, mitochondrial 10-formyl-THF synthetase, MTHFD1L, and utilized for cytosolic OCM. In fact, up to 75% of 1-C units in the cytosol are derived from mitochondrial formate (Pike et al. 2010). Thus, MTHFD1L is essential for cytosolic OCM.

Mouse embryos lacking the gene, *Mthfd1l,* were found to be non-viable beyond E12.5 and phenotypically presented severe developmental delay, orofacial clefts, and NTDs (Momb et al. 2013; Shin et al. 2019). Maternal supplementation with exogenous formate decreased the prevalence and severity of the observed phenotypes and prolonged viability (Momb et al. 2013). The human gene, *MTHFD1L*, has been implicated in birth defects as well. Three alleles in a common polymorphism, rs3832406, were identified in

an Irish population with variable influences on risk for NTDs, and an additional single-nucleotide polymorphism in the 3' UTR of *MTHFD1L* was also associated with these same congenital anomalies (Parle-McDermott et al. 2009; Minguzzi et al. 2014). One of the rs3832406 alleles was further found to slightly enhance maternal risk of having a neural tube defect-affected infant in a U.S. Hispanic cohort (McKenzie 2018). Another *MTHFD1L* variant, rs11754661, was associated with Alzeheimer's Disease in a Han Chinese population (Ren et al. 2011; Ma et al. 2012), while a study in Hungary and the United Kingdom demonstrated strong association between *MTHFD1L* variant, rs11754661, and ruminative response style, suggesting the gene may play a role in the etiology of depression and other disorders associated with mental and cognitive health (Eszlari et al. 2016). Yet another polymorphism, rs6922269, has been associated with patient outcomes after acute coronary syndrome (Palmer et al. 2014; Hubacek et al. 2015). Finally, the most recent line of published research sharply focuses on this enzyme's role in cancer progression and metabolism, suggesting MTHFD1L may be a strong candidate target for future therapeutic strategies (Lee et al. 2017; Yang et al. 2018; Agarwal et al. 2019; Eich et al. 2019; Li et al. 2019). Given, the extensive and diverse roles for MTHFD1L thus far associated with human health outcomes, understanding the underlying mechanisms through which MTHFD1L influences normal cellular metabolism and function is of critical interest.

To investigate these questions, a functional analysis of mouse embryonic stem (ES) cells lacking *Mthfd1l* was performed. Consistent with impaired *de novo* nucleotide metabolism, we observed proliferation defects in the *Mthfd1l* knockout ES cells compared to wildtype, which could be rescued with either exogenous formate, or co-supplementation with hypoxanthine and thymidine. We also observed that ES cells lacking *Mthfd1l* were sensitive to hypoxia in a gene dose-dependent manner, and that this sensitivity was related

to cell survival, not proliferative capacity. Finally, we found evidence in mouse embryo gene expression analysis suggesting a metabolic switch in catabolism of mitochondrial 10-formyl-THF away from MTHFD1L-dependent formate synthesis occurring between E8.5 and E10.5. The implications and relevance of these findings related to underlying mechanisms of NTD pathology are also discussed.

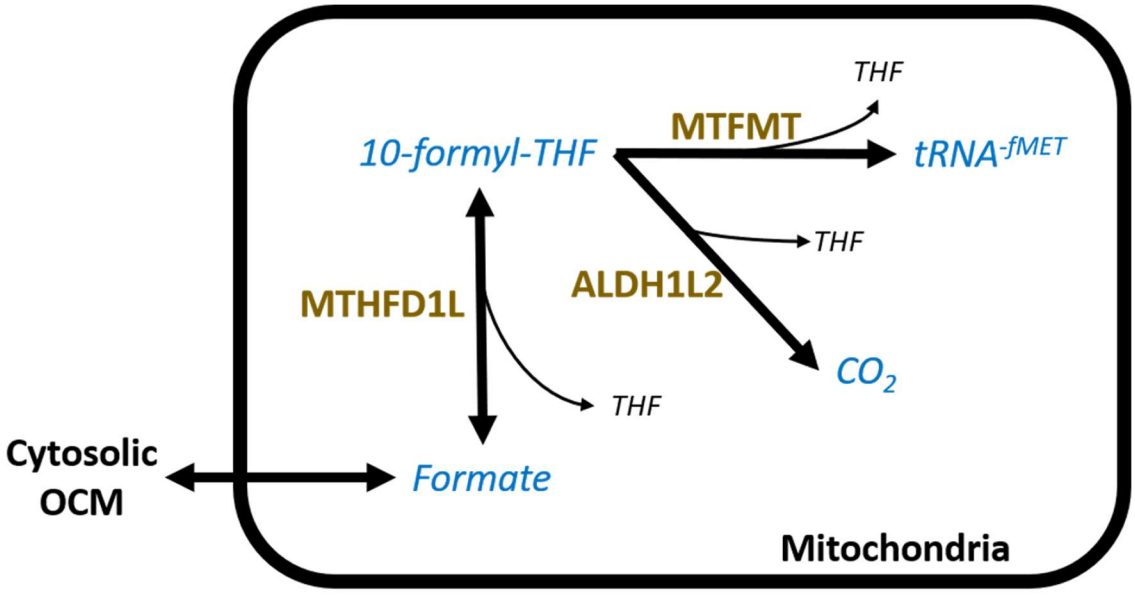

Figure 3.1 Fates for 10-formyl-THF in Mitochondrial One-carbon Metabolism

THF = tetrahydrofolate; tRNA-fMET = N-formylmethionyl-tRNA; MTFMT = methionyl-tRNA formyltransferase; ALDH1L2 = aldehyde dehydrogenase 1-like-2; MTHFD1L = methylene-tetrahydrofolate dehydrogenase 1-like (10-formyl-THF synthetase); OCM = one-carbon metabolism.

3.2 Materials and Methods

3.2.1 Mouse Embryonic Stem Cell Culture

Mouse ES cell lines were generated as described by Nichols et al. (2009) from *Mthfd1l*$^{+/+}$, *Mthfd1l*$^{+/z}$, and *Mthfd1l*$^{z/z}$ mouse embryos (described in Momb et al. (2013)) and cryopreserved in liquid nitrogen for long term storage. ES cells were maintained on gelatin coated plates (EMD Millipore, ES-006-B) with daily feedings of 2i media, which consisted of a 50:50 mix of Neurobasal (Gibco, 21103049) and DMEM/F-12 (Gibco, 11320082) supplemented with 0.5x Ndiff Neuro-2 (EMD Millipore, SCM012), 0.5x B-27 (Gibco, 17504044), 3μM CHIR 99021 (Cayman Chemical, 13122), 1μM PD03259010 (Sigma, PZ0162), 100μM 2-mercaptoethanol (Gibco, 21985023), and 50 ng/mL recombinant mLIF (EMD Millipore, LIF2050). The cells were passaged as needed using Accutase (EMD Millipore, SF006) for 3 minutes at 37°C.

3.2.2 Embryonic Stem Cell Growth Curve Analysis

Since DMEM/F-12 contains thymidine and hypoxanthine, which would prevent the cells from utilizing *de novo* nucleotide synthesis in favor of nucleotide salvage, DMEM/F12 was replaced with DMEM (Gibco, 11965118) in the 2i cocktail for the growth curve experiments. The cells were gradually weaned onto this modified 2i media for two days leading up to the experiments by reducing the ratio of Ham's F-12 (Gibco, 11765054) by half with each feeding. *Mthfd1l*$^{+/+}$ and *Mthfd1l*$^{z/z}$ ES cells were plated in 6-well cell culture plates at a density of 30,000 cells per well. The cells were cultured for five days in the modified 2i media containing DMEM, and the media was either left un-supplemented or supplemented with 400μM sodium formate, or 30μM hypoxanthine and 3μM thymidine based on the conventional media formulation for Ham's F-12. Each day, three replicate

wells from each genotype and treatment were harvested with Accutase and counted by hemocytometer.

3.2.3 Hypoxia Experiments

3.2.3.1 CyQUANT Assay

Hypoxic cell culture conditions were generated by culturing cells in a humidified, one-shelf C-chamber (Biospherix, C174) placed inside a 37°C cell culture incubator. Oxygen was regulated using the ProOx P110 oxygen controller (Biospherix, P110) using a custom gas mixture of 5.55% CO_2 balanced with nitrogen. The purpose of the custom gas mixture is to maintain a 5% CO_2 environment as ambient oxygen gets displaced.

Mthfd1l$^{+/+}$, *Mthfd1l*$^{+/z}$, and *Mthfd1l*$^{z/z}$ ES cells were plated in 96-well plates at a density of 6,000 cells per well, with three replicate wells per genotype. The cells were allowed to attach overnight and subsequently placed at either 1% O_2 or ambient incubator O_2 (approximately 18-19%) conditions for 48 hours. The media was then removed, and the cells were gently washed once with PBS. The plates were then frozen at -80°C for one hour and allowed to thaw at room temperature. Relative cell density in each well was then measured using the CyQUANT Cell Proliferation Assay (Thermo Fisher, C7026) via a fluorescent 96-well plate reader.

3.2.3.2 EDU Proliferation Assay

Mthfd1l$^{+/+}$, *Mthfd1l*$^{+/z}$, and *Mthfd1l*$^{z/z}$ ES cells were plated in 6-well plates at a density of 200,000 cells per well, with three replicate wells per genotype. An additional well of *Mthfd1l*$^{+/+}$ was utilized as a negative control. The cells were allowed to attach overnight and subsequently placed at 1% O_2 for 24 hours. At the 22 hour mark, EdU (ethynyl deoxyuridine) was quickly added without changing the media to each well at a

final concentration of 10μM (from a 10mM stock) and the cells were allowed to incubate for an additional 2 hours at 1% O_2. Afterwards, cells were lifted with Accutase, washed once with PBS, fixed, permeabilized, and the incorporated EdU was labelled using the Click-iT Plus EdU Flow Cytometry Assay Kit (Life Technologies, C10633) as per manufacturer protocols. The fixative and saponin-based permeabilization buffer were supplied as part of the kit. Negative control wells were treated with EdU, washed, fixed, and permeabilized the same as all other samples, but were not treated the Alexa Fluor 647 picolylazide detection reagent. Cells were then washed twice in 5mL of PBS, incubated with Hoescht 33342 (1μg/mL) in PBS for 10 minutes, and washed again with 5mL of PBS. Cells were then placed in 1mL of PBS while EdU and Hoescht incorporation were measured via fluorescence-based flow cytometry using an Attune NXT (T103) Cell Analyzer in BCM's Cytometry and Cell Sorting Core. The plots in Figure 3.4A represent concatenations of three replicates. Between 7,000 and 10,000 cells were analyzed for each replicate.

3.2.3.3 Cellular Viability Assay

Mthfd1l$^{+/+}$, *Mthfd1l*$^{+/z}$, and *Mthfd1l*$^{z/z}$ ES cells were plated in 6-well plates at a density of 200,000 cells per well, with three replicate wells per genotype. Two additional wells of *Mthfd1l*$^{+/+}$ were utilized as positive and negative controls. The cells were allowed to attach overnight and subsequently placed at 1% O_2 for 24 hours. The cells were lifted with Accutase, washed once with PBS, resuspended in 1mL of PBS and 1mL of 2X LIVE/DEAD Cell Imaging Kit 488 probe (Life Technologies, R37601) was added to each well, except for the negative control. The positive controls were heated at 42°C for 10 minutes to induce cell death prior to adding probe. The cells were then incubated at room temperature for 15 minutes followed by two 5mL washes with PBS. The cells were then

incubated with Hoescht 33342 (1μg/mL) in PBS for 10 minutes and washed once more with 5mL of PBS. Cells were then placed in 1mL of PBS while FITC and Hoescht fluorescence were measured via flow cytometry using an Attune NXT (T103) Cell Analyzer in BCM's Cytometry and Cell Sorting Core. The plots in Figure 3.5A represent concatenations of three replicates. Between 7,000 and 10,000 cells were analyzed for each replicate. Gates were established using the positive and negative controls.

3.2.4 Mouse Embryo Gene Expression Analysis Between E8.5 and E10.5

C57/BL6 mice were obtained from BCM's Center for Comparative Medicine, were housed in BCM's Neurosensory mouse facility on 12-hour light/dark cycles with standard chow and maintained according to protocols approved by the Institutional Animal Care and Use Committee (IACUC) at BCM. Timed mating and euthanasia were performed as described in Section 2.2.1. Embryos were collected from pregnant dams at E8.5, E9.5, and E10.5. Total mRNA was extracted as described in Section 2.2.6 using Tri-reagent. cDNA synthesis and qPCR were also performed as described in Section 2.2.6. The following genes were targeted for qPCR: *Slc25a32, Shmt2, Shmt1, Mthfd2L, Mthfd1L, Mthfd1, Folr1, Gapdh, Actb, Aldh1l1,* and *Aldh1l2*. Differential gene expression was determined using the comparative CT method with *Gapdh* and *Actb* used as housekeeping genes.

3.2.5 Statistics

All statistical analyses were performed using GraphPad Prism (La Jolla). Statistics comparing genotypes and treatments at each time point for the ES cell growth curve analysis were conducted using student's t tests (α=0.05). Statistical significance for the CyQUANT, EdU, and cellular viability assays were determined using two-way ANOVA with Dunnett's multiple comparisons tests (α=0.05). Significant differences in embryo

gene expression between E8.5 and E10.5 was determined by one-way ANOVA with Dunnett's multiple comparisons tests (α=0.05). All error bars represent mean +/- standard error of the mean (SEM).

3.3 RESULTS

3.3.1 Embryonic Stem Cell Growth Curve Analysis

We initially did not observe proliferation defects in our ES cell lines, which was not consistent with previous observations in *Mthfd1l*$^{z/z}$ MEFs (Bryant 2017) and CRISPR-mediated knockouts of mitochondrial OCM in HEK-293T cells (Ducker et al. 2016). It was hypothesized that the standard 2i media formulation may provide sufficient levels of hypoxanthine and thymidine for the cells to utilize nucleotide salvage for purine and pyrimidine synthesis. To test this hypothesis, a modified 2i media was formulated lacking hypoxanthine and thymidine (see Section 3.2.2). Consistent with the hypothesis, ES cells lacking *Mthfd1l* grew significantly slower in this modified 2i media (Figure 3.2). Differences between the number of *Mthfd1l*$^{+/+}$ cells and *Mthfd1l*$^{z/z}$ cells were statistically significant at every timepoint measured between days two and five of the experiment, and the ratio of wildtype to knockout cells increased each day. Formate supplementation did improve growth of knockout cells, although formate-supplemented knockouts never completely caught up to wildtype ES cells. It should also be noted that formate supplementation in *Mthfd1l*$^{+/+}$ significantly impaired growth, although not comparably to total loss of *Mthfd1l* (data not shown). Notably, *Mthfd1l*$^{z/z}$ cells co-supplemented with hypoxanthine and thymidine grew comparable to wildtype ES cells, confirming our hypothesis.

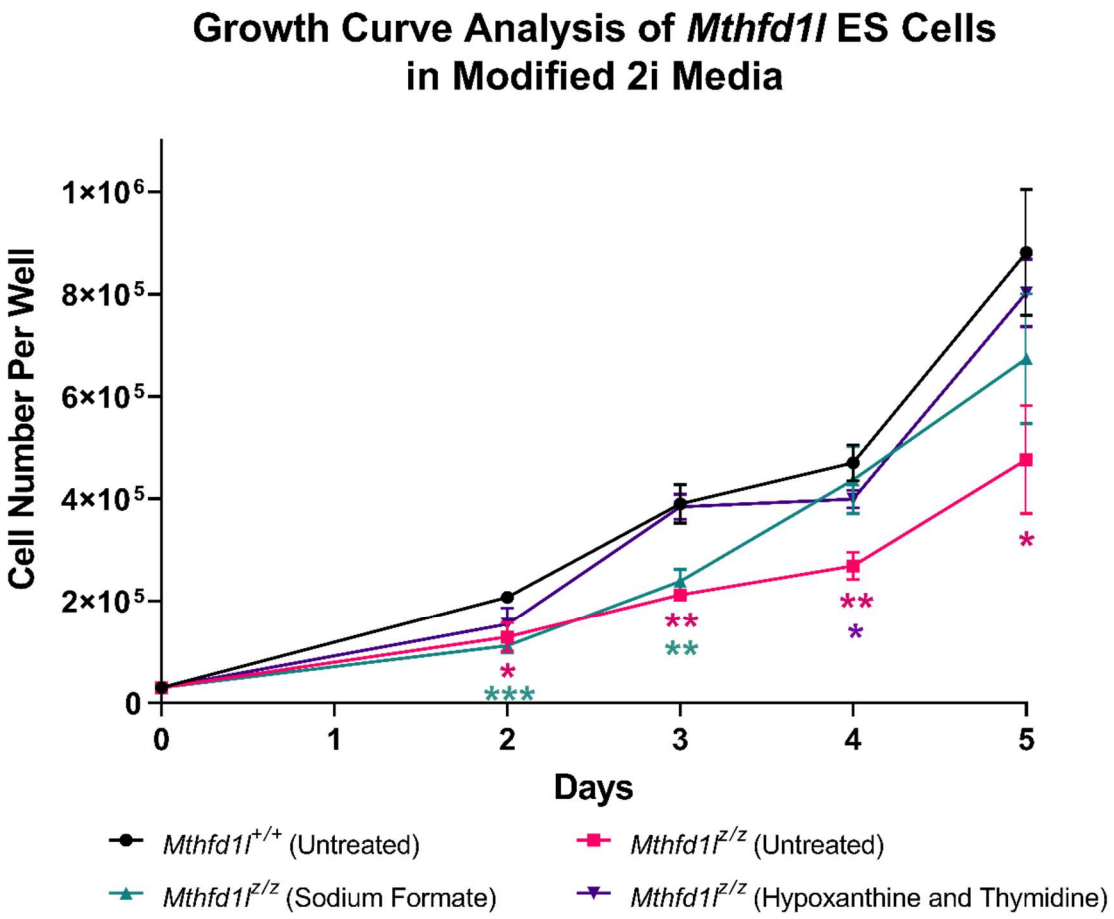

Figure 3.2 Growth Curves Comparing *Mthfd1l*$^{+/+}$ and *Mthfd1l*$^{z/z}$ Embryonic Stem Cells

Growth curves of un-supplemented *Mthfd1l*$^{+/+}$ and *Mthfd1l*$^{z/z}$ ES cells cultured in modified 2i media lacking hypoxanthine and thymidine over five days. Growth of formate supplemented (400μM sodium formate) *Mthfd1l*$^{z/z}$ cells and *Mthfd1l*$^{z/z}$ cells co-supplemented with hypoxanthine (30μM) and thymidine (3μM) is also displayed.

*Statistical significance was determined by student's t tests (α=0.05). *, $p<0.05$. **, $p<0.01$. ***, $p<0.001$.

3.3.2 Embryonic Stem Cells Lacking *Mthfd1l* are Sensitive to Hypoxia

Given the role of mitochondrial OCM in mediating cellular redox balance, it was hypothesized that *Mthfd1l*$^{z/z}$ ES cells may exhibit hypoxia-specific phenotypes. To test this hypothesis, *Mthfd1l*$^{+/+}$, *Mthfd1l*$^{+/z}$, and *Mthfd1l*$^{z/z}$ ES cells were cultured at 1% O_2, and a CyQUANT proliferation assay was performed. It is important to note that while the CyQUANT kit is marketed as a "proliferation assay," the detection method relies on DNA content; thus, this assay can only detect cellular density and is not able to discern between proliferation rate and cell viability. After 48 hours under ambient O_2 conditions in a normal CO_2 cell culture incubator (O_2 = approx. 18-19%), there were no differences in cell numbers between *Mthfd1l*$^{+/+}$, *Mthfd1l*$^{+/z}$, and *Mthfd1l*$^{z/z}$ ES cells (Figure 3.3). This experiment was performed in standard 2i media to differentiate between mitochondrial OCM's role in producing purines and pyrimidines from its supportive role in cellular redox homeostasis. Thus, those observations are consistent with our previous observations regarding proliferation in these ES cells under those conditions. At 1% O_2 however, wildtype cells performed better compared to wildtype cells at ambient oxygen (Figure 3.3). This is consistent with observations that many cell lines, including stem cells and primary cells, perform better at lower than atmospheric oxygen, possibly because these conditions are more physiologically relevant and cells are genetically designed to adapt under these conditions (Bates 2012). Interestingly, an *Mthfd1l* genotype-dependent reduction in cell density was observed under these hypoxic conditions, with *Mthfd1l*$^{+/z}$ performing half as well as wildtype, and *Mthfd1l* knockouts performing substantially poorer (Figure 3.3). Thus, it appears *Mthfd1l* may be critical for cellular adaptation to hypoxia.

3.3.3 Hypoxia Sensitivity in *Mthfd1l* Embryonic Stem Cells is Characterized by Viability Defects

We wanted to see whether this observed hypoxia sensitivity associated with *Mthfd1l* genotype was a result of impaired cellular proliferation or decreased viability. An EdU cell proliferation assay was performed on *Mthfd1l*$^{+/+}$, *Mthfd1l*$^{+/z}$, and *Mthfd1l*$^{z/z}$ ES cells cultured at 1% O_2. After 2 hours EdU exposure, no significant differences were observed between genotypes in the proportions of cells at each phase of the cell cycle (G0/G1, S, and G2) (Figure 3.4). Thus, it was concluded that hypoxia sensitivity was not caused by impaired proliferative capacity.

However, in the viability assay, only 83.29% (+/- 1.24%) of *Mthfd1l*$^{z/z}$ cells clustered with the viable negative controls, compared to 86.25% (+/- 0.57%) in *Mthfd1l*$^{+/z}$ cells and 90.67% (+/- 0.08%) in *Mthfd1l*$^{+/+}$ cells (Figure 3.5). This result was statistically significant; thus, it was concluded that hypoxia decreases cellular viability in ES cells lacking *Mthfd1l*.

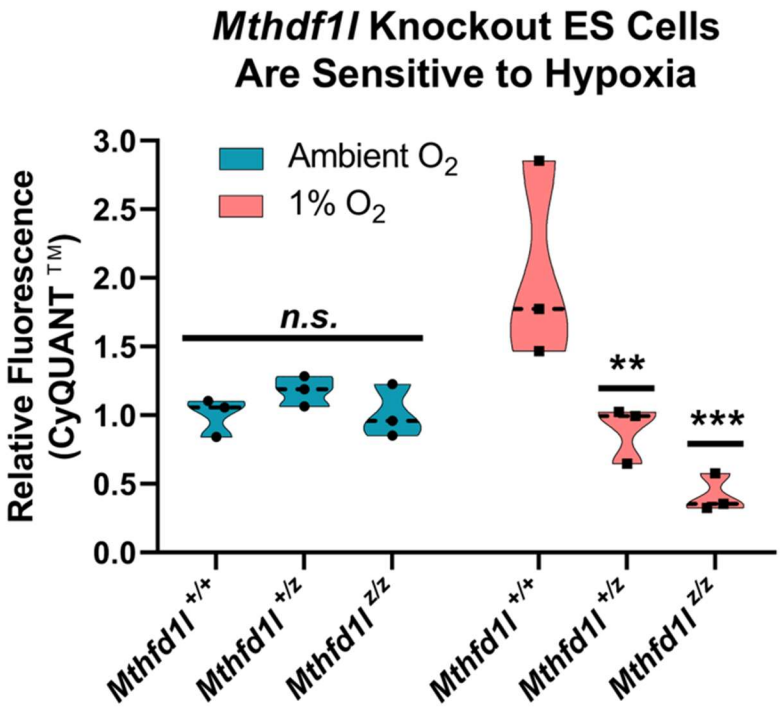

Figure 3.3 Hypoxia Sensitivity in *Mthfd1l*$^{z/z}$ Embryonic Stem Cells

CyQUANT proliferation assay showing relative cellular abundance (based on sample DNA content) in *Mthfd1l*$^{+/+}$, *Mthfd1l*$^{+/z}$, and *Mthfd1l*$^{z/z}$ ES cells cultured for 48 hours under at ambient O_2 or 1% O_2.

*Statistical significance was determined using two-way ANOVA with Dunnett's multiple comparisons tests (α=0.05). *, $p<0.05$. **, $p<0.01$. ***, $p<0.001$.

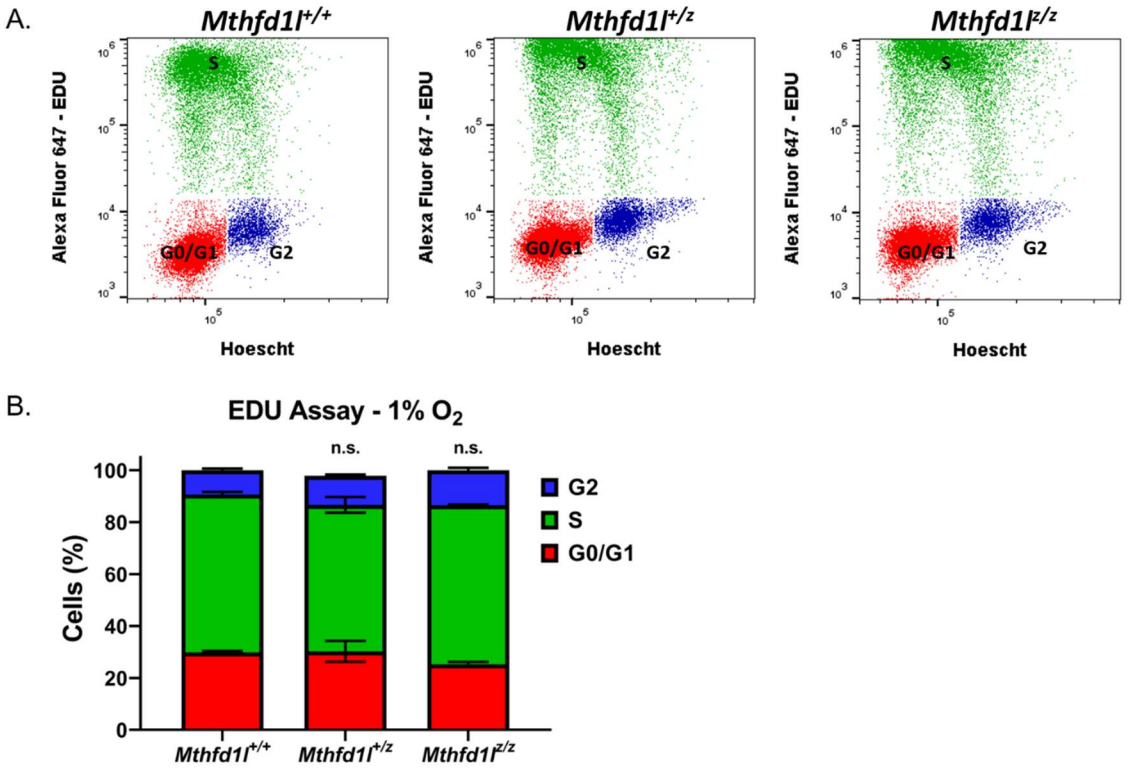

Figure 3.4 Effect of Hypoxia on Proliferation of *Mthfd1l*$^{z/z}$ Embryonic Stem Cells

A) Concatenated scatter plots of flow cytometry data from EdU proliferation assays conducted in *Mthfd1l*$^{+/+}$, *Mthfd1l*$^{+/z}$, and *Mthfd1l*$^{z/z}$ ES cells cultured for 24 hours at 1% O_2. The gated cell populations shown in red, green, and blue represent cells in G0/G1, S-phase, and G2 of the cell cycle, respectively.

B) Stacked column chart showing the average (n=3) proportions of cells in each phase of the cell cycle based on EdU incorporation.

*Statistical significance was determined using two-way ANOVA with Dunnett's multiple comparisons tests (α=0.05). *, $p<0.05$. **, $p<0.01$. ***, $p<0.001$. ****, $p<0.0001$.

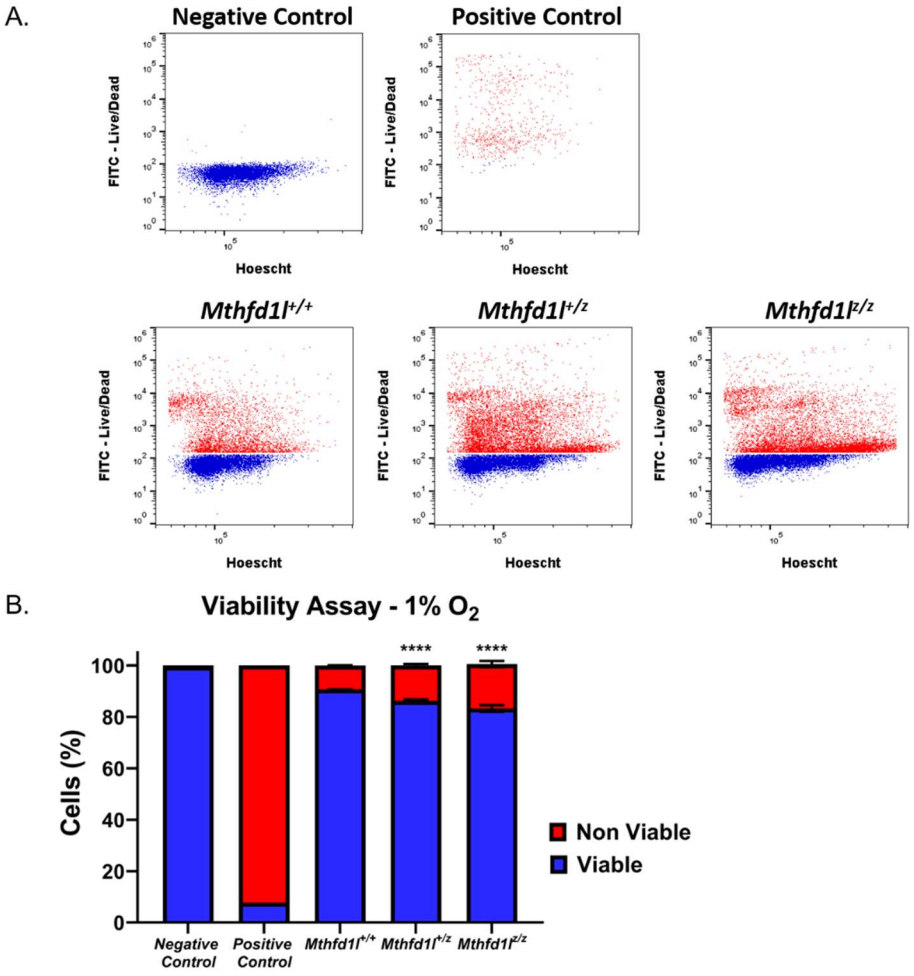

Figure 3.5 Effect of Hypoxia on Viability of *Mthfd1l*$^{z/z}$ Embryonic Stem Cells

A) Concatenated scatter plots of flow cytometry data from viability assays conducted in *Mthfd1l*$^{+/+}$, *Mthfd1l*$^{+/z}$, and *Mthfd1l*$^{z/z}$ ES cells cultured for 24 hours at 1% O_2. The gated cell populations shown in blue and red represent viable and non-viable cells respectively as confirmed by positive and negative controls.

B) Stacked column chart showing the average (n=3) proportions of viable and non-viable cells based on FITC signal.

*Statistical significance was determined using two-way ANOVA with Dunnett's multiple comparisons tests (α=0.05). *, p<0.05. **, p<0.01. ***, p<0.001. ****, p<0.0001.

3.3.4 Changes in Gene Expression Suggest Metabolic Switch in Mitochondrial 10-formyl-THF Utilization in Mouse Embryos Between E8.5 and E10.5

Since the window of mouse embryo development between E8.5 and E10.5 is a time of drastic changes, both in terms of vascularization and neural tube closure, we decided to look at expression of mitochondrial and cytosolic OCM genes during this timeframe. Of the genes examined, six were differentially expressed between E8.5 and E10.5 (Figure 3.6). Downregulation of the folate receptor, *Folr1*, after neural tube closure was already known (Piedrahita et al. 1999), and thus serves as a validation of the results. Notably, *Shmt2* expression decreased between E8.5 and E10.5, but *Shmt1* expression did not. This may suggest a reduction in mitochondrial serine catabolism. More interestingly, we observed decreased expression of *Mthfd1l* and *Mthfd1*, consistent with results published in Shin et al. (2014). Decreased expression of these genes occurred concomitant with substantial increases in *Aldh1l1* and *Aldh1l2* expression. The diametrical changes in gene expression between these two classes of enzymes with a common substrate suggest a change in embryonic utilization of 10-formyl-THF between E8.5 and E10.5. MTHFD1L and MTHFD1 direct interconversion of formate and 10-formyl-THF between the mitochondria and cytosol, allowing for direction of 1-C units from 10-formyl-THF into continued utilization by OCM; but ALDH1L1 and ALDH1l2, both catalyze the irreversible oxidation of the formyl group to CO_2 (see Figure 3.1). This result taken with decreased expression of *Shmt2* suggests mouse embryos may decrease mitochondrial OCM activity after neural tube closure at the levels of serine catabolism and formate synthesis, at least in terms of gene expression.

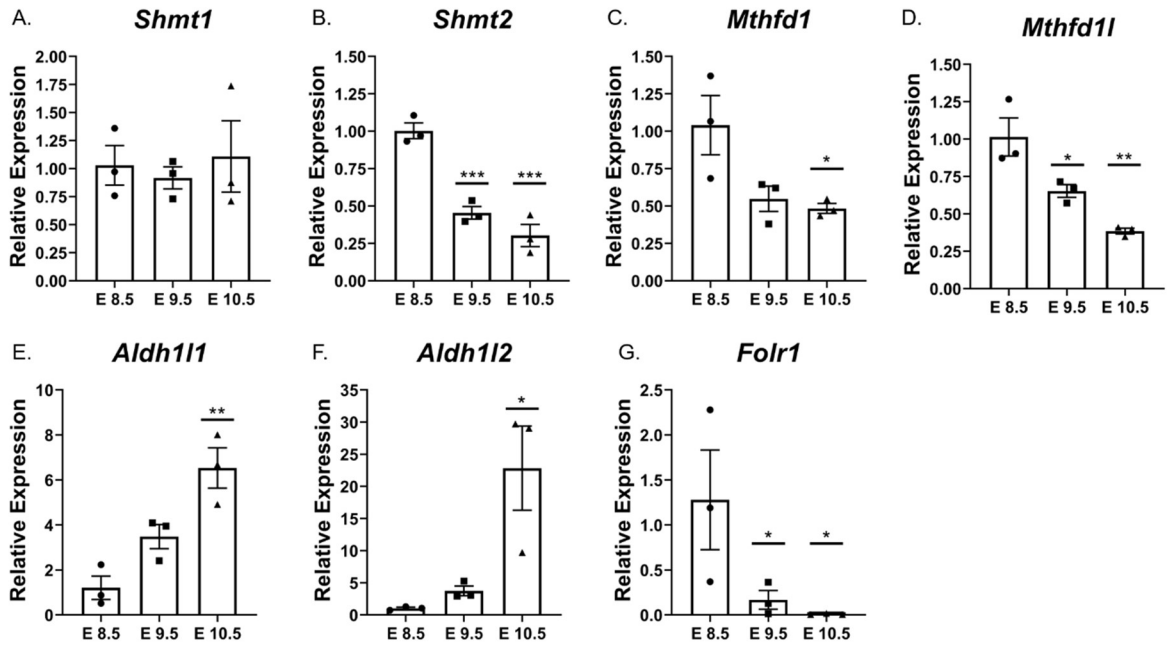

Figure 3.6 Expression of One-carbon Metabolism Genes in C57 Mouse Embryos Between E8.5 and E10.5

Gene expression of OCM genes in C57/BL6 mouse embryos at E8.5, E9.5, and E10.5.

*Statistical significance was determined using one-way ANOVA with Dunnett's multiple comparisons tests (α=0.05). *, p<0.05. **, p<0.01. ***, p<0.001. ****, p<0.0001.

3.4 DISCUSSION

The growth curve analysis in ES cells lacking *Mthfd1l* demonstrates that this gene is essential for ES cell growth in a manner dependent on purine and pyrimidine metabolism. It is notable that no proliferation defects were observed in *Mthfd1l* knockout cells on standard 2i media. Modifying the media to remove Ham's F12, which contains thymidine and hypoxanthine induced an apparent deficiency in knockout cells compared to wildtype. This suggested that thymidine and hypoxanthine would be sufficient to restore normal proliferation in knockout cells, likely because thymidine could be used directly in pyrimidine metabolism, and hypoxanthine could promote purine synthesis via nucleotide salvage. This hypothesis was confirmed when co-supplementation of hypoxanthine and thymidine restored growth in knockout ES cells back to wildtype levels. This raises the question as to whether hypoxanthine and thymidine supplementation, or supplementation with other nucleotides or nucleobases can rescue NTDs in *Mthfd1l* knockout mouse embryos. It was previously demonstrated that supplementation of nucleotides could rescue NTDs in the FA-resistant *Curly Tail* mice (Leung et al. 2013). In *Mthfd1l* knockout mice, maternal supplementation with a "cocktail" of various nucleotides was not capable of preventing any of the observed phenotypes, nor was thymidine supplementation (Jessica Momb, The University of Texas at Austin, personal communication). However, 20mg/kg/d of hypoxanthine did prevent up to 20% of NTDs in the *Mthfd1l* knockouts (Jessica Momb, The University of Texas at Austin, personal communication). However, Dr. Momb did not test tandem supplementation with hypoxanthine and thymidine as we tested here in the ES cell experiment. Thus, the efficacy of these two compounds as co-supplements for NTD prevention remains an open question in this model and a project for future exploration. Formate supplementation also rescued growth defects observed in *Mthfd1l* knockout ES cells as expected, although not as efficiently. More interestingly, formate inhibited growth

in wildtype cells, which is consistent with observations in Ducker et al. (2016) where formate supplementation impaired growth in mitochondrial OCM mutant HEK-293T cells. Bryant et al. (2018) found that formate and co-supplemented hypoxanthine and thymidine were effective at rescuing growth defects in *Mthfd1l*$^{z/z}$ MEFs, supporting our observations in ES cells, while thymidine supplementation on its own did not rescue growth deficiency in *Mthfd1l*$^{z/z}$ MEFs. Bryant et al. (2018) also performed metabolic analysis of *Mthfd1l*$^{z/z}$ embryos with and without calcium formate supplementation. They found that formate supplementation restored metabolic imbalance in energy metabolism and a few amino acid pathways. However, it appeared general 1-C metabolic pathways such as methane metabolism and serine/glycine/threonine metabolism were still significantly perturbed. For example, formate did not restore relative abundances of glycine (which was diminished in *Mthfd1l*$^{z/z}$ embryos) and serine (which accumulated in *Mthfd1l*$^{z/z}$ embryos). Thus, while formate may rescue cytosolic OCM and its constituent functions, the defect in mitochondrial OCM remains. We therefore hypothesized that ES cells lacking *Mthfd1l* may display other phenotypes under conditions of mitochondrial stress, such as hypoxia.

The developing mammalian embryo is a hypoxic environment (Chen, Fujinaga, and Giaccia 1999; Burton and Jaunaiux 2001; Dunwoodie 2009), particularly around the time of neural tube closure as hypoxia-dependent vascularization of the embryo occurs around that time, at least in the mouse (Walls et al. 2008). While hypoxia may be a normal, and possibly even required aspect of development, hypoxia does require unique metabolic adaptations that are necessary to maintain cellular redox balance under hypoxic conditions (Miyata, Takizawa, and van Ypersele de Strihou 2011). Recent research in cancer metabolism suggests mitochondrial OCM may play a role in cellular adaptation to hypoxia, supporting tumor growth and survival (Martinez-Reyes and Chandel 2014). Ye et al. (2014) found that in hypoxia-resistant, myc-amplified neuroblastoma cells, there was

significantly enhanced expression of SHMT2, which was induced by hypoxia-inducible factor (HIF1α). Ablation of this SHMT2 activity resulted in hypoxia-sensitivity and oxidative stress. Moreover, MTHFD1L itself appears to be implicated as hypoxia-sensitive in the literature. The prokaryotic equivalent enzyme that performs 10-formyl-THF synthetase activity, Fhs, is more commonly found in anaerobic bacteria and facultative anaerobes, but does not appear to be required for aerobic species (Sah et al. 2015). Moreover, it was found that transformation with the *fhs* gene conferred a metabolic advantage to *Escherichia coli* under anaerobic conditions (Sah et al. 2015). Thus, we hypothesized that ES cells lacking *Mthfd1l* may also exhibit hypoxia sensitivity.

While *Mthfd1l* knockout cells exhibited no observable phenotypes at ambient O_2 so long as they received hypoxanthine and thymidine supplemented media, cell survival was impacted in a genotype-dependent manner under hypoxic conditions (1% O_2). We also ruled out the possibility that this phenotype was associated with *Mthfd1l*'s role in formate synthesis and nucleotide metabolism, since the knockout cells did not appear to be proliferating slower under hypoxia compared to wildtype cells but were in fact less viable. Recently, it was shown that knockdown of *MTHDF1L* in human tumor squamous cell carcinoma resulted in reduced NADPH and increased reactive oxygen species under stress conditions, including hypoxia and glucose deprivation (Li et al. 2019). Our data also support a role for MTHFD1L in maintaining cellular redox homeostasis under hypoxic stress and potentially other forms of oxidative stress. Work on mitochondrial OCM mutant mouse models have thus far focused on mitochondrial OCM as a source for 1-C units involved in purine, thymidine, and methionine metabolism. However, the role of mitochondrial OCM in redox homeostasis and its implications for NTC have been largely ignored. While that is understandable given how difficult redox experiments can be to control, especially *in vivo*, a developing body of evidence supports that mitochondrial

OCM's redox properties may be critical to understanding this pathway's role in neural tube development.

Finally, the changes in OCM gene expression observed between E8.5 and E10.5 in mouse embryos suggests that embryonic utilization of 10-formyl-THF may shift during this timeframe from favoring mitochondrial formate synthesis at E8.5, to aldehyde dehydrogenase activity at E10.5. While these data may be considered preliminary, since more evidence beyond gene expression would be needed to confirm this hypothesis, there are two possible explanations as to why this may be a beneficial metabolic switch for embryos. First, the enzymatic activity of ALDH1L1 and ALDH1L2 catalyzes the irreversible oxidation of the formyl group from 10-formyl-THF to CO_2, regenerating THF in the process. This reaction utilizes $NADP^+$ as a cofactor and yields one molecule of NADPH. Thus, this switch may reflect the embryo's metabolic requirements for reducing equivalents during the transition from predominantly anaerobic to aerobic metabolism. Furthermore, Ducker et al. (2016) demonstrated that in cell culture, mitochondrial OCM flux exceeds demand for cytosolic 1-C units, and that the rate of mitochondrial formate excretion was closely linked to expression of mitochondrial OCM genes, specifically *MTHFD2*, *SHMT2*, and *MTHFD1L*. While these observations have not been confirmed *in vivo*, it seems a reasonable hypothesis that embryonic demand for 1-C units may decrease after NTC. If that is the case, mitochondrial OCM continuing to produce more formate beyond 1-C demand may lead to accumulation of formate, which can be toxic in the 5-30mM range via inhibition of cytochrome c oxidase (Nicholls 1975; Pietzke, Meiser, and Vazquez 2020). Thus, disposing of 1-C units by shuttling them into complete oxidation by ALDH1L1 and ALDH1L2 may be a metabolic strategy to cope with decreased 1-C demand. Pursuing this hypothesis in future experiments may yield insight into the role of mitochondrial OCM both during NTC and at other stages of development.

PART TWO: MECHANISMS OF NEURAL TUBE DEFECTS CAUSED BY PHARMACEUTICAL EXPOSURE TO VALPROIC ACID OR DOLUTEGRAVIR

Chapter 4: Identifying Predictive Biomarkers of Valproic Acid Sensitivity in Neural Tube Defect-affected and Unaffected Murine Embryos

4.1 INTRODUCTION

The teratogenic mechanism by which valproic acid (VPA) causes neural tube defects (NTDs) and other congenital anomalies remains an unanswered question. Preventing VPA-induced NTDs (or other AED-induced defects for that matter) while still enabling women of childbearing potential to safely benefit from the therapeutic properties of these drugs requires us to understand the underlying mechanism of action. That said, even the therapeutic mechanism of VPA is debatable (Lloyd 2013). Enhancing γ-aminobutyric acid (GABA) concentrations within the brain (Johannessen and Johannessen 2003), and reduction of excitatory neurotransmission through inhibition of voltage gated sodium channels (Pugsley et al. 1999; Large et al. 2009) or reduction in synaptic aspartate levels (Morland, Nordengen, and Gundersen 2012) have all been proposed. Ultimately, several undefined mechanisms may contribute to VPA's anticonvulsant effects (Lloyd 2013).

Several potential mechanisms of VPA teratogenesis are being researched. Physiologically, around 97% of the drug is metabolized in the liver through uridine diphosphate glucuronidation, β-oxidation, and cytochrome P450 activity (Sankar 2007). It appears that VPA is asymmetrically distributed across the placenta, with higher concentrations of VPA accumulating in the embryo than in maternal blood, possibly resulting in a toxic dose for the embryo despite a conventionally safe dose for the mother (Vajda 2012). Even managing maternal dose can be tricky during pregnancy, since plasma concentrations of VPA may decrease by up to 50% (Sabers and Tomson 2009; Wlodarczyk et al. 2012). It has also been demonstrated that VPA functions as a histone-deacetylase

(HDAC) inhibitor, which suggests VPA may disrupt epigenetic regulation of embryonic gene expression (Lloyd 2013). Other evidence indicates VPA may cause oxidative stress. For example, hepatic metabolism of VPA results in several reactive compounds including 4-ene VPA, which can undergo β-oxidation to form the reactive species (E)-2,4-diene VPA which competes with the glutathione redox cycle by oxidizing NADPH (Liu et al. 2009). It has also been suggested that VPA may antagonize the activities of folate and OCM by directly antagonizing the folate receptor (Fathe, Palacios, and Finnell 2014) or through antagonism of DHFR, thus depleting cellular folate pools (Hsieh et al. 2012). Regardless, given the extensive metabolic activity of VPA and its constituent metabolites, a metabolism-dependent mechanism of VPA sensitivity is highly plausible.

Moreover, there is undoubtedly an underlying genetic component predisposing to AED risk. Studies in mice demonstrate that VPA sensitivity is strain-dependent, and that this sensitivity can be mapped to a specific genetic locus in Swiss-Vancouver (SWV) mice (Finnell et al. 1988; Finnell et al. 1997; Beck 1999; Finnell et al. 2000; Beck 2001; Lundberg et al. 2004). Even within the same litter, not all VPA-exposed embryos develop NTDs. For example, DBA/2J mice appear entirely resistant to VPA, while about 20% of LM/BC and C57/BL6 embryos develop NTDs. SWV mouse embryos appear even more susceptible displaying a 35% occurrence of NTDs after VPA exposure (Finnell et al. 1988; Lundberg et al. 2004). Regardless, elucidating the underlying genetic or metabolic factors contributing to risk for valproate-affected pregnancies may lead to development of non-teratogenic anticonvulsants, novel prevention strategies, or more targeted methods for managing epileptic pregnancies.

Previous metabolomic studies have been performed in mice comparing VPA-treated and untreated embryos (Akimova et al. 2017). However, as mentioned, less than half of exposed embryos actually develop NTDs; thus, these studies did not adequately

discern between metabolic alterations caused by VPA exposure and metabolic alterations associated with VPA sensitivity. No comparison has yet been made between VPA-treated embryos that developed NTDs and those that did not. Using tandem liquid chromatography-mass spectrometry (LC-MS), we performed an untargeted metabolomic profiling of murine C57/BL6 embryos (a moderately sensitive strain) exposed *in utero* to VPA on gestational day E8.5 and compared metabolic alterations between VPA-affected (developed an NTD) and unaffected embryos at gestational days E9.5 (26 hours post exposure), and E10.5 (50 hours post exposure). Moreover, by observing metabolic variation between untreated control embryos and VPA-treated embryos on E8.5 (two hours post exposure and prior to neural tube closure) we identified predictive biomarkers associated with VPA exposure that may be determinative of sensitivity to VPA-induced NTDs.

4.2 Materials and Methods

4.2.1 VPA Treatment and Embryo Collection

C57/BL6 mice were obtained from BCM's Center for Comparative Medicine and were housed on 12-hour light/dark cycles with standard chow (5V5R, Lab Supply) and maintained according to protocols approved by the Institutional Animal Care and Use Committee (IACUC) at BCM. Timed crosses were performed, and copulation was confirmed by morning checks for vaginal plugs. Pregnancy was confirmed by comparing dam weight on the date the plug was observed to weight measured on gestational day E8.5. Pregnant dams were euthanized using CO_2 asphyxiation followed by cervical dislocation. At 11 AM on gestational day E8.5, 9 pregnant dams received an intraperitoneal injection of a 600mg/kg dose of VPA dissolved in PBS. 9 pregnant control dams did not receive the injection. Embryos were collected from three dams of each treatment group on E8.5 at 1

PM, two hours post-injection. Embryos were also collected from three dams of each treatment group 26 hours post-injection (E9.5) and 50 hours post-injection (E10.5). E 9.5 and E10.5 embryos were scored as being VPA-affected if they presented with an open neural tube, and unaffected if they presented with a closed neural tube and otherwise normal development. Somite number was counted at each timepoint. E8.5 embryos could not be scored as the process of neural tube closure is still ongoing at that time. 22 VPA-treated embryos were collected at E8.5. 24 VPA-treated embryos were collected at E9.5, of which 6 were scored as affected (25%). 26 VPA-treated embryos were collected at E10.5, of which 5 were scored as affected (19.2%).

Upon dissection, the embryos were washed once in sterile milli-Q water and snap frozen in liquid nitrogen. All VPA-treated embryos and 8 untreated control embryos from each timepoint were selected for metabolomics. Metabolites were extracted in a 1:1 aqueous methanol solution with 10mM chloroform, which was then evaporated using a refrigerated speed vac at -5ºC.

4.2.2 Liquid Chromatography-Mass Spectrometry (LC-MS)

An untargeted metabolomic analysis of polar fraction extracts was performed on a Hybrid quadrupole-Orbitrap mass spectrometer (Q Exactive, Thermo Scientific, Waltham, MA, USA) hyphenated with a Thermo Scientific Accela 1250 UHPLC system via electrospray ionization source, simultaneously operating in positive/negative polarity switching ionization mode. To ensure consistency in data acquisition over the entire batch, quality control (QC) samples, prepared for each group and pool of all samples, were run every 8 samples.

4.2.3 Data Analysis and Statistics

All raw MS datasets were processed using Sieve 2.2 (Thermo Fisher Scientific) and features with a coefficient of variation (CV) lower than 25% in the QC samples were considered for further analysis. Peaks were scaled and normalized according to a PQN algorithm (Dieterle et al. 2006) and features were then mined against an in house database of accurate masses and retention times generated in the Stefano Tiziani laboratory (The University of Texas at Austin, Dell Medical School) through the IROA300 (Lu, Solmonson, et al. 2017) Mass Spectrometry Metabolite Library of Standards (MSMLS; IROA Technologies, Bolton, MA) using the same experimental conditions used for data acquisition of this dataset. In addition, databases of accurate masses taken from the KEGG database and the Human Metabolome database were also mined. Univariate (student's t test) and multivariate (principal component analysis) statistical data analyses were performed using statistics and bioinformatics toolboxes for MATLAB as described in the following publications: (Lodi et al. 2011; Tiziani et al. 2011; Lodi et al. 2013; Tiziani et al. 2013; Kang et al. 2014; Sweeney et al. 2016; Lodi et al. 2017; Lu, Salmoson, et al. 2017), or in Microsoft Excel with Analyze-It statistical package. Statistical significance was set at $p<0.05$. False discovery rate (FDR) was calculated using the Benjamini-Hochberg method (Benjamini and Hochberg 1995). Pathway analyses were performed using MetaboAnalyst (McGill University, Montreal, Canada).

4.3 RESULTS

4.3.1 Comparison of Affected and Unaffected Embryos at E9.5 and E10.5

All putatively identified metabolites (based on exact mass) and confirmed MS peaks were plotted in heat maps following hierarchical clustering (Figures 4.1 and 4.2). Major metabolic alterations were observed between gestational days E8.5 and E10.5 for

control as well as VPA-treated embryos (See Appendix II for a list of significantly altered metabolites between E8.5, E9.5, and E10.5 in VPA-treated embryos). To better visualize the extent of the metabolic differences between the control and treated embryos at each gestational day, principal component analysis (PCA) was performed using all putatively identified MS peaks for all embryo samples and different groups (control and treated) separately (Figure 4.3). It can be clearly seen in Figure 4.3A that control and treated embryo groups at each gestational day overlap with one another indicating metabolic similarity among them, whereas clear separation between each gestational day of the control and treated embryo groups indicates significant metabolic changes between different embryonic developmental stages. That said, overall metabolism of VPA-affected and unaffected embryos was remarkably similar (Figure 4.3B).

A more detailed analysis of metabolic alterations in VPA treated embryos at gestational day E10.5 (compared to E8.5) indicated accumulation of citrate cycle metabolites (citrate, fumarate and malate) as well as hydroxyglutarate. Significant effects on glycolysis and the pentose phosphate pathway (PPP) were observed with accumulation of glucose, fructose-1,6-biphosphate, glycerol-2-phosphate, phosphoenolpyruvate, nucleotides (mono-, di-, and tri-phosphates), and downregulation of ribose-5-phosphate, glycerate, inosine, xanthine, hypoxanthine, uracil, uric acid, uridine, cytidine and thymidine. Similarly, accumulation of glycine, serine and methionine suggests alteration of one-carbon metabolism and nucleotide biosynthesis. Upregulation of NAD^+, NADH, tryptophan, kynurenine and hydroxykynurenine indicates modulation of *de novo* NAD^+ biosynthesis (Appendix II).

In addition, we performed an in-depth analysis of the metabolic differences between VPA-affected and unaffected embryos at gestational days E9.5 and E10.5. As mentioned earlier, the PCA plot demonstrated little to no variation between E9.5 and E10.5

embryos classified as affected or unaffected (Figure 4.3B). Confirming this assessment, univariate statistical analyses (student's t tests) uncovered very few metabolites significantly altered between VPA-affected and unaffected embryos at these two timepoints. There was significant downregulation of the nucleotide diphosphate, adenosine diphosphate, the nucleotide-sugar, uridine 5-diphosphogalactose, the pentose-phosphate intermediate, ribose 5-phosphate, and the glycolysis pathway intermediates, phosphoenolpyruvic acid and fructose-1,6-biphosphate (Figure 4.4). We also found significantly decreased abundance of methionine at E10.5 concomitant with a significant increase in 2-ketobutyric acid, a metabolite produced during conversion of cystathionine to cysteine (Figure 4.4G and 4.4H). These data suggest persistent disruption of cysteine and methionine metabolism in VPA-affected embryos, even as late as 50 hours post exposure.

4.3.2 Metabolic Effects of VPA in E8.5 Embryos

Previous metabolomic analyses of VPA-treated embryos only examined metabolic alterations at E9.5 when VPA-induced defects become apparent (Akimova et al. 2017). However, in our analysis, we noticed the greatest variation between VPA-treated and untreated embryos was observable at E8.5 (two hours post-injection). Thus, it appears VPA induces large-scale metabolic changes very quickly, within a few hours of exposure, and analyzing metabolic alterations at that timepoint would be more informative. We therefore compared metabolism at E8.5 between VPA-treated embryos and untreated controls.

Seventy-five metabolites of significantly differential abundance were identified in E8.5 VPA-treated embryos after adjusting for false discovery rate (FDR) (Appendix III). Pathway analysis revealed that pyrimidine and purine metabolism were the most overrepresented pathways, with 10 and 12 altered metabolites respectively (Table 4.1).

Purines and pyrimidines in their nucleobase or glycosylated nucleoside forms were significantly upregulated, while their mono-, di-, and tri-phosphate nucleotide analogs were significantly downregulated (Appendix III), suggesting impairment of nucleoside kinase activity, which are ATP-dependent enzymes. There were also a significant number of dysregulated amino acids, explaining enrichment of the pathway aminoacyl-tRNA biosynthesis. There were six metabolites of differential abundance representing cysteine and methionine metabolism (Table 4.1), including upregulation of S-adenosyl-homocysteine and methionine, and downregulation of taurine, hypotaurine, and oxidized glutathione (Appendix III), suggesting impairment of homocysteine and cysteine catabolism via the transsulferation pathway.

4.3.3 Predictive Biomarkers of VPA Sensitivity in E8.5 Embryos

Scoring E8.5 embryos as either VPA-affected or unaffected through observation of overt phenotypes is not possible since NTDs cannot be confirmed prior to neural tube closure, which occurs between E9.0 and E9.5 in mouse embryos (Greene and Copp 2009). However, there were disappointingly few metabolites differentiating VPA-affected and unaffected embryos at E9.5 and E10.5. Since E8.5 is a more developmentally critical timepoint to assess metabolic influence on neural tube closure, and since VPA seemed to induce the largest metabolic alterations at that time, we sought to identify metabolites at E8.5 that might be predictive of VPA sensitivity.

To address this challenge, we performed a multivariate analysis of all MS peaks for VPA-treated and untreated embryos at E8.5 only (Figure 4.5). We noticed that the greatest stratification between control embryos (n=8) and treated embryos (n=22) occurred along principal component 2 (PC2). While their ranges overlapped, with approximately half of treated embryos clustering within the range of the controls, the other half clustered outside

that range. This alone, however, cannot be predictive of VPA-sensitivity since NTD-affected embryos only accounted for 19.2% and 25% of E10.5 and E9.5 embryos, respectively. Thus, using the standard deviation (σ) of the controls, we looked for a number of standard deviations along PC2 outside the range of the control embryos that isolated approximately that proportion of treated embryos (Table 4.2). We found that 5 treated embryos (22.73%) clustered more than five standard deviations from the range of the controls (Figure 4.5 and Table 4.2). Assuming that embryos with the greatest metabolic deviation from controls are more sensitive to VPA, we categorized these embryos as *likely affected*. Treated E8.5 embryos that clustered within five standard deviations of the control range were categorized as *likely unaffected*. Hierarchical clustering of confirmed metabolite peaks in E8.5 embryos demonstrated that the five *likely affected* embryos clustered together with a distinguished metabolic signature relative to the other treated embryos and the controls (Figure 4.6). Only one other embryo classified as *likely unaffected* appeared hierarchically related to these *likely affected* embryos and we noted that this embryo was the next closest in the PCA (Figure 4.5) to the *likely affected* embryos.

We next compared MS peaks between the *likely affected* and *likely unaffected* E8.5 embryos and identified 31 metabolites of significantly differential abundance after adjusting for FDR (Appendix IV). Pathway analysis showed that purine and pyrimidine metabolism were not overrepresented, as was the case when comparing all VPA-treated embryos with controls. Instead, glyoxylate/dicarboxylate metabolism and the mitochondrial citrate cycle were significantly affected (Table 4.3). The metabolites of differential abundance in these pathways were oxaloacetate, citrate/isocitrate, succinate, fumarate, and D-glyceric acid (Figure 4.7). Each of these metabolites was found to be significantly reduced in *likely affected* embryos compared to *likely unaffected* embryos; but notably, only oxaloacetate was significantly reduced in *likely unaffected* embryos

compared to untreated controls. Thus, impairment of the other citrate cycle intermediates may be uniquely predictive markers of VPA sensitivity.

While cysteine and methionine metabolism were not significantly overrepresented in the pathway analysis, we did observe a notable number of metabolites with differential abundance representing this pathway (Appendix IV). These metabolites included methionine and serine, which were upregulated, and the downregulated metabolites, taurine and 2-sulfinoalanine (also known as L-cysteine sulfinic acid) (Figure 4.8). Serine is required for conversion of homocysteine to cystathionine while 2-sulfinoalanine is an intermediate in the catabolism of cysteine to taurine. Notably, these two metabolites were dysregulated in *likely affected* embryos, but not *likely unaffected* embryos relative to untreated controls.

Since metabolites that are significantly altered in *likely affected* embryos but not in *likely unaffected* embryos are arguably more predictive of VPA sensitivity, we sought to identify all metabolites that were of differential abundance in *likely affected* embryos compared to *likely unaffected* embryos, but not in the *likely unaffected* group compared to untreated controls. The goal in this case was to differentiate between metabolic alterations associated with VPA exposure and those associated with VPA sensitivity. We identified 14 metabolites that met these criteria (Table 4.4). Notably, all of the upregulated metabolites are amino acids, suggesting accumulation of these compounds possibly through impaired catabolism. This hypothesis is supported when examining the downregulated metabolites, which predominantly appear to be products of catabolism or intermediates of catabolic pathways. Notably, among these downregulated metabolites are the citrate cycle intermediates, succinate, fumarate, and citrate/isocitrate. Moreover, the catabolic “waste” compounds, urate and its oxidation product allantoin, were two of the most significantly depleted metabolites.

Arginine was the most significantly accumulated metabolite in *likely affected* embryos (Table 4.4). Interestingly, arginine abundance was highly distinguishing between *likely affected* embryos and both untreated controls and *likely unaffected* embryos (Figure 4.9A). It is notable that the only embryo from the *likely unaffected* group that falls within the range of the *likely affected* embryos in terms of arginine abundance was the one that was hierarchically related to the *likely affected* group in Figure 4.6. Thus, it appears accumulation of arginine is the most predictive biomarker indicative of VPA sensitivity, and the strongest component associated with the distinguishing metabolic signature of *likely affected* embryos as determined by hierarchical clustering.

Arginine is converted to citrulline either indirectly via the urea cycle or directly through the activity of nitric oxide synthase (NOS) enzymes. NOS catalyzes the oxygen dependent conversion of arginine to citrulline, producing nitric oxide (NO) as a byproduct. Citrulline was not identified in our analysis looking for markers specifically associated with VPA sensitivity, but only because the metabolite was excluded after correcting for FDR. When we examined the MS peaks for citrulline, we found that the metabolite was significantly reduced in *likely affected* embryos compared to both *likely unaffected* embryos and untreated controls (Figure 4.9B). Since interconversion of arginine and citrulline is performed by NOS and may therefore be a readout of NO levels, we looked at the arginine/citrulline ratio for each individual embryo. We found that the arginine/citrulline ratio was increased nearly four-fold in *likely affected* embryos compared to the *likely unaffected* group, and nearly 10-fold compared to untreated controls (Figure 4.9C). Comparatively, embryos classified as *likely unaffected* only showed a 2.5-fold increase compared to controls. These data would suggest VPA impairs NOS enzyme activity and subsequent NO production (Figure 4.9D), and that the severity of this impairment may be predictive of VPA sensitivity.

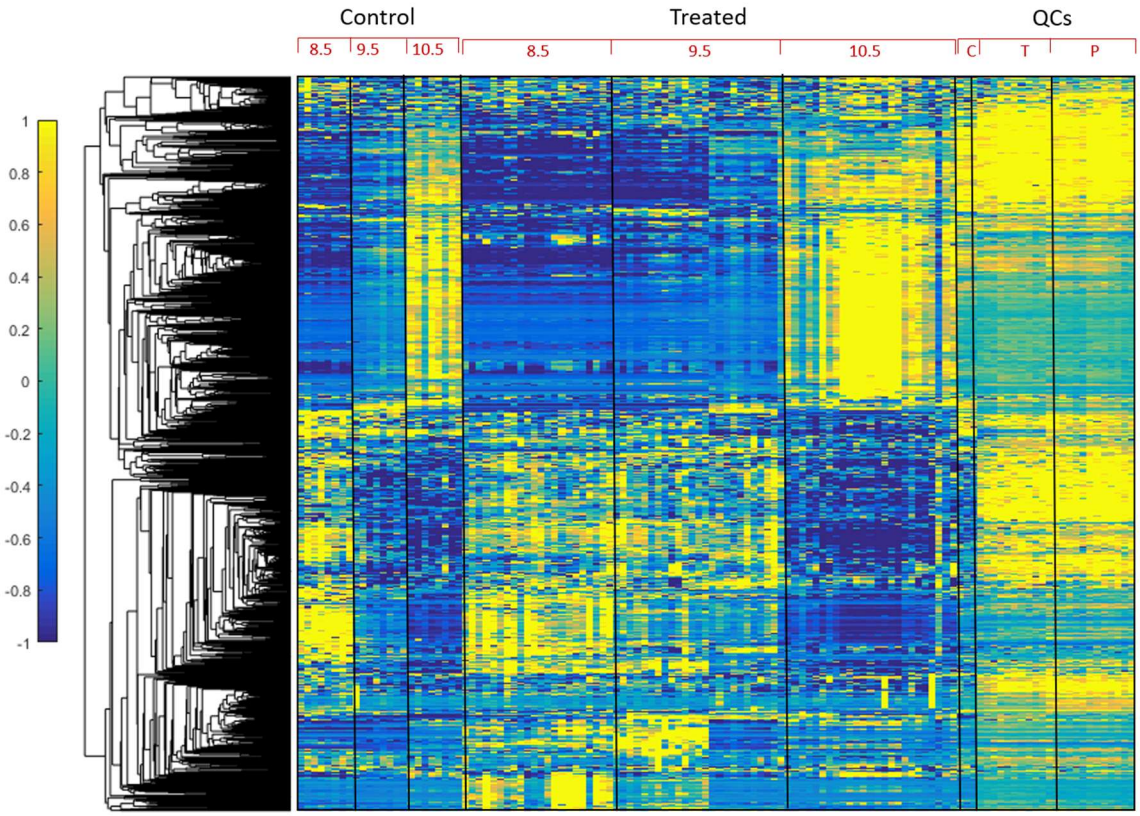

Figure 4.1 Hierarchical Clustering of Putatively Identified Metabolites in Control and VPA-treated Embryos

Untargeted hierarchical clustering of all putatively identified MS peaks in VPA-treated and control embryos at E8.5, E9.5, and E10.5, and in QC samples. Clustering was performed by Pearson correlation using complete linkage

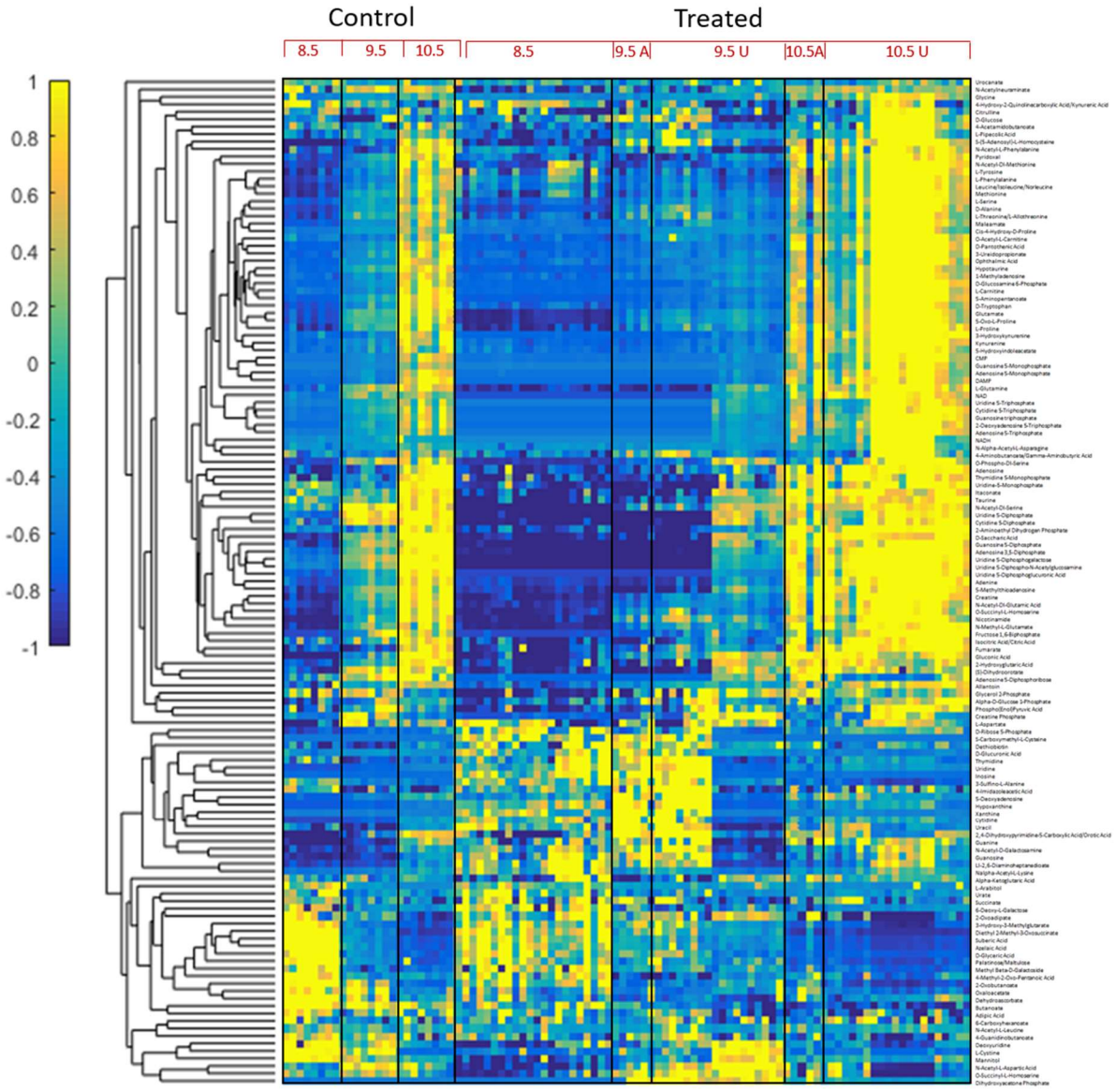

Figure 4.2 Hierarchical Clustering of Confirmed Metabolites in Control and VPA-treated Embryos

Untargeted hierarchical clustering of all confirmed MS peaks in VPA-treated and control embryos at E8.5, E9.5, and E10.5. Clustering was performed by Pearson correlation using complete linkage.

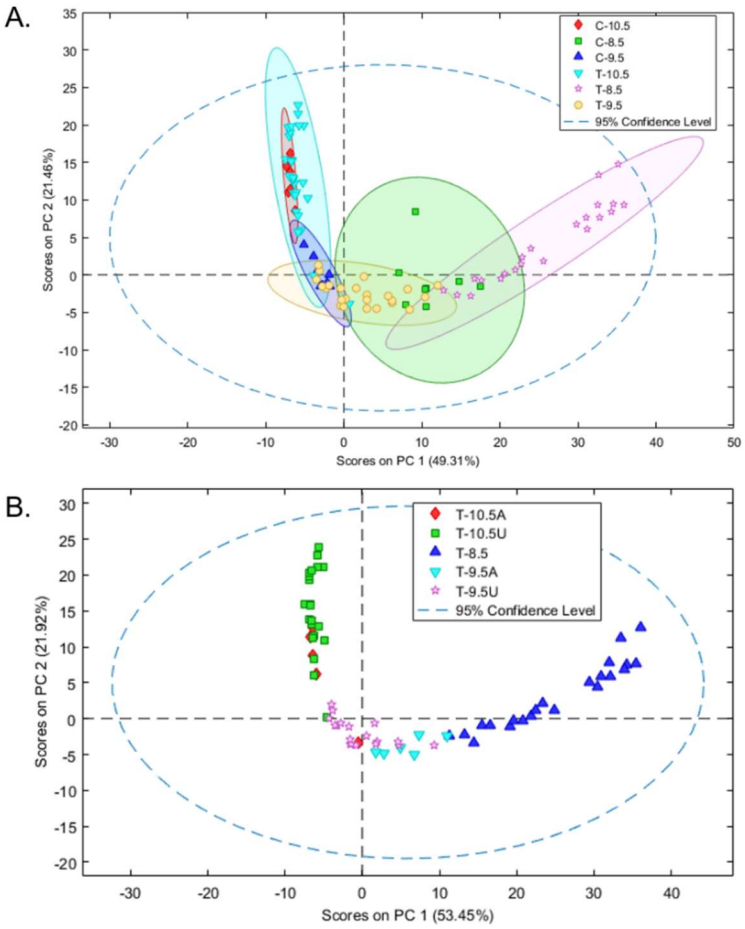

Figure 4.3 Principal Component Analysis of All Confirmed Peaks in Control and VPA-treated Embryos

A) Principal component analysis of all confirmed MS peaks comparing control (C) and VPA-treated (T) embryos at each time point (E8.5, E9.5, and E10.5). The largest variation observed between control and VPA-exposed embryos occurred at E8.5, two hours post-injection.

B) Principal component analysis of all confirmed MS peaks comparing affected (A) and unaffected embryos (U) at each timepoint (E8.5, E9.5, and E10.5) in VPA-treated embryos (T). Notably, there was little separation between affected and unaffected embryos at E9.5 and E10.5.

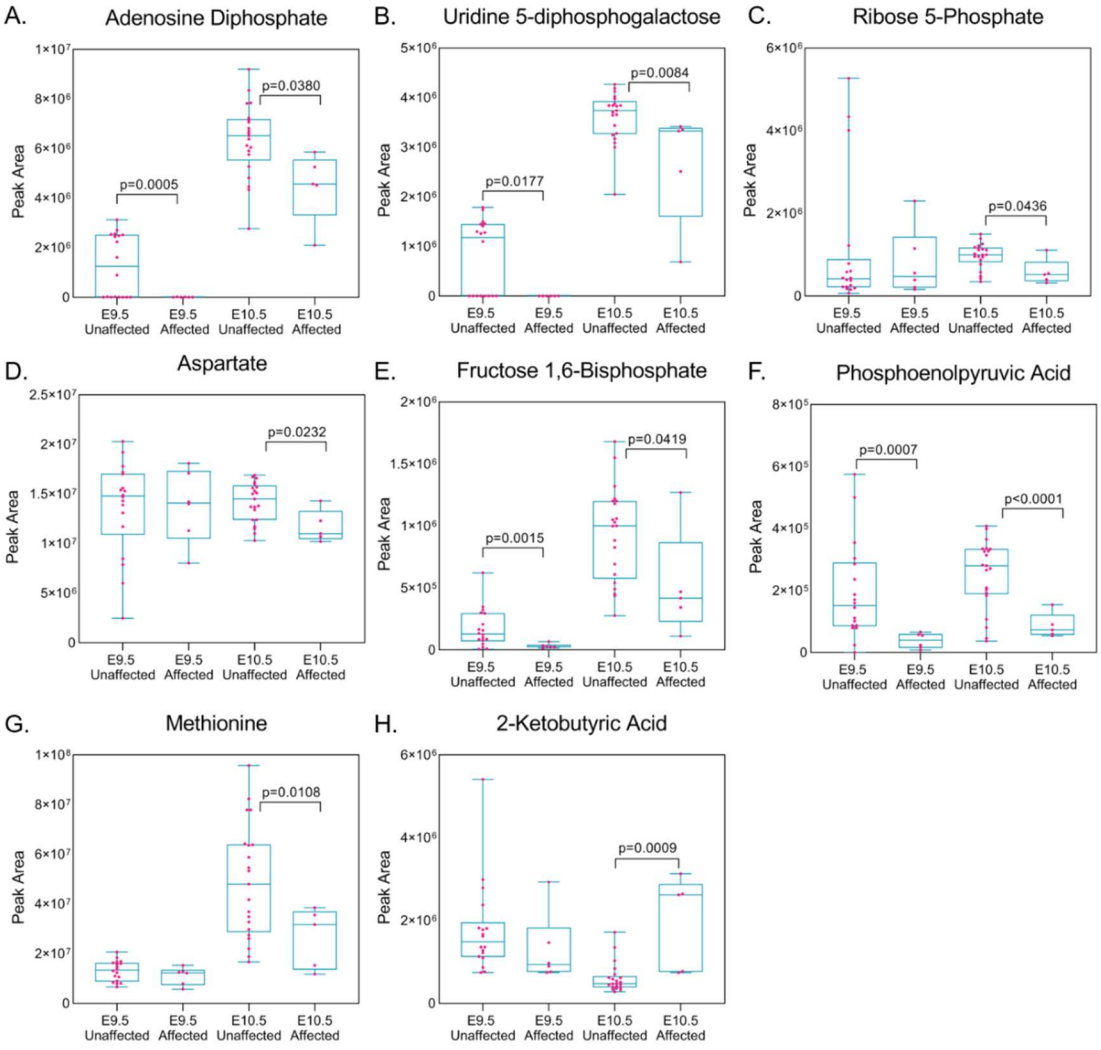

Figure 4.4 Metabolites of Differential Abundance in VPA-affected and Unaffected Embryos at E9.5 and E10.5

MS peak areas from VPA-treated embryos at E9.5 and E10.5 comparing differential abundance of metabolites between affected and unaffected embryos. These metabolites included (A) adenosine diphosphate, (B) uridine 5-diphosphogalactose, (C) ribose 5-phosphate, (D) aspartate, (E) fructose 1,6-bisphosphate, (F) phosphoenolpyruvate, (G) methionine, and (H) 2-ketobutyric acid. *Statistical significance was determined by unpaired t tests with Welch's correction (α=0.05).

Table 4.1 Pathway Analysis Comparing VPA-treated and Untreated Embryos at E8.5

Metabolic pathways found to be significantly altered in VPA-treated E8.5 embryos compared to untreated controls. Pathway analysis was performed using MetaboAnalyst.

Pathway Name	Total Compounds	Match Status*	p value	FDR	Impact
Pyrimidine metabolism	39	10	5.33E-06	4.48E-04	0.38282
Purine metabolism	66	12	2.63E-05	0.001105	0.14111
Aminoacyl-tRNA biosynthesis	48	9	2.36E-04	0.0066	0
Alanine, aspartate and glutamate metabolism	28	6	0.00136	0.028553	0.71235
Arginine biosynthesis	14	4	0.003011	0.046515	0.19289
Cysteine and methionine metabolism	33	6	0.003323	0.046515	0.19088

***** *Match status reflects the number of altered metabolites identified in each pathway.*

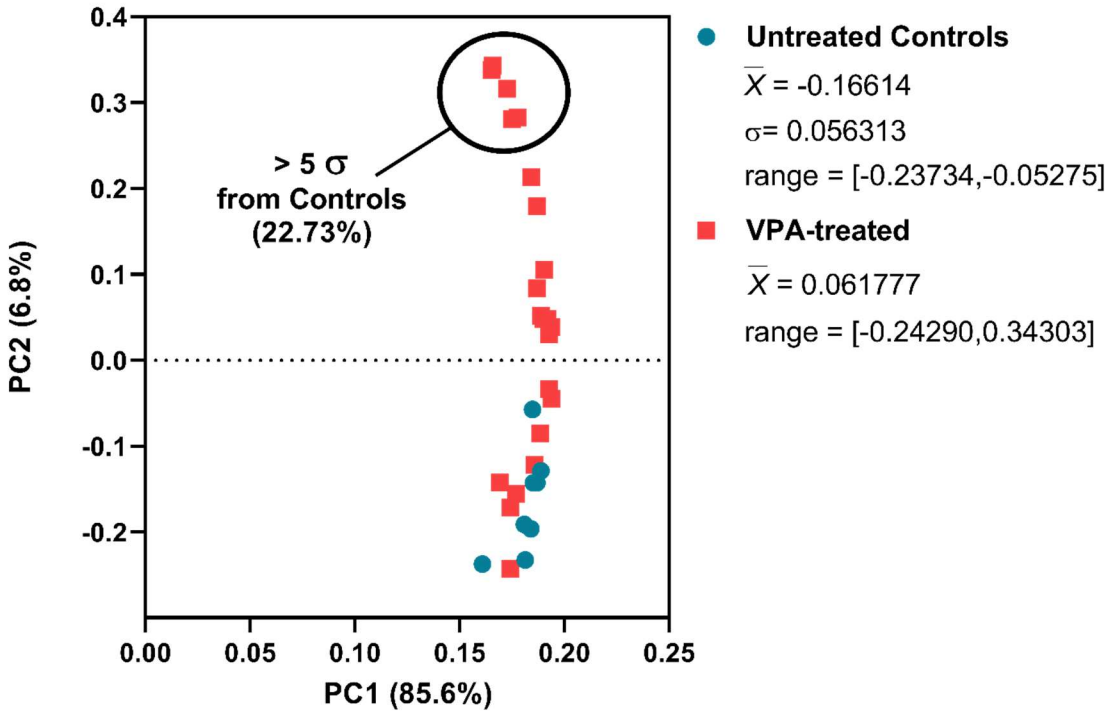

Figure 4.5 Principal Component Analysis of All Confirmed Peaks in E8.5 Embryos

Principal component analysis of confirmed MS peaks in E8.5 embryos comparing untreated controls (n=8) and VPA-treated embryos (n=22). The component predicting greatest variance between treated and untreated embryos was principal component 2 (PC2). The mean ($\bar{X}$) and ranges of the controls and VPA-treated embryos along PC2 are displayed to the right, along with the standard deviation (σ) of the controls along PC2. Five VPA treated embryos (black circle), representing 22.73% of VPA-treated embryos, were found to cluster more than five standard deviations outside the range of the controls. These embryos were classified as *likely affected*.

Table 4.2 Proportion of VPA-treated Embryos Clustering More Than a Given Number of Standard Deviations Outside the Range of Control Embryos on PC2

Criteria for differentiating VPA-affected and unaffected embryos at E8.5 based on the principal component analysis from Figure 4.5. Embryos clustering more than five standard deviations from the controls were classified as *likely affected* (approximately 22.73% of embryos).

Mean of Controls (PC2)	-0.16614	
Mean of Treated (PC2)	0.061777	
Standard Deviation of Controls (PC2)	0.056313	
Range of Controls (PC2)	-0.23734	-0.05725

σ from Max of Controls	**No. of Treated Embryos**	**Percentage of Treated Embryos**
1	10	45.45455
2	9	40.90909
3	7	31.81818
4	7	31.81818
5	**5**	**22.72727**
6	3	13.63636
7	0	0

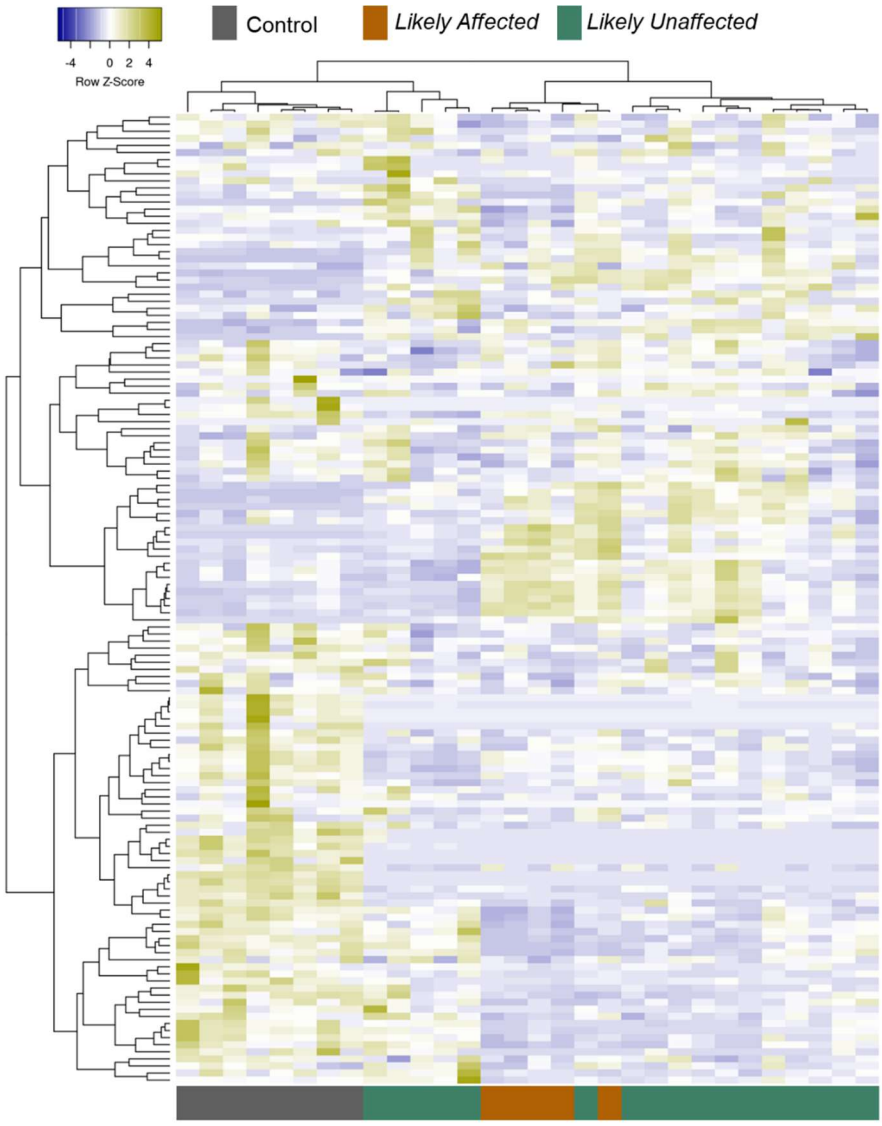

Figure 4.6. Hierarchical Clustering of Confirmed Metabolite Peaks in E8.5 Embryos

Untargeted hierarchical clustering of confirmed MS peak areas for 136 metabolites in both VPA-treated (n=22) and untreated control (n=8) embryos at E8.5. Metabolites are clustered in the rows and columns represent individual embryos. Each column is marked with a color coding (bottom) signifying the classification of the corresponding embryos as control (grey, n=8), *likely affected* (orange, n=5), or *likely unaffected* (green, n=17). The row and column dendrograms represent clustering by Pearson correlation using complete linkage.

Table 4.3. Pathway Analysis Comparing *Likely Affected* and *Likely Unaffected* Embryos at E8.5

Metabolic pathways found to be significantly altered in *likely affected* E8.5 embryos compared to *likely unaffected* VPA-treated embryos at E8.5. Pathway analysis was performed using MetaboAnalyst.

Pathway Name	Total Compounds	Match Status*	p value	FDR	Impact
Aminoacyl-tRNA biosynthesis	48	8	2.02E-06	1.70E-04	0.16667
Alanine, aspartate and glutamate metabolism	28	6	1.03E-05	4.32E-04	0.29407
Glyoxylate and dicarboxylate metabolism	32	5	3.07E-04	0.008585	0.17726
Citrate cycle (TCA cycle)	20	4	4.98E-04	0.01045	0.27074
Arginine biosynthesis	14	3	0.002241	0.031448	0.07614
Phenylalanine, tyrosine and tryptophan biosynthesis	4	2	0.002246	0.031448	1

***** *Match status reflects the number of altered metabolites identified in each pathway.*

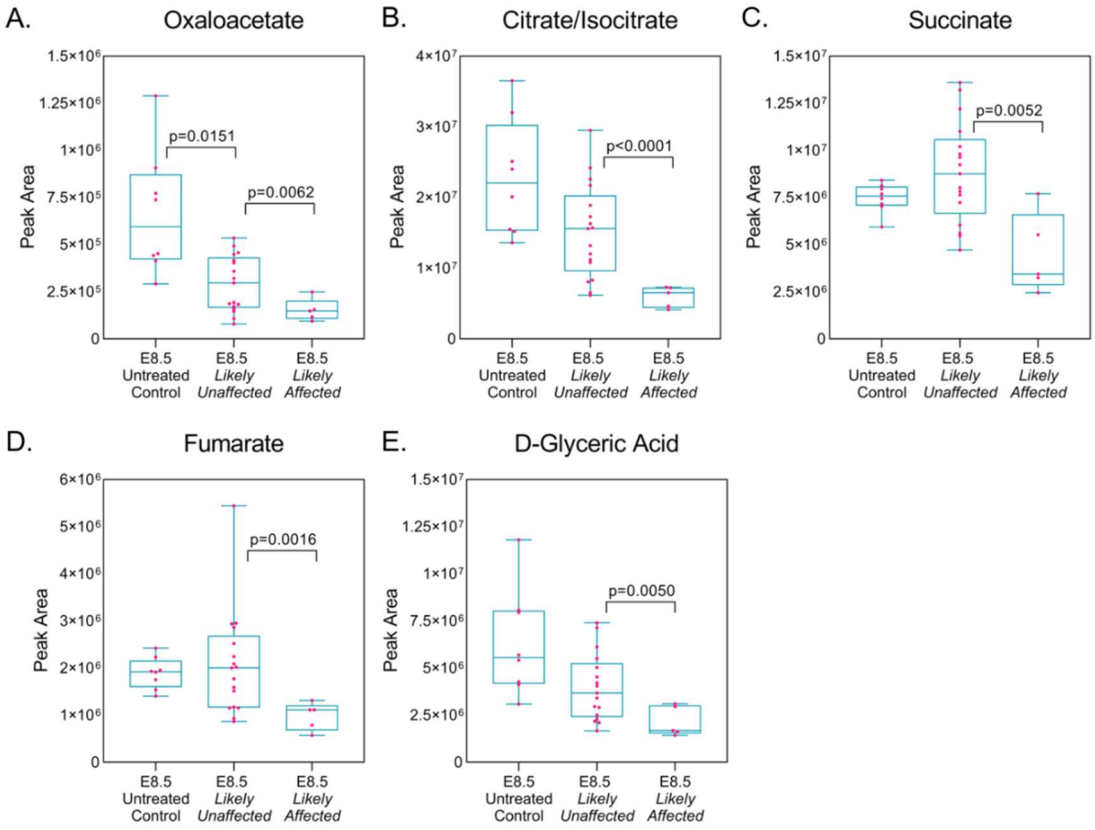

Figure 4.7. Metabolites of Differential Abundance Related to the Citrate Cycle and Glyoxylate/Dicarboxylate Metabolism in E8.5 Embryos

MS peak areas from VPA-treated embryos at E8.5 comparing differential abundance of metabolites between control (n=8), *likely affected* (n=5), and *likely unaffected* (n=17) embryos. These metabolites were associated with the citrate cycle and glyoxylate/dicarboxylate metabolic pathways, and included (A) oxaloacetate, (B) citrate/isocitrate, (C) succinate, (D) fumarate, and (E) D-glyceric acid.

*Statistical significance was determined by unpaired t tests with Welch's correction (α=0.05).

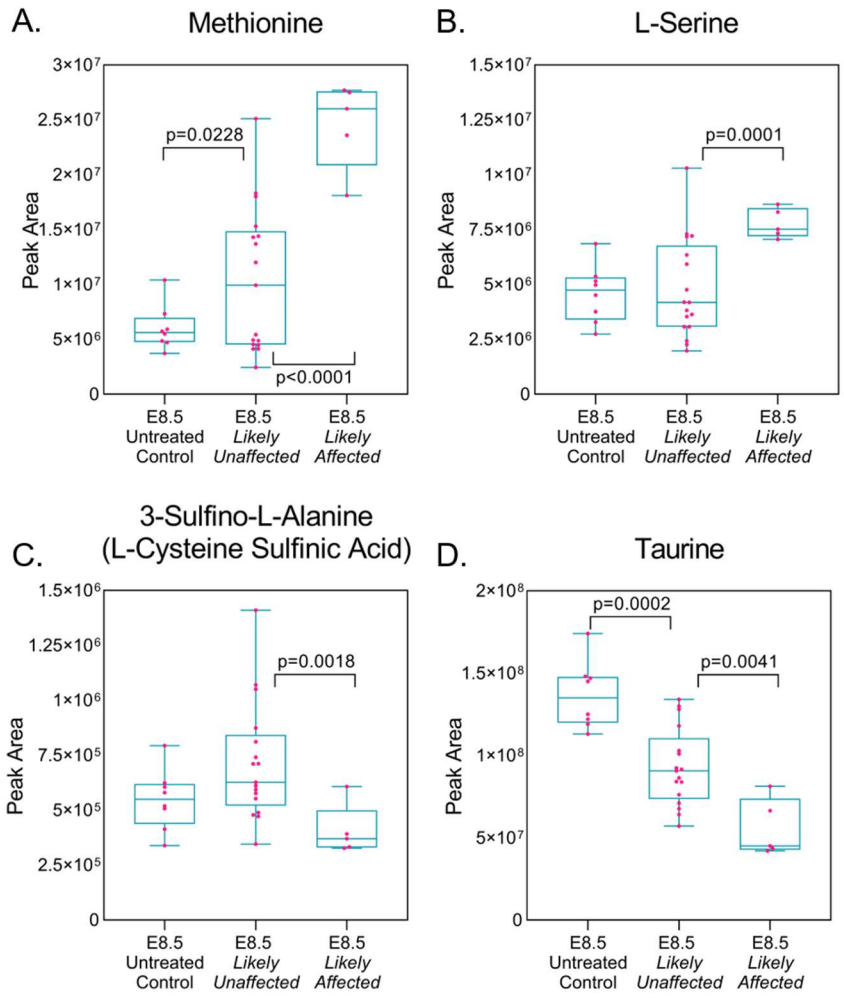

Figure 4.8. Metabolites of Differential Abundance Related to Cysteine and Methionine Metabolism in E8.5 Embryos

MS peak areas from VPA-treated embryos at E8.5 comparing differential abundance of metabolites between control (n=8), *likely affected* (n=5), and *likely unaffected* (n=17) embryos. These metabolites were associated with cysteine and methionine metabolism, and included (A) methionine, (B) serine, (C) 3-sulfino-L-alanine (also known as L-cysteine sulfinic acid), and (D) taurine.

*Statistical significance was determined by unpaired t tests with Welch's correction (α=0.05).

Table 4.4 Metabolites of Differential Abundance Only in *Likely Affected* E8.5 Embryos

Metabolites found to be significantly altered in *likely affected* E8.5 VPA-treated embryos compared to *likely unaffected* VPA-treated embryos, but not significantly altered in unaffected embryos compared to untreated controls.

Metabolite	**FC**[a]	**$\log_2$(FC)**	**FDR (U[b]vA[c])**	**FDR (C[d]vU)**
Arginine	3.12	1.644898	0.01124	0.214088
D-Tryptophan	2.20	1.139785	1.58E-05	0.070694
L-Tyrosine	1.81	0.858123	0.001362	0.063553
L-Serine	1.63	0.701088	0.001515	0.822323
L-Threonine/L-Allothreonine	1.40	0.489917	0.008042	0.224635
D-Alanine	1.38	0.464912	0.015809	0.405604
3-Sulfino-L-Alanine	0.57	-0.81135	0.012647	0.094568
D-Glyceric Acid	0.54	-0.88308	0.025359	0.103572
3-Hydroxy-3-Methylglutarate	0.52	-0.95715	0.016398	0.074156
Succinate	0.51	-0.98357	0.02518	0.110221
Fumarate	0.47	-1.082	0.011435	0.606414
Allantoin	0.41	-1.27858	0.004987	0.47988
Isocitric Acid/Citric Acid	0.39	-1.34976	0.000644	0.080757
Urate	0.27	-1.89217	0.008476	0.183783

a) FC = fold change, b) U = likely unaffected, c) A = likely affected, d) C = control

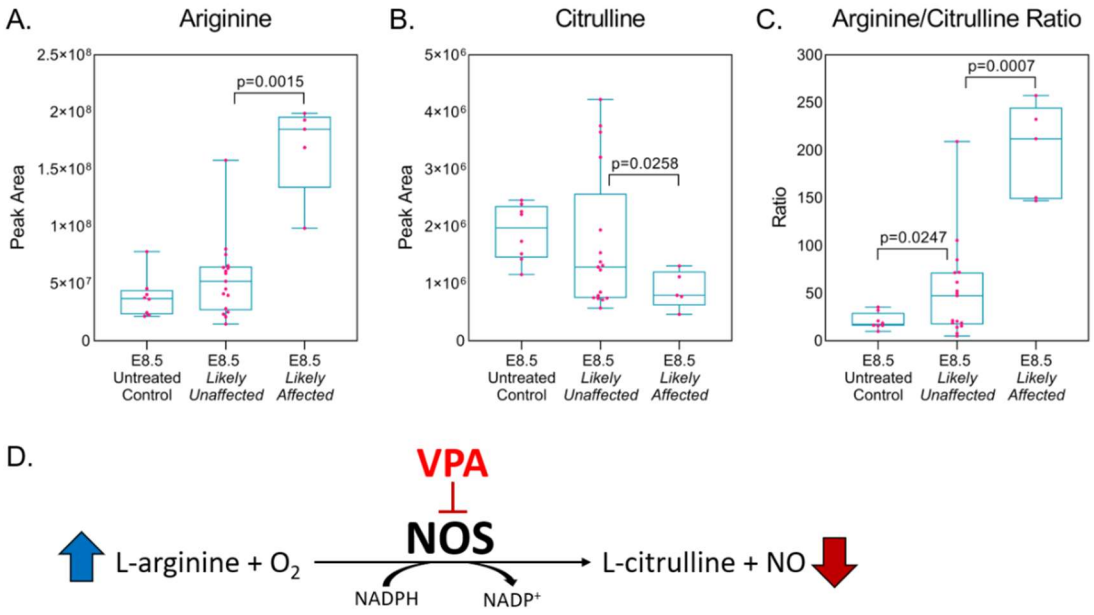

Figure 4.9 Differential Abundance of Arginine and Citrulline in *Likely Affected* E8.5 Embryos

MS peak areas from VPA-treated embryos at E8.5 comparing differential abundance of (A) arginine and (B) citrulline between control (n=8), *likely affected* (n=5), and *likely unaffected* (n=17) embryos. (C) The ratio of the metabolites arginine and citrulline in control, *likely affected*, and *likely unaffected* embryos. The ratio was highest in the embryos classified as likely affected suggesting impairment of arginine-citrulline interconversion. Statistical significance was determined by unpaired t tests with Welch's correction (α=0.05). (D) Proposed model of VPA-sensitivity predicted by impairment of nitric oxide synthase (NOS) enzymes.

*Statistical significance was determined by unpaired t tests with Welch's correction (α=0.05).

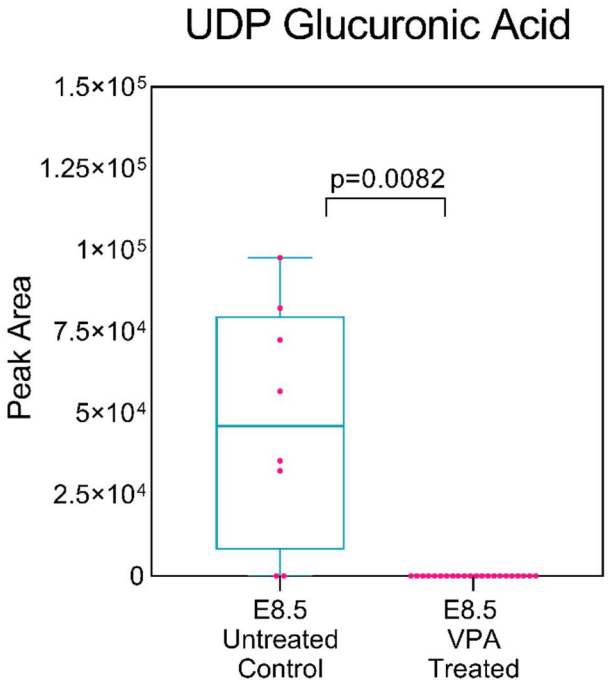

Figure 4.10 Ablation of UDP Glucuronic Acid in VPA-exposed E8.5 Embryos

MS peak areas for UDP glucuronic acid in VPA-exposed E8.5 embryos compared to untreated controls.

*Statistical significance was determined by unpaired t tests with Welch's correction (α=0.05).

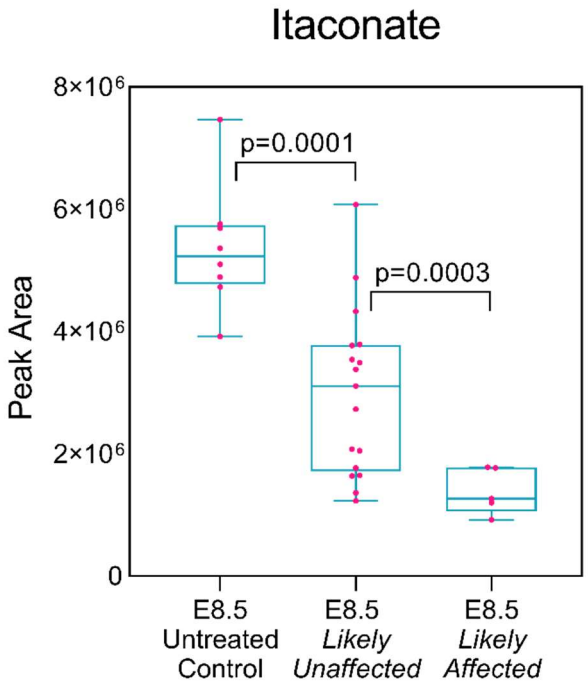

Figure 4.11 Decrease in Itaconate Abundance in VPA-treated E8.5 Embryos

MS peak areas for itaconate in VPA-exposed E8.5 embryos compared to untreated controls.

*Statistical significance was determined by unpaired t tests with Welch's correction (α=0.05).

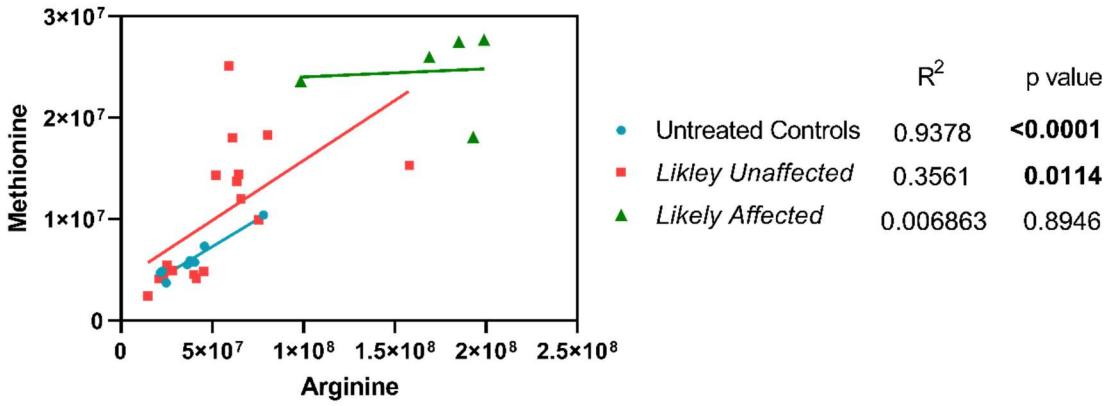

Figure 4.12 Correlation of Arginine and Methionine Abundance in E8.5 Embryos

Scatter plot demonstrating correlation between MS peak areas of arginine and methionine in E8.5 embryos. Arginine and methionine abundance are highly correlated in untreated control embryos.

*Statistical significance was determined by simple linear regression (α=0.05).

4.4 DISCUSSION

In a previous study, Akimova et al. 2017, our group demonstrated that VPA exposure in mouse embryos on gestational day E8.5 resulted in very little metabolic alteration by E9.5 compared to control embryos, so long as the mice were fed a diet with a standard amount of folic acid (2 ppm) (Akimova et al. 2017). In fact, only two metabolites were demonstrated to have statistically significant abundance, adenine and thymine (Akimova et al. 2017). It is important to note that Akimova et al. found that a high folic acid diet (10 ppm) resulted in more severe metabolic alterations associated with VPA exposure, alterations predominantly related to nucleotide, carnitine, and one-carbon metabolisms. They also found that VPA-treated embryos on the high folic acid diet had more severe developmental anomalies and developmental delay characterized by lower somite number (Akimova et al. 2017). We did observe marginally lower somite numbers at E9.5 and E10.5 in VPA-treated embryos, but no difference in somite number was observed at E8.5 (data not shown). Since mice in our study were fed a chow with 3.6 ppm folic acid, considerably lower than 10 ppm, the fact that we did not observe metabolome wide changes in the VPA-treated embryos at those timepoints appears consistent with previous results. Moreover, the previous study only looked at metabolism in VPA-treated embryos that had NTDs, thus excluding apparently non-sensitive embryos from analysis (Akimova et al. 2017). Since the goal of our current study was to identify metabolism indicative of VPA sensitivity, we considered it more prudent to compare affected and unaffected embryos.

Adenosine diphosphate, uridine 5-diphosphogalactose, fructose 1,6-bisphosphate, and phosphoenolpyruvate were decreased in affected embryos both at E9.5 and E10.5. Downregulation of the latter two metabolites would suggest persistent impairment of glycolysis in NTD embryos, while changes in nucleotide diphosphates are consistent with

observations from Akimova et al (Akimova et al. 2017). The decrease in uridine 5-diphosphogalactose is likely related to VPA's suppression of uridine diphosphate glucuronidase activity (Wlodarczyk et al. 2012), consistent with our observation that uridine diphosphoglucuronic acid (UDP glucuronic acid) was completely ablated in all VPA-treated embryos at E8.5 (Figure 4.10). We also found that aspartate levels were decreased in E10.5 affected embryos relative to unaffected embryos, but that there was no apparent difference at E9.5. While we found aspartate was not significantly different between VPA-treated embryos and controls at either timepoint, it is still difficult to draw conclusions from these results regarding aspartate as a marker for VPA sensitivity. We also observed an interesting relationship between methionine and cysteine metabolism at E10.5. Methionine abundance was decreased in affected embryos at E10.5, while a product of homocysteine and cysteine metabolism, 2-ketobutyrate was increased. This would suggest that at this timepoint, affected embryos are favoring utilization of homocysteine for transsulfuration of cysteine as opposed to regeneration of methionine. This result is interesting since the opposite effect was observed at E8.5, where we saw increased methionine in VPA-treated embryos along with decreased abundance of cysteine metabolism intermediates.

That said, given the small number of altered metabolites and large-scale shifts in metabolism between E8.5 and E10.5 (Appendix II), it is ultimately difficult to extract informative insights by comparing affected and unaffected embryos at E9.5 and E10.5. First, there were few observed VPA-affected metabolic alterations at those gestational dates, and while using those timepoints does allow for direct scoring of embryos as affected or unaffected based on visual observations, it is important to note that the VPA-induced defects have already occurred by E9.5. Thus, we cannot be certain that we are measuring metabolism associated with VPA sensitivity or metabolism associated with NTDs

themselves. As such, we chose to focus the rest of our analysis on E8.5 embryos, not only because it is a more developmentally relevant timepoint, but also because we noticed VPA had the greatest influence on embryonic metabolism at that time, likely because it was the earliest timepoint collected post exposure. After all, the half-lives of VPA and its 2-ene-VPA metabolite are only 0.8 and 1.2 hours, respectively (Nau and Zierer 1982; Nau 1985).

We first examined metabolic alterations between control and VPA-treated embryos at E8.5 since, to our knowledge, no previous metabolomic study at that timepoint has been published. We observed large-scale changes in embryonic metabolism associated with acute VPA exposure, predominantly in purine and pyrimidine metabolism. This is consistent with observations in Akimova et al. where it was hypothesized impairment of purine and pyrimidine synthesis through disrupted one-carbon metabolism may be causative of VPA-induced NTDs (Akimova et al. 2017). However, our findings do not support this hypothesis since we actually observed increased abundance of purine and pyrimidines and their nucleoside analogs; it was their phosphate-linked nucleotide analogs that were depleted as a result of VPA exposure. Phosphorylation of nucleosides to manufacture nucleoside monophosphates, diphosphates, and triphosphates is mediated by nucleoside kinases, and it is ultimately an ATP-dependent process (Lehninger, Nelson, and Cox 2013). Thus, the observed alterations in purine and pyrimidine metabolism do not appear to be a result of disrupted purine and pyrimidine synthesis but may actually be suggestive of dysfunctional energy metabolism.

While comparing untreated controls and VPA-treated embryos can be revealing as to how VPA exposure influences global metabolism, the ultimate goal of our study was to identify markers specifically associated with VPA-sensitive embryos. To address this challenge, we initially employed a machine learning algorithm that attempted to predict VPA-affected and unaffected embryos at E8.5 using metabolites of differential abundance

identified at E9.5. However, this approach did not yield a satisfyingly predictive model as it estimated approximately 60% of E8.5 embryos would be affected. We know this cannot be the case since we only observe around 20-25% of E9.5 and E10.5 embryos with NTDs. It is possible this strategy failed due to the lack of metabolic variation observed between affected and unaffected embryos at E9.5 and E10.5, even between control and VPA-treated embryos for that matter, and of course the large metabolome-wide shifts observed between gestational timepoints. These factors likely hampered the robustness of the model. We thus decided to employ a more conventional strategy by isolating a proportion of E8.5 embryos that demonstrated the greatest separation from untreated control embryos in a basic multivariate analysis. We found that approximately 23% (five embryos) of the treated E8.5 group clustered more than five standard deviations away from control embryos, and thus made a quantitative assumption that these five embryos are *likely affected*, based on them demonstrating the greatest metabolic sensitivity to VPA. We believe our five-standard deviation cutoff was ultimately conservative, as at least one other embryo lying within the cutoff appeared metabolically related to the selected embryos (Figure 4.6).

The metabolic signature that characterized the *likely affected* embryos was strongly distinguished by increased abundance of several amino acids, particularly arginine, and decreased abundance of citrate cycle intermediates. Despite altered purine and pyrimidine metabolism being the most impactful markers of VPA exposure, disruption of these pathways was not associated with VPA sensitivity in the *likely affected* cohort. That said, it is notable that decreased abundance of urate and allantoin were two makers strongly indicative of VPA sensitivity. Urate is a product of purine catabolism and allantoin is an oxidative product of urate synthesized via the enzyme urate oxidase (Lehninger, Nelson, and Cox 2013). Humans lack functional urate oxidase, but can still produce allantoin from urate non-enzymatically in the presence of free radicals (Grootveld and Halliwell 1987).

In fact, urate acts as an antioxidant due to its capacity for free radical scavenging, and is endogenously produced in response to oxidative stress caused by hypoxia (Baillie et al. 2007). The developing mammalian embryo constitutes a hypoxic environment, especially around the time of neural tube closure (Chen, Fujinaga, and Giaccia 1999), and hypoxia-induced oxidative stress has been implicated as a mechanism of NTDs associated with diabetes (Li et al. 2005). While it is unknown how important urate's antioxidant properties are during this critical window of development, it is conceivable that reduced capacity to handle VPA-induced oxidative stress may distinguish between VPA-sensitive and resistant embryos. This hypothesis is supported by a previous study which demonstrated that coadministration of VPA with antioxidants was ameliorative with respect to both oxidative stress and unsavory developmental and morphological endpoints, including NTDs (Tung and Winn 2011). Regardless, it is a notable observation that purines accumulated in VPA-treated embryos but that their catabolic product, urate, was diminished only in apparently sensitive embryos, suggesting impairment of purine catabolism may be a marker of VPA sensitivity.

Decreased abundance of citrate cycle intermediates was also a unique predictor of VPA-sensitive embryos. It has been previously demonstrated that VPA may reduce excitatory neuronal activity by inhibiting Krebs's cycle and impairing production of ATP (Johannessen et al. 2001), and that VPA inhibits mitochondrial uptake of pyruvate (Aires et al. 2008). It is notable, however, that disruption of most of these citrate cycle intermediates, specifically succinate, fumarate, and citrate/isocitrate, was exclusive to VPA-sensitive embryos. We also observed VPA-dependent reduction of another citrate-related metabolite, itaconate, which was significantly reduced in all VPA-treated embryos, but more so in the *likely affected* group (Figure 4.11). Itaconate is a metabolite of cis-aconitate, the intermediate of interconversion of citrate and iso-citrate, and plays a role in

metabolic reprogramming of macrophages during an inflammatory response (Ferreira, Netea, and Dominguez-Andres 2019; O'Neill and Artyomov 2019). It has also been shown that itaconate modulates redox metabolism through activation of nuclear factor erythroid 2-related factor 2 (Nrf2) in models of oxidative reperfusion injury (Cordes et al. 2020; Yi et al. 2020). Since inhibition of Nrf2 has been linked to NTDs (Liu et al. 2018), and activation of Nrf2 has been shown to prevent NTDs in certain models (Dong, Reece, and Yang 2016), itaconate deserves further exploration as a possible mechanistic component of VPA-sensitive NTDs. Even so, a metabolic profile associated with an impaired citrate cycle has implications for both central energy production and oxidative metabolism that may be explanatory of VPA sensitivity.

The marker most strongly associated with the distinguished metabolic signature of *likely affected* embryos at E8.5 was accumulation of arginine and subsequent depletion of citrulline as demonstrated by the 10-fold elevation of the arginine/citrulline ratio. NO is synthesized by NOS enzymes, of which there are several isoforms, by NADPH-dependent reduction of arginine and molecular oxygen to produce citrulline and NO as products (Groves and Wang 2000). Our data suggest the severity of VPA-induced NOS inhibition may be determinative of VPA sensitivity (Figure 4.9D). Recent evidence has emerged indicating functional interaction between VPA and NO synthesis; although in some models VPA appears to attenuate NO production, while in other cases it has an enhancing effect (Mairuae and Cheepsunthorn 2018; Nieto-Patlan et al. 2019; Okubo et al. 2019). Coadministration of VPA with a NOS inhibitor, L-NAME, in mice at E8 was shown to enhance VPA's teratogenic effects, resulting in a four-fold increase in NTDs and an 18% increase in skeletal defects (Tiboni, Chiarelli, and Verrotti 2013). It is also known that exposing chick embryos to exogenous NO induces NTDs through inhibition of vitamin B12-dependent methionine synthase, and that these defects can be rescued with folic acid

supplementation (Weil et al. 2004). Inhibition of NOS enzymes in chick embryos also causes NTDs through modulation of methionine synthase activity (Nachmany et al. 2006).

Since we observed elevated methionine in *likely affected* embryos and a reduction in markers associated with homocysteine metabolism, we looked deeper into the relationship between arginine and methionine in our dataset. We found that abundance of arginine and methionine was highly correlated in untreated control embryos at E8.5, but less so in VPA-treated embryos (Figure 4.12). As arginine levels increased, so too did levels of methionine, but their relationship became increasingly uncoupled as these two metabolites increased in abundance. *Likely affected* embryos showed the highest levels of both metabolites, but the correlation between their relative abundances was ablated (Figure 4.12). These data would suggest that arginine metabolism and methionine synthesis are coupled in embryos at this developmental stage, and that this coupling is most likely mediated by NO-dependent modulation of methionine synthase activity. Further experimentation is needed to confirm this mechanism of VPA sensitivity. It is also interesting to note that NO is reported to play a role in modulating metabolic reprogramming in inflammatory macrophages via the citrate cycle and itaconate (Bailey et al. 2019). Thus, it is possible that each of these aspects characterizing the unique metabolic signature in VPA-sensitive embryos may be functionally linked to one another through nitric oxide. Either way, the predictive biomarkers of VPA-sensitivity identified in our study point to impairment of NOS and subsequent NO production as a novel mechanism of VPA teratogenicity that warrants further experimental exploration.

To conclude, our metabolomic comparison of VPA-affected and unaffected murine embryos identified predictive biomarkers of VPA sensitivity associated with the citrate cycle, urate, cysteine and methionine metabolism, and arginine-dependent nitric oxide synthesis. The findings presented herein lay a groundwork for future studies exploring

metabolic mechanisms of VPA sensitivity and may help to identify underlying components of genetic susceptibility to VPA-induced congenital defects. Understanding these susceptibilities may allow for more informed decisions regarding the safe use of VPA or other AEDs during pregnancy, the design of alternative AEDs with lower teratogenic potential, or the development of intervention strategies that may reduce the risk of adverse pregnancy outcomes associated with VPA and other AEDs.

Chapter 5: Calcium Enhances Interactions Between Folate, FOLR1, and the Integrase Inhibitor, Dolutegravir

5.1 INTRODUCTION

The work in this chapter represents the dissertation author's contribution to a research article published in the journal *AIDS*, *"The antagonism of folate receptor by dolutegravir: developmental toxicity reduction by supplemental folic acid."* (Cabrera et al. 2019). The previously published material will be denoted with quotes and additional indentation.

> "Dolutegravir (DTG) is the clinically preferred integrase inhibitor, available as a single agent (Tivicay, ViiV Healthcare, Brentford, UK) for use with other antiretroviral therapy (ART) medications, and available in combination formulation (e.g., Triumeq, ViiV Healthcare) for HIV ART. A teratogenic risk for DTG was recently reported after neural tube defects (NTDs) were observed in four infants from mothers who had been taking DTG at the time of conception in Botswana (Zash, Makhema, and Shapiro 2018). The WHO subsequently provided guidelines that DTG use be avoided by women of childbearing potential unless they used adequate contraception methods (WHO 2018)."
>
> "Preclinical studies reported DTG was administered orally at up to 1000mg/kg daily, in rats and rabbits, during the period of organogenesis, days 16-17 and 16-18, respectively. Although not statistically significant, examination of these data indicates one occurrence (1/167) of cranioschisis (anterior NTD) at 40mg/kg in rabbits (Oral Study For Effects of S-349572 Sodium on Embryofetal Development in Rabbits). There was also a rat pup with meningocele, that is spina bifida, at 1000mg/kg in study SG10306 (Reproductive and Developmental Toxicity: Effects on Pre and Post-Natal Development Including Maternal Function,

in Rats). An ongoing observational human cohort study in Botswana reported a six to nine-fold increase for NTD risk in the offspring of mothers receiving DTG (Zash, Makhema, and Shapiro 2018; Zash 2018)."

In Cabrera et al. (2019), we demonstrated developmental toxicity in zebrafish (*Danio rerio*) exposed to 100μM DTG beginning between one and five hours post fertilization, with 80-100% embryo mortality. However, mortality was reduced to 0-7.69% in *D. rerio* embryos co-exposed to 60ng/mL folic acid. We also hypothesized that DTG is a FOLR1 antagonist and demonstrated that DTG produces partial antagonism "with an unadjusted half-maximal inhibitory concentration (IC_{50}) of approximately 4.4 μmol/L" using a FOLR1-folate binding microtiter assay. The dissertation author designed and performed cell culture experiments building on these results and found that DTG inhibited cellular folate uptake in NIH-3T3 cells and in a human placental trophoblast cell line (HTR-8/SVneo). Using fluorescently labelled folic acid, it was demonstrated that therapeutic concentrations of DTG result in dose-dependent cytotoxicity, altered localization of cellular folate, and enhanced cellular folate binding, but only in cell culture media and not in buffered saline. These results suggested that an ingredient in cell culture media modifies DTG-folate interactions, and calcium was subsequently identified to be the modifying factor. Using the FOLR1-folate binding microtiter assay, it was discovered that calcium enhances both FOLR1-folate interactions and FOLR1-folate-DTG interactions. The data generated by these experiments are presented herein, and the implications of these findings regarding plausible mechanisms of DTG's contribution to NTD risk are discussed.

5.2 Materials and Methods

5.2.1 General Cell Culture

HTR-8/SVneo (ATCC, CRL-3271) (Graham et al. 1993) human trophoblast cells were cultured under standard conditions (5% CO_2, 37°C) in RPMI media with 5% FBS. NIH-3T3 and HeLa cells were cultured under standard conditions in DMEM with 10% FBS. Experiments were carried out in folic acid-free RPMI 1640 or DMEM with 1% FBS to limit the contribution of undefined folate in the serum. Depending on the experiment, unlabeled folic acid or labelled folic acid was added back to the media at concentrations specified by the described experimental parameters.

5.2.2 Microscopy and Image Analysis

> "Live cell imaging using near-infrared-labeled folate (50 nmol/l, FolateRSense 680; Perkin Elmer, Waltham, Massachusetts, USA), prepared in DPBS [or folic acid-free media] with 1% FBS, was used to determine the impact of DTG on folate interactions [in cell culture]. Cations, Ca^{+2}, Fe^{+3}, Mg^{+2}, and K^{+}, were prepared from calcium chloride (1.8 mmol/l), iron III sulfate (250 nmol/l), magnesium sulfate (810 μmol/l), or potassium chloride (5.3 mmol/l). These ion concentrations are typical for cell culture media or serum. Folic acid (0-60 ng/ml) and DTG (0-100 μmol/l) were likewise dissolved in DPBS with 1% FBS for testing. Following incubation (1 h) with test compounds, cells were washed in DPBS with 1% FBS. Live-cell nuclei were stained using Hoechst 33342 (1 μg/ml, 10 min) (Thermo Fisher Scientific, Waltham, Massachusetts, USA). Images were captured and analyzed on the Operetta High Content Imaging System (Perkin Elmer)."

5.2.3 Quantification of Cellular Folate Uptake

NIH-3T3 or HTR-8/SVneo were cultured for 24 hours in 80% confluent 6-well plates in their respective folic acid-free media with 100nM unlabeled folic acid added back. Low-folate controls were cultured with only 10nM folic acid. Cells received either 2μM, 10μM, or 20μM DTG or were left untreated except with DMSO as a vehicle control. There were six replicates for each control and treatment group. After 24 hours, cells were lifted with 0.05% Trypsin-EDTA, washed twice with PBS and then lysed in TBS-T with 0.1% ascorbic acid by boiling (described in Chapter 2, Section 2.2.5). The resulting protein pellet was reserved for protein quantification using a DC Protein Assay (BioRad, 5000111). Relative folate was quantified in the supernatant of each lysate using the FOLR1 competitive microtiter binding assay methods described in Chapter 2, Section 2.2.5. Samples were normalized to total protein for relative comparison.

5.2.4 Microtiter Assay for FOLR1 Antagonism

The FOLR1 competitive microtiter binding assay was also used to test calcium-dependent modulation of DTG-FOLR1 antagonism as described in Chapter 2.

> "For all testing, stock DTG solutions were prepared at 100 mmol/l in dimethyl sulfoxide (DMSO). DTG was diluted (1:1000, producing 100 μmol/l DTG, 0.1% DMSO) into tris-buffered saline with 0.01% Tween-20 (TBS-T), and serial diluted (1:1) in TBS-T for testing. Vehicle dilutions were done in parallel with 0.1% DMSO serial diluted into TBS-T. Based on the results of in-vitro studies, calcium was also examined for interactions with FOLR1-folate binding by DTG. Calcium was tested by adding serial diluted calcium chloride (0, 0.125-2 mmol/l) to the competitive binding buffer [TBS-T, DTG, folic acid-horseradish peroxidase (FA-HRP, Ortho Clinical Diagnostics, Raritan, New Jersey, USA)]."

More specifically, large volume serial dilutions of calcium chloride (0, 0.125-2 mM) were made in TBS-T/1:10 FA-HRP (competitive binding buffer). Four separate serial dilutions of DTG (0, 0.25-32μM) were made into each calcium-competitive binding solution. At least three replicates of each combination were conducted. These samples were plated into FOLR1 labelled 96-well assay plates, which were then incubated, washed, imaged, and analyzed as described in Chapter 2, Section 2.2.5.

5.2.5 Statistics

All statistical analyses were performed using GraphPad Prism (La Jolla). Statistical significance was determined by one-way ANOVA with Dunnett's multiple comparisons tests (α=0.05).

5.3 RESULTS

5.3.1 Dolutegravir Inhibits Cellular Folate Uptake and Elicits Cytotoxicity

Consistent with our findings that DTG antagonizes folate binding to FOLR1, we observed a dose-dependent decrease in cellular folate uptake in HTR-8/SVneo and NIH-3T3 cells (Figure 5.1). In both cell lines, relative cellular folate in the 10nM (low) folic acid controls was lower compared to cells exposed to 100nM folic acid. Mean relative cellular folate decreased as DTG exposure increased. Notably, relative cellular folate in NIH-3T3 cells appeared to be more strongly disrupted by DTG than in HTR-8/SVneo. In NIH-3T3, mean cellular folate was decreased to 83%, 50%, and 9% in 2μM, 10μM, and 20μM DTG-treated samples, respectively, compared to that of unexposed cells. In HTR-8/SVneo, mean cellular folate was decreased to 93%, 87%, and 78% in 2μM, 10μM, and 20μM DTG-treated samples, respectively, compared to that of unexposed cells. While the observed decrease in HTR-8/SVneo was not statistically significant, the general decreasing

trend was still present. As to why NIH-3T3 were more sensitive to DTG, obviously there is the underlying genetic history, the fact that these cells were derived from separate individuals, and the fact that these cells are completely different cell types all likely factoring into the explanation. However, these results may also be explained by our subsequent findings that calcium modulates DTG-FOLR1-folate interactions at physiological concentrations, since DMEM, the base media for NIH-3T3, contains 1.8mM Ca^{+2}, while RPMI 1640, the base media for HTR-8/SVneo only contains 0.42mM Ca^{+2}. Regardless, the data obtained from both cell lines confirm that DTG inhibits cellular folate uptake.

We also observed that DTG elicited a dose-dependent cytotoxicity in HTR-8/SVneo. After 24 hours of exposure to 2.5μM, 5μM, 10μM, or 20μM DTG, nuclear area decreased to 98%, 92%, 88% and 60%, respectively compared to that of control cells (Figure 5.2A). Nuclear contraction is often associated with apoptotic and pre-apoptotic cells (Tone et al. 2007). Furthermore, we observed a dose-dependent decrease in the number of cells in each imaged well, suggesting a decrease in overall cellular viability. We do not believe cellular proliferation was a contributing factor, because these experiments were performed under low folate (100nM) and serum starvation conditions (1% FBS).

5.3.2 Calcium Modifies Cellular Folate Distribution in Dolutegravir-treated Cells

Based on our findings that DTG was a FOLR1 antagonist, we hypothesized that by using a near-IR-labeled folic acid, we could visualize decreased cellular folate in cells. Surprisingly, we found that when we performed the labelling experiment with HeLa cells in PBS, we did not observe any detectable differences in signal intensity per cell with or without DTG exposure (2.5μM, 5μM, 10μM, or 20μM), nor was there a dose response, at least after one hour of co-exposure. However, when we repeated the experiment in cell

culture media, we observed a dramatic change in cellular folate distribution concomitant with DTG exposure (Figure 5.3). In PBS and media, the labelled folate appeared to distribute evenly throughout the cytosol, and in PBS this was the case even with 20μM DTG. However, in cell culture media with 20μM DTG, we observed that labelled folate appeared highly restricted to small puncta of intense near-IR signal within cells. It is not clear whether these puncta represent clustered folate-receptor-DTG complexes on the cell surface, in the cytosol, or possibly within sub-cellular compartments. It might be the case that these folate-receptor-DTG complexes sequester folate and disrupt its sub-cellular distribution, possibly by blocking internalization of folate receptor, preventing release of internalized folate from endosomes, or decreasing solubility of folate. Either way, it appears that some component of cell culture media that is lacking in PBS modifies DTG-folate interactions.

Since DTG and similar drugs target HIV integrases through binding of cations in the integrases' active sites (Song et al. 2015), we hypothesized that metal cations in cell culture media, of which there are five (Ca^{+2}, Fe^{+3}, Mg^{+2}, K^{+}, and Na^{+}), are the modifying factors affecting DTG-folate interactions. To test this hypothesis, we repeated the near-IR folic acid labelling experiment of HeLa cells in PBS but added back concentrations of these individual cations to see which, if any, elicited the phenotypes observed in cell culture media upon DTG treatment. We excluded Na^{+} from this experiment since it is present in both PBS and the media. Only coadministration of Ca^{+2} and DTG reproduced the altered cellular folate distribution observed in cell culture media (Figure 5.4). It also appeared that calcium enhanced folate levels within the cells. The total near-IR signal associated with the labelled folate increased 180% compared to DTG-treated cells that received no cations (Figure 5.5). Comparatively, iron and magnesium resulted in 32% increases, while potassium elicited a 30% increase. To be certain that this was not a HeLa-specific

phenomenon, we repeated the experiment using HTR-8/SVneo using 20μM DTG in PBS for one hour, with and without calcium chloride (1.8mM). We observed the same increase in cellular folate accumulation and punctate distribution of labelled folate within cells (Figure 5.6). These results suggest that calcium cations are a modifier of DTG-folate interactions at the cellular level.

5.3.3 Calcium Enhances Interactions Between Folate, FOLR1, and Dolutegravir

Building on these findings, we hypothesized that calcium may modify DTG's antagonism of FOLR1. To test this hypothesis, we repeated the competitive microtiter binding assay using calcium chloride-supplemented competitive binding buffer. We did not observe any changes in binding of FA-HRP to FOLR1 or DTG's antagonism of said binding at 0.125mM or 0.5mM Ca^{+2}. At 2mM, however, calcium enhanced FA-HRP binding to FOLR1 by 42.3% even in the absence of DTG (Figure 5.7). It was further observed that DTG enhanced this effect up to a certain concentration, such that at 4μM DTG, binding of FA-HRP to FOLR1 was two-fold higher compared to 0μM DTG. At higher concentrations of DTG, however, 8-32μM, it appears DTG became stoichiometrically superior and it was clear that increasing concentrations of DTG resulted in antagonistic properties. These data confirm that calcium enhances both folate-FOLR1 interactions as well as folate-FOLR1-DTG interactions at physiologically relevant concentrations. It also appears that calcium's ability to modify these interactions is dependent on the stoichiometric ratios of the reactants.

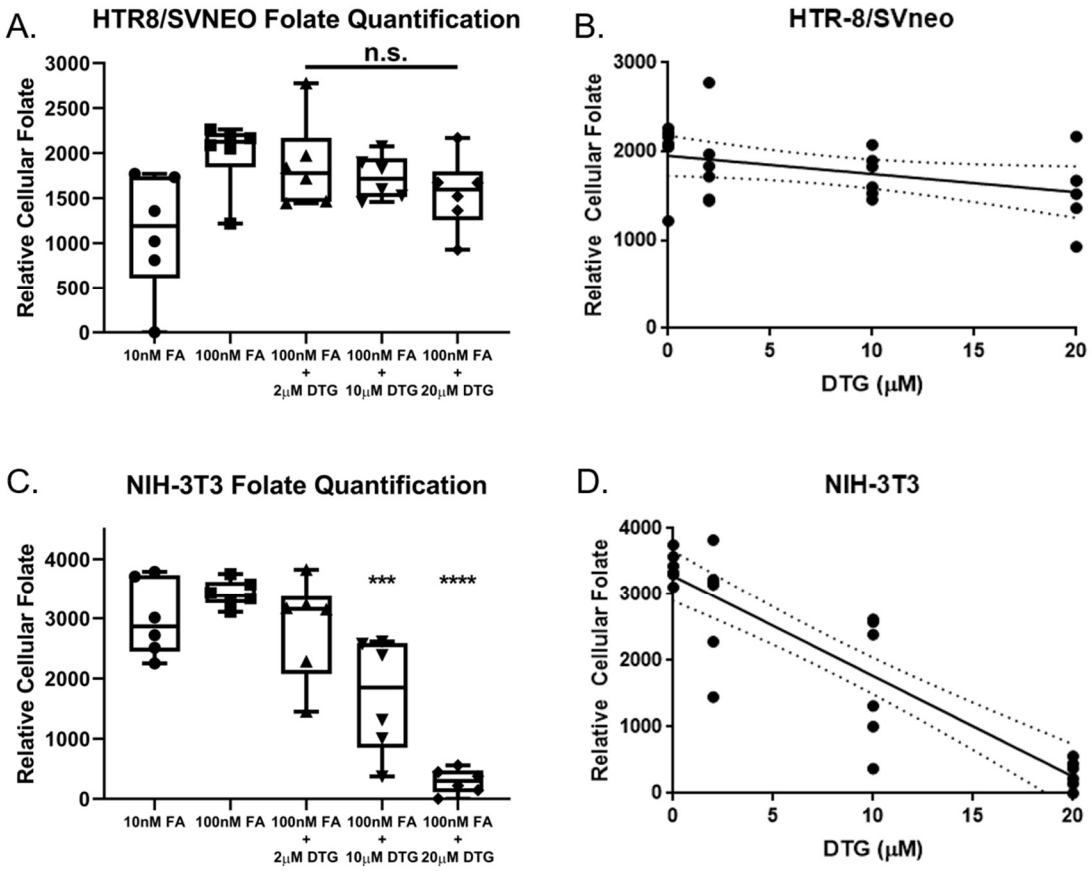

Figure 5.1 Effect of Dolutegravir on Cellular Folate Uptake in HTR-8/SVneo and NIH-3T3

Charts depicting dose-dependent reduction in relative cellular folate after 24 hours DTG exposure in HTR-8/SVneo (A and B) and NIH-3T3 (C and D).

*Statistical significance was determined using one-way ANOVA with Dunnett's multiple comparisons tests (α=0.05). n=6 for all groups. *, $p<0.05$. **, $p<0.01$. ***, $p<0.001$. ****, $p<0.0001$.

(Figure from Cabrera et al. (2019))

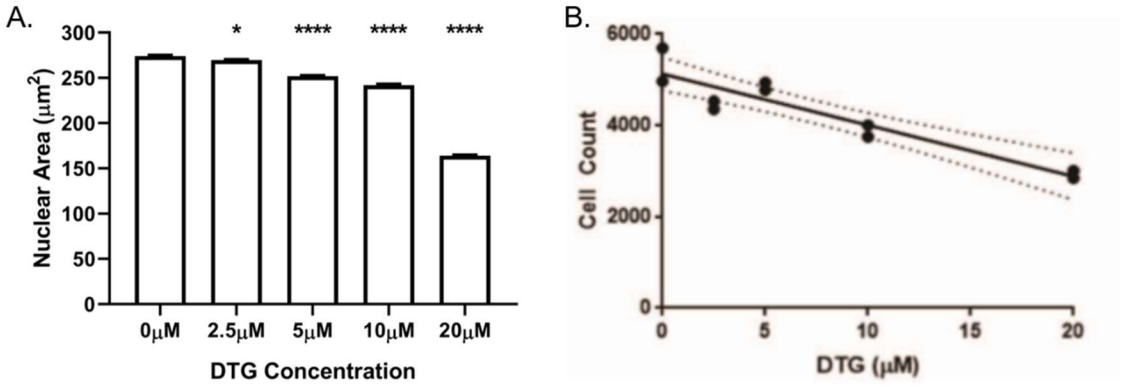

Figure 5.2 Therapeutic Concentrations of Dolutegravir Cause Cytotoxicity in HTR-8/SVneo

A) Dose-dependent contraction of nuclear area in HTR-8/SVneo after 24 hours DTG exposure.

B) Dose-dependent reduction in total cell count in HTR-8/SVneo after 24 hours DTG exposure.

*Statistical significance was determined using two-way ANOVA with Dunnett's multiple comparisons tests (α=0.05). *, $p<0.05$. **, $p<0.01$. ***, $p<0.001$. ****, $p<0.0001$.

(Figure from Cabrera et al. (2019))

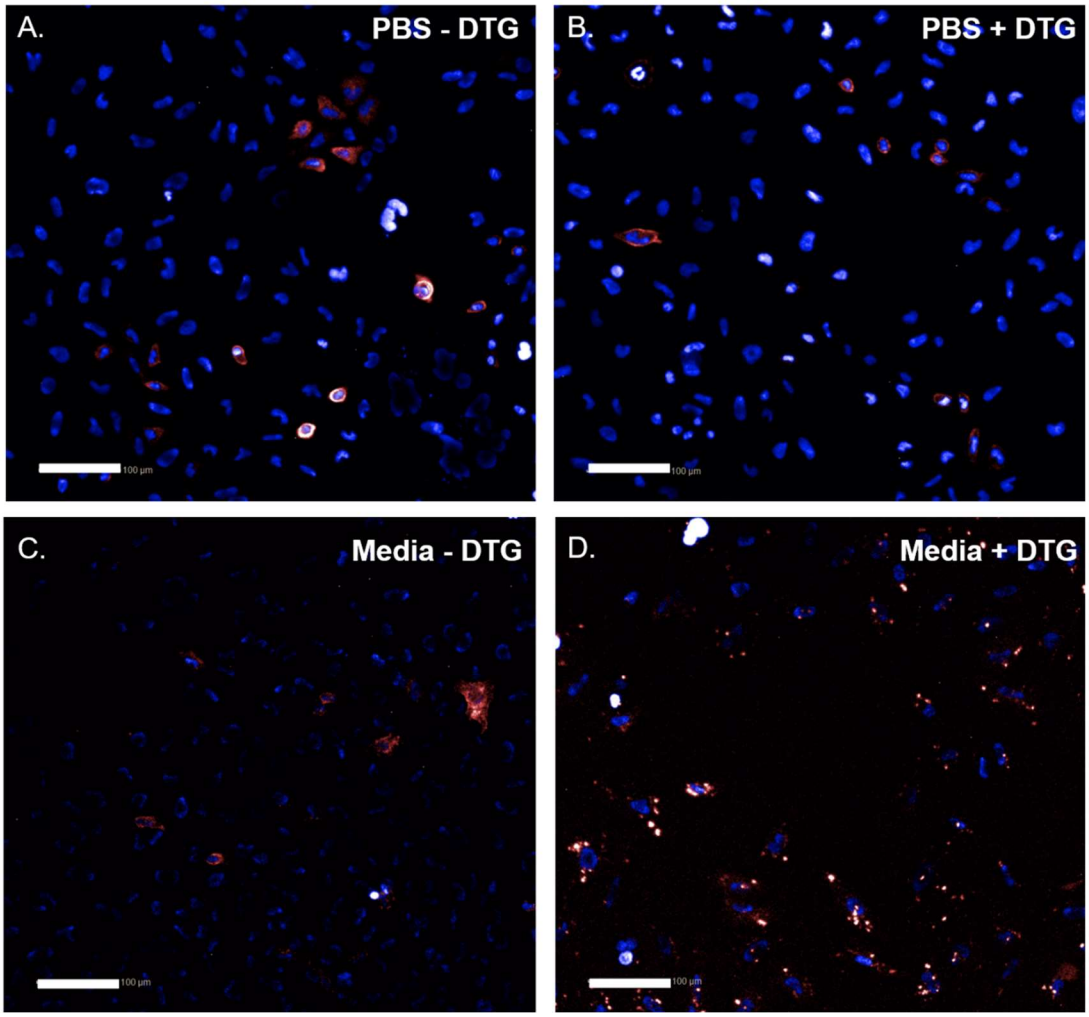

Figure 5.3 Dolutegravir Modifies Cellular Folate Distribution in a Media-Dependent Manner

Microscopy images demonstrating disrupted cellular folate distribution after one hour of 20µM DTG exposure in HeLa cells in cell culture media (C and D) but not PBS (A and B). Scale bars represent 100µm

Red = FolateRSense 680 labelled folic acid (Perkin Elmer)

Blue = Hoescht 33342 nuclear label

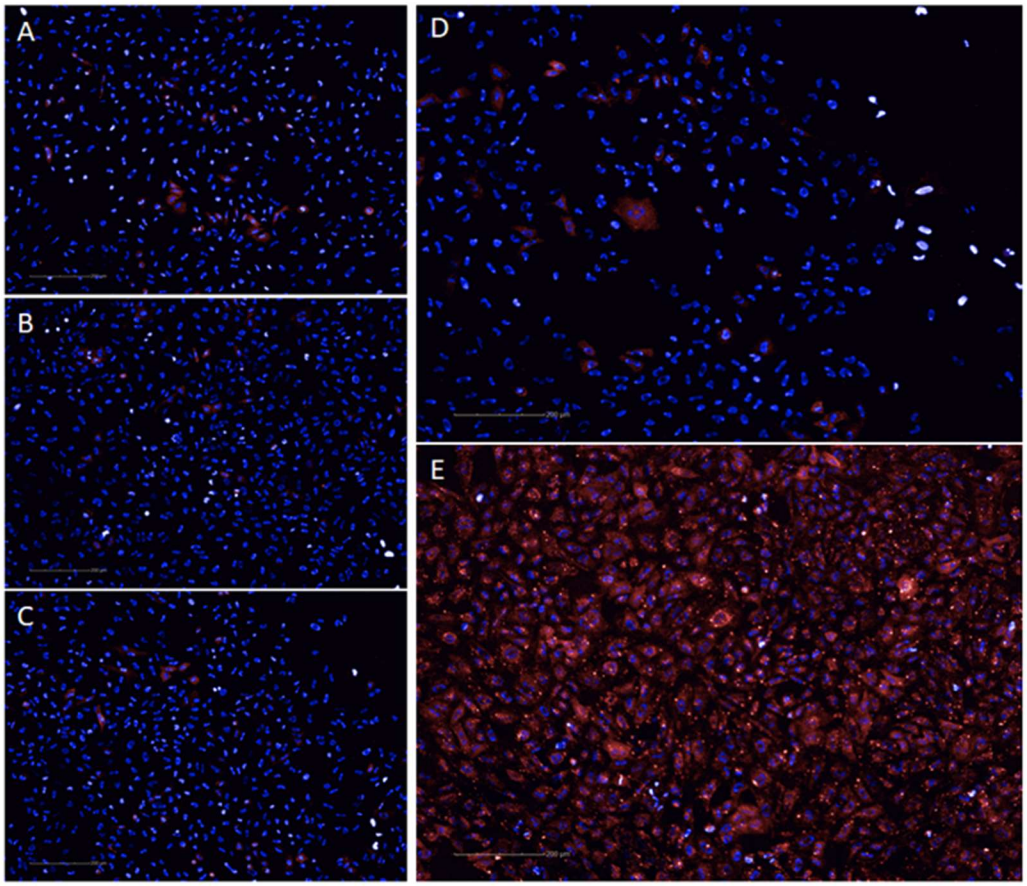

Figure 5.4 Effect of Various Cations on Cellular Folate Binding in Dolutegravir-exposed HeLa Cells – Microscopy Images

Microscopy images demonstrating effect of various cations [(A) potassium chloride (5.3mM), (B) magnesium sulfate (810 μM), (C) iron III sulfate (250nM), (D) no cation control and (E) calcium chloride (1.8mM)] on cellular folate uptake and distribution in HeLa cells after one hour of 20μM DTG exposure in PBS.

Scale bars represent 200μm

Red = FolateRSense 680 labelled folic acid (Perkin Elmer)

Blue = Hoescht 33342 nuclear label

(Figure from Cabrera et al. (2019))

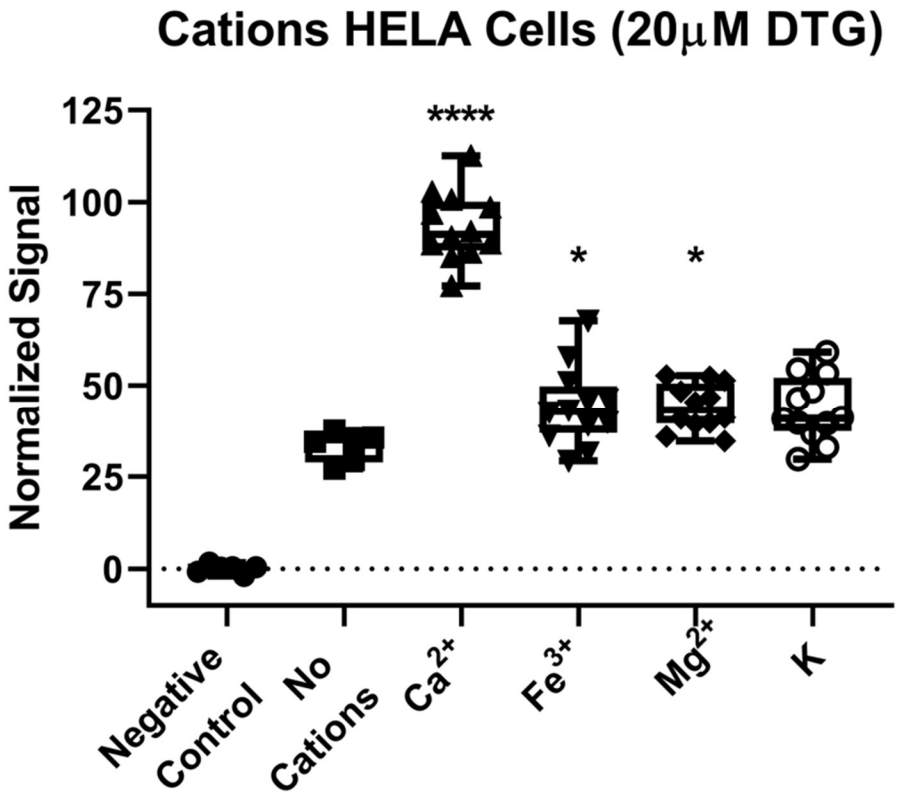

Figure 5.5 Effect of Various Cations on Cellular Folate Binding in Dolutegravir-exposed HeLa Cells – Quantification

Quantification of FolateRSense 680 signal demonstrating effect of various cations [potassium chloride (5.3mM), magnesium sulfate (810 μM), iron III sulfate (250nM), and calcium chloride (1.8mM)] on cellular folate uptake in HeLa cells after one hour of 20μM DTG exposure in PBS.

*Statistical significance was determined using one-way ANOVA with Dunnett's multiple comparisons tests (α=0.05). n=6 for negative and no cation controls. n=12 for all cation-treated groups. *, $p<0.05$. **, $p<0.01$. ***, $p<0.001$. ****, $p<0.0001$.

(Figure from Cabrera et al. (2019))

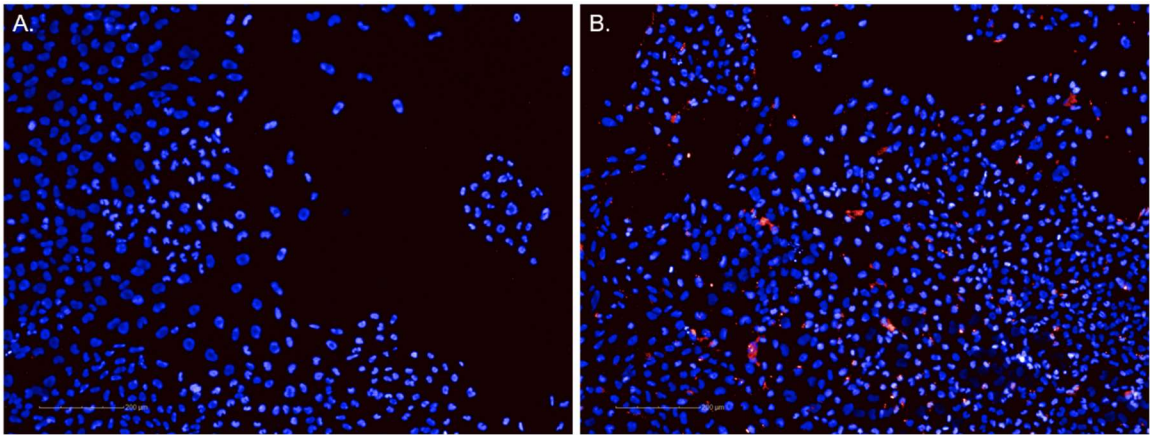

Figure 5.6 Calcium Modifies Cellular Folate Binding in Dolutegravir-exposed HTR-8/SVneo

Microscopy images demonstrating effect of A) no calcium and B) calcium (calcium chloride, 1.8mM) on cellular folate uptake and distribution in HTR-8/SVneo after one hour of 20μM DTG exposure in PBS.

Scale bars represent 200μm

Red = FolateRSense 680 labelled folic acid (Perkin Elmer)

Blue = Hoescht 33342 nuclear label

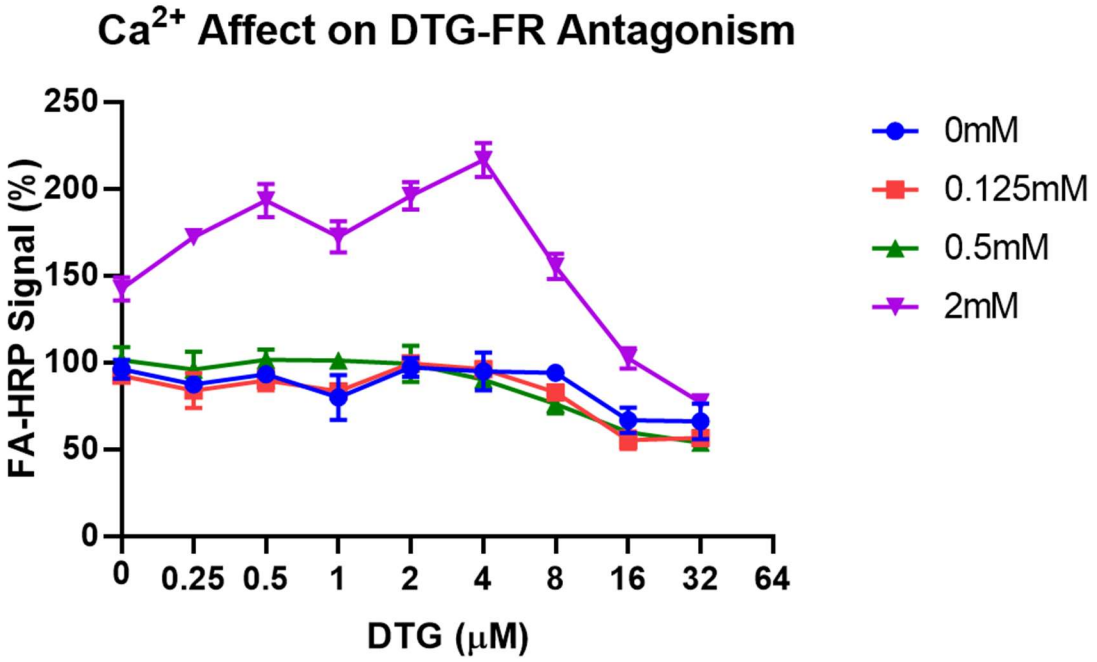

Figure 5.7 Calcium Enhances Folate-FOLR1-Dolutegravir Interactions

"Calcium (2mM) modified folate binding to FOLR1 in the microtiter protein-ligand binding assay. In the presence of Ca^{+2} (2mM) and absence of DTG, folate receptor bound 42.3% more FA-HRP. The response to DTG in the presence of 2mM Ca^{+2} appeared biphasic. The dolutegravir-Ca-FOLR1 interaction below 4μM increased folate binding, but at concentrations above 4μM, the binding fell to 77%, or decreased -23% compared to untreated wells."

(Figure from Cabrera et al. (2019))

5.4 DISCUSSION

"Adverse interactions with DTG have been reported clinically with coadministered polyvalent cations, including calcium and iron (Tivicay, 09/2018, Summary of Effect of Coadministered Drugs on the Pharmacokinetics of Dolutegravir). The clinical concern is that coadministration can result in decreased DTG uptake and lower serum concentrations (Song et al. 2015). The increase in folate binding in cells with DTG (< 4 μmol/L) was unexpected based on the FOLR1-folate binding microtiter assay. The increase in folate-FOLR1 interactions (+42.3%) produced by calcium alone appears biologically relevant to folate-FOLR1 interactions. This interaction is supported by another report that indicated calcium chloride (1 mmol/L) resulted in doubling of folate binding to rat intestinal mucosal cells (Colman, Hettiarachchy, and Herbert 1981)." The studies in HeLa cells and HTR-8/SVneo demonstrate that calcium is indeed a modifier of cellular folate binding, and the resulting cytotoxicity observed is supported by "a red blood cell study that reported DTG produces cytotoxicity in the presence of extracellular calcium (Al Mamun Bhuyan et al. 2016)." Furthermore, "the microtiter assay reproduced the increased folate binding observed in the cell culture assay[s] with 2 mmol/L [Calcium]." These concentrations are physiologically relevant, as extracellular calcium in blood is approximately 2mM. "These data indicate that calcium is a modifier of FOLR1-folate binding, and we propose DTG chelation of calcium modifies FOLR1 interactions and cytotoxicity."

"Mechanistically, DTG binds to magnesium at the active site of the HIV integrase enzyme, thereby preventing integration of viral DNA into the host genome. Drugs in this class are unfortunately susceptible to cation interference if coadministered with mineral supplements of antacids (Song et al. 2015). The results

support the increased folate detected in the trophoblast model [and HeLa cell model] is a result of DTG-Ca-FOLR1-folate interactions, and the increase in signal represents localized increased concentrations of DTG and folate due to interaction with FOLR1. As soluble calcium increases folate-FOLR1 interactions and also interactions with DTG, the resulting chelation decreases DTG-Ca-FOLR1-folate solubility. This model is consistent with nuclei contraction and decreased cell numbers observed when DTG was coadministered with calcium and folate. We propose the increase in FOLR1-folate binding in cells exposed to DTG is due to DTG binding of calcium, and calcium-responsive FOLR1-folate binding, producing DTG-FOLR1-folate or DTG-Ca-FOLR1-folate complexes with limited DTG-folate solubility and increased cytotoxicity. The FOLR1 epitopes involved in DTG or Ca^{+2} binding, structural and stoichiometric interaction of these molecules, and testing of other ART medications for similar interactions are open topics for future studies."

"We have previously reported that homozygous deletion of *Folr1* in mice is lethal, but folate supplementation if *Folr1* mutants produces a range of developmental defects that vary by genetic background and range from lethality, to NTDs, to complete rescue (Piedrahita et al. 1999; Cabrera 2018). Based on these results, we propose the recommended folic acid (2-3 mg/kg) content in laboratory animal chow may limit the developmental toxicity of DTG. We propose future mammalian animal testing of DTG developmental toxicity is warranted, but preimplantation, peri-implantation, and post-implantation DTG exposure should be explored in studies using both low-folate diet (e.g. 0.3 mg/kg) and standard-folate diet to examine folate responsive defects and folate masking of DTG developmental toxicity. Furthermore, as more human cohort data is generated, or additional

clinical studies are performed on DTG, biological interactions and clinical correlations between natural folate intake, supplemental folic acid, fortified diets, calcium intake and resultant DTG, folate, and calcium in blood and serum should be investigated. It has been previously reported that in human populations where folate fortification is in place, the prevalence of folate deficiency is approximately 0.1% or one per 1000 individuals, but in unfortified populations, the base line incidence may be more than 20%, one in five, or possibly higher (Rogers et al. 2018). This 100-200-fold difference in the incidence of folate deficiency lowers the average serum folate, increases NTD risk and may also increase the risk of NTDs associated with early gestational *in-utero* DTG exposure. According to a WHO review from 1993 to 2005, 42% of pregnant women had iron-folate-related anemias worldwide and almost 90% of anemic women reside in Africa or Asia (Sanghvi, Harvey, and Wainwright 2010). On the other hand, preclinical animal studies are expected to approach 0% folate-deficient on standard diets, because they all have adequate folate intake. We propose the combination of fortified diets coupled to a critical period in zebrafish that parallels pre-gastrulation mammalian embryos (Carnegie Stage <8) limited previous detection of DTG-induced developmental toxicity. The data reported in this study indicate that the research and medical communities should consider folic acid supplementation and maternal folate status as a major modifier of DTG-induced developmental toxicity. The results from these studies are also expected to inform and guide future animal models and clinical studies of DTG-based ART in women of childbearing age."

Chapter 6: Summary and Future Directions

6.1 Part One Summary

Part One of this dissertation explored mechanisms of impaired mitochondrial OCM in NTDs using mouse and stem cell knockout models of the mitochondrial genes, *Slc25a32* and *Mthfd1l*. In Chapter 2, a novel digenic interaction was identified between *Slc25a32* and the Wnt co-receptor encoding gene, *Lrp6*. By crossing *Slc25a32*$^{+/gt}$ mice with *Lrp6*$^{+/cd}$, it was discovered that a proportion of resulting co-heterozygous offspring presented with NTDs, suggesting the point of *Lrp6*-folate interactions may be in mitochondrial OCM. Further experiments demonstrated that *Lrp6* regulates expression of mitochondrial OCM genes in mouse embryos, while CHO cells lacking *Slc25a32* demonstrated impaired autonomous Wnt signaling that could be rescued with glycine. Building on that data, it was discovered that maternal glycine supplementation could prevent NTDs in *Slc25a32* null embryos similarly to formate as previously reported (Kim et al. 2018); and preliminary data suggests that glycine or serine supplementation may reduce NTD risk associated with *Cd* heterozygosity. Thus, the experiments in Chapter 2 clearly identify a mechanistic interaction between canonical Wnt signaling and mitochondrial OCM and suggests that glycine or serine may serve as novel intervention strategies for NTDs arising from human *LRP6* variants or other mitochondrial OCM interactors. Future experiments will explore more detailed mechanisms underlying this interaction, and the efficacy of glycine and serine as NTD preventative supplements. For example, this dissertation demonstrated that mitochondrial OCM gene expression is impaired in *Lrp6 Cd* embryos at the level of mitochondrial folate transport, serine catabolism/glycine synthesis, and glycine catabolism. While expression levels of mitochondrial OCM genes have previously been shown to modify 1-C flux in cell culture (Ducker et al. 2016), it has not been demonstrated

in embryos. Thus, 1-C flux and incorporation analyses in *Lrp6 Cd* embryos using deuterium-labelled serine and ^{13}C-labelled glycine may inform as to whether these observed changes in gene expression translate to impaired OCM (Ducker and Rabinowitz 2017; Leung et al. 2017). Furthermore, it has not been shown that the observed *Lrp6*-dependent reduction in expression of *Slc25a32* results in reduced abundance in mitochondrial folate pools to any significant degree. Thus, mitochondrial folate levels and speciation in *Lrp6 Cd* embryos should be quantified to answer this question. β-catenin activity in *Slc25a32* null and heterozygous embryos should be measured to determine if MFT-dependent Wnt signaling is replicated *in vivo*. Finally, it has yet to be determined if NTDs resulting from *Lrp6*/mitochondrial OCM mutants are FA-resistant, whether Lrp6 can interact with other mitochondrial OCM genes (such as *Mthfd1l*), or whether glycine, serine, or formate can rescue NTDs associated with compound *Lrp6*/mitochondrial OCM mutations. Thus, future experiments will explore these questions.

In Chapter 3, it was demonstrated that ES cells lacking *Mthfd1l* have proliferation defects and are sensitive to hypoxia. It was notable that co-supplementation with hypoxanthine and thymidine appeared more efficient than formate at rescuing proliferation defects associated with loss of *Mthfd1l*. Thus, future experiments may look into the efficacy of hypoxanthine and thymidine as co-supplements for prevention of NTDs in the *Mthfd1l* knockout mouse model. Chapter 3 experiments also demonstrated that ES cells lacking *Mthfd1l* display hypoxia sensitivity in a manner independent of *Mthfd1l*'s role in nucleotide metabolism and proliferation. ES cells displayed a hypoxia-induced decrease in cell viability that was determined by *Mthfd1l* gene dosage, with nulls being most sensitive. These results imply alternative mechanisms by which *Mthfd1l* or impaired mitochondrial OCM may cause NTDs apart from simply insufficient production of formate for cytosolic 1-C units. These alternate mechanisms may include mitochondrial OCM's role in

producing the reducing equivalents NADPH and NADH, as well as supporting glutathione synthesis, thus modulating cellular redox balance. While the cancer research-community has already been exploring these mechanisms in their models, deciphering these same mechanisms in embryos is much more challenging. Finally, Chapter 3 identified changes in murine embryonic expression of mitochondrial OCM genes, specifically down regulation of *Shmt2*, *Mthfd1l*, and *Mthfd1*, concurrent with upregulation of *Aldh1l1* and *Aldh1l2*, between E8.5 and E10.5. These changes suggest a metabolic switch away from production of mitochondrial 10-formyl-THF and utilization of 10-formyl-THF for formate synthesis and cytosolic OCM after NTC. Future experiments will explore whether these changes in gene expression translate into actual changes in metabolism, and to determine the factors driving and requiring this theorized metabolic switch.

6.2 PART TWO SUMMARY

Part Two of this dissertation explored mechanisms through which pharmaceutical exposures to VPA or DTG may cause NTDs. For Chapter 4, by comparing metabolites of differential abundance between VPA-affected and unaffected embryos, we were able to identify metabolic markers that are predictive of VPA sensitivity. Our results confirmed previous reports that VPA disrupts embryonic purine and pyrimidine metabolism, but we found that this alone was not associated with VPA sensitivity. Metabolites in affected embryos suggest impairment of nitric oxide synthase enzymes as a mechanism for valproate-induced neural tube defects. Disruption of the citrate cycle and alterations in amino acid interconversion were also predictive, especially methionine and cysteine metabolism. These results identify previously unexplored metabolic mechanisms through which valproic acid may cause congenital defects, thus establishing a groundwork for further investigation that could evolve strategies for preventing these defects. Future

experiments will test mechanistic hypotheses prioritized based on the findings presented in this study. Moreover, since some mouse strains are more resistant than others, an alternative future approach could be to perform a comparative metabolic analysis in embryos after VPA exposure in a relatively sensitive strain, such as SWV, and a relatively VPA-resistant strain, such as LM/BC. Ultimately, identifying mechanisms underlying VPA-sensitivity in NTDs may lead to the development of novel intervention strategies or alternative, nonteratogenic pharmaceuticals for treatment of epilepsy in women of childbearing potential.

The work presented in Chapter 5 explored mechanisms underlying interactions between folate, FOLR1, and the HIV integrase inhibitor, DTG. The cell culture experiments built on the findings of Cabrera et al. (2019) that DTG is a folate receptor antagonist at therapeutic concentrations. It was discovered that an unknown component in cell culture media modifies cellular folate distribution and uptake in the presence of DTG, and subsequent experiments demonstrated that calcium was the modifying component. Using a competitive folate binding assay, it was demonstrated that calcium enhances DTG-FOLR1-folate interactions, and it was proposed that these interactions may not only antagonize folate uptake but may also sequester sub-cellular folate and reduce bioavailability of folates by decreasing their solubility. While Cabrera et al. (2019) demonstrated developmental toxicity in zebrafish resulting from DTG exposure, and that supplemental FA reduced said toxicity, more teratology and human epidemiological studies are needed to assess NTD risk associated with DTG. Future experiments are planned to assess developmental toxicity in mouse embryo models using dams on low-folate diets, thus more adequately accounting for DTG-folate interactions compared to the initial teratology studies performed for the drug's approval. The role of calcium as a modifier will also be assessed in these studies.

Ultimately, the work presented in this dissertation identifies new mechanisms through which impaired mitochondrial OCM or drug exposure to VPA or DTG may cause NTDs. Building on the work presented here may eventually lead to novel strategies for the prevention of NTDs or development of safer anti-epileptic or anti-retroviral pharmaceuticals.

Appendices

APPENDIX I: PRIMERS FOR QPCR

Table I.1 Primers for qPCR

***Gene* (*species*)**	**Forward Primer (5' to 3')**	**Reverse Primer (5' to 3')**
Actb (C. griseus)	ATGACGATATCGCTGCGCTC	GCCACAGGATTCCATACCCAG
Actb (M. musculus)	CCACCATGTACCCAGGCATT	AGGGTGTAAAACGCAGCTCA
Aldh1l1 (M. musculus)	TCTTTGACCTTGGGTGCCTT	GAACACACCCACCACCTCAT
Aldh1l2 (M. musculus)	TGAAGCGAAGCACTCAACCC	TTGAAATAAACCCGGCTGGTG
Amt (M. musculus)	ATGCAGGACAAGGTCAAGGAG	GTGGGTCCTTGCAGAGCTAACA
Bhmt (M. musculus)	GAGGCAGTTCGTCAGCTTCA	GCTTCGTTGACTTTCTGCCC
Dhfr (M. musculus)	GACGGCAATCCTAGCGTGAA	CTCGTTCCTGAGCGGAGGC
Folr1 (M. musculus)	ACAAGAAAGGAGGCTGACGG	CCGAGGTTTAGTGGCCTGAA
Gapdh (C. griseus)	CCTGGAGAAACCTGCCAAGTA	CGGTGTGGGGGTTATTGGAC
Gapdh (M. musculus)	GCACAGTCAAGGCCGAGAAT	GTGGTTCACACCCATCACAA
Gldc (M. musculus)	AGAAGCCACAGAAATCGCCA	AGCCACATACCCTCTTGCAC
Hprt (C. griseus)	GCAGCGTTTCTGAGCCATTG	CATCATCGCTAATCACGACGC
Hprt (M. musculus)	ACAGGCCAGACTTTGTTGGA	ACTTGCGCTCATCTTAGGCT
Lrp6 (C. griseus)	TGGATGGACAACACCGACAG	CGGTCCAATACATAAATCCTTC
Mtfmt (M. musculus)	GTGTACCACAGACCATCGCA	ATCCAGCCATCCTTACAGCG
Mthfd1 (M. musculus)	GACCCAGACAGACAAGGCTC	TGGTGGGTTCAGTCTTCTCA
Mthfd1l (M. musculus)	CCACCCGACCCTGCTTTTAT	CTTGACCGCATCTTGCCCAG
Mthfd2l (M. musculus)	GCCGGAGACACGAAGCC	GGTGTGGCTTGCTGGGTTAT
Mthfr (M. musculus)	TGAGCAGATCGGGATGAACC	GATTCCTGCTGAAGGGTGG
Mtr (M. musculus)	AATACTTGCTGGCTGGAGCA	ATCCGGTAGGCCAAGTGTTC
Polm (C. griseus)	CGATCCAAAGGCTTCCGCAT	CCACGTGTGTCACCTCTGTA
Polm (M. musculus)	TCTCTCCTTCTCCAGAGCGG	CAGCAGCTCCTGGATTACTCT
Rpl13a (C. griseus)	CATGCTGCCCCACAAGACTA	CCTGGTATTTCCACCCGACC
Rpl13a (M. musculus)	TGACAAGAAAAAGCGGATGGTG	GCTGTCACTGCCTGGTACTT
Shmt1 (M. musculus)	GGAGGTGTTGCTGTGGTCA	ACTGGTTCAGAGTTGCCTTGT
Shmt2 (M. musculus)	CAGAGATGTGGTCAGCTGGT	GCAGAAGTTCTCTGAGGCGA
Slc25a32 (M. musculus)	CGTAGCAGCAACATACCCGT	ATGCCTTCTTTCCTCCACGTC
Wnt1 (C. griseus)	AGCTGGGTTTCTGCTACGTT	GTTCACGATGCCCCACCATC

Table I.1 continued

Wnt10a (C. griseus)	CTGTAGGACCAGTGCCAGGA	CAACTCCTGGTGCCTCCCAA
Wnt10b (C. griseus)	GGCTTTGTTCACTCGGGCT	GGGAAGTTTTAGGCCCAGGAT
Wnt11 (C. griseus)	AAGCCAATAAACTGATGCGG	GGCACGTAGAGCCTGTCTCC
Wnt16 (C. griseus)	TCCAGTACGGCATGTGGTT	CGACAGCCTGCCTTCCC
Wnt2 (C. griseus)	TCCTCCGAAGTAGTCGGGAAT	GGTCACAGGAGCAGGACTTT
Wnt2b (C. griseus)	CCATGCGGTCGCAGCTC	TCCCAATATCTCCGTCCCCC
Wnt3 (C. griseus)	GAAAACAGACCTGATGCCCG	CAGGATGGTCGTGCGGC
Wnt3a (C. griseus)	GGAAGAACCAAAACGGAGCC	CCACAGCTAAAGACCACCAGA
Wnt4 (C. griseus)	GAAAAGTGTGGCTGTGACCG	TGGAAACCCTGTGGGCTGAC
Wnt5a (C. griseus)	TACCAGTTTCGGCATCGGAG	GTCTCTCTGCTGCCTATTTGC
Wnt5b (C. griseus)	CAACACGTCTGTCTTCGGCA	CAGTCTCCCGGCTACCTATC
Wnt6 (C. griseus)	GAGACGATGTGGACTTCGG	GCGTGTGCTACGCACCA
Wnt7a (C. griseus)	GCCTGGACGAGTGTCAGTTT	CCGGCTCCCCACTTTAAGC
Wnt7b (C. griseus)	GCCAACAGTTCCGATTC	GCCTCACGACTCCCTACTCG
Wnt8a (C. griseus)	ATCCCCGTTCACCTCAGTTT	TCAGATAGGCCTTGGGACCTG
Wnt8b (C. griseus)	TCGTAGTGCTAACCGGGAGA	CGGGAGTCATCACAACA
Wnt9a (C. griseus)	CCGCGCTCAATGGCTCATAG	CCTGTTAGCCGGGATCTAGC
Wnt9b (C. griseus)	GCATCAAGGCTGTGAAGAGTG	TAGCGTAGCTTCAGCACCTG

APPENDIX II: SIGNIFICANTLY ALTERED METABOLITES BETWEEN E8.5, E9.5, AND E10.5 IN VPA-TREATED EMBRYOS

Table II.1 Significantly Altered Metabolites Between E8.5, E9.5, and E10.5 in VPA-treated Embryos

Fold change (FC) and p values are relative to E8.5.

Metabolite	FC-9.5	FC-10.5	p val-9.5	p val-10.5
Cytidine 5-Triphosphate	2.11E+05	1.88E+06	1.763E-03	6.948E-07
Uridine 5-Triphosphate	1.43E+05	1.35E+06	1.992E-03	2.398E-05
Uridine 5-Diphosphoglucuronic Acid	2.11E+04	2.35E+05	8.375E-04	2.306E-19
NADH	8.98E+03	2.33E+05	5.643E-03	1.238E-04
2-Deoxyadenosine 5-Triphosphate	6.83E+03	1.11E+05	1.612E-03	4.236E-08
Guanosine triphosphate	1.61E+03	2.18E+04	3.058E-03	1.461E-07
Adenosine 5-Triphosphate	3.06E+02	8.49E+03	1.504E-03	5.382E-07
NAD	7.21E+02	5.64E+03	6.001E-04	2.205E-11
Uridine 5-Diphosphogalactose	3.88E+02	2.14E+03	4.393E-04	2.045E-25
DAMP	2.63E+01	9.32E+02	2.244E-02	4.796E-10
Uridine 5-Diphospho-N-Acetylglucosamine	1.50E+02	8.98E+02	4.802E-04	7.068E-26
Guanosine 5-Diphosphate	1.16E+02	5.19E+02	1.115E-03	2.053E-23
Adenosine 3,5-Diphosphate	4.89E+01	3.07E+02	7.663E-04	1.216E-21
CMP	9.86E+00	2.76E+02	2.886E-03	5.415E-08
3-Hydroxykynurenine	4.53	222.30	2.667E-02	6.682E-14
Guanosine 5-Monophosphate	2.27	168.77	1.256E-02	1.426E-06
Adenosine 5-Monophosphate	4.84	142.81	2.429E-02	1.205E-08
Uridine 5-Diphosphate	44.03	137.15	6.985E-04	1.211E-17
Fructose 1,6-Biphosphate	21.29	131.76	1.547E-04	1.608E-12
O-Phospho-Dl-Serine	41.35	118.68	1.922E-06	1.660E-08
D-Glucosamine 6-Phosphate	7.24	96.68	6.442E-04	1.217E-10
Oxidized glutathione	6.12	71.49	1.677E-06	2.336E-07
L-Carnitine	2.77	51.94	8.940E-10	3.803E-10
Adenosine 5-Diphosphoribose	23.95	51.61	9.943E-04	1.090E-03
Cytidine 5-Diphosphate	8.93	27.69	1.493E-03	2.302E-16
Hypotaurine	3.76	26.32	8.670E-10	2.282E-08
D-Pantothenic Acid	1.93	25.23	1.161E-10	3.874E-11
Dihydroxyacetone Phosphate	107.83	23.32	4.144E-08	2.301E-08
5-Aminopentanoate	1.94	22.68	2.944E-07	9.738E-11
1-Methyladenosine	1.42	15.02	1.861E-08	2.107E-08
Cis-4-Hydroxy-D-Proline	1.49	14.01	6.058E-13	3.852E-06
Glutamate	3.61	13.57	8.874E-17	8.241E-12

Table II.1 continued

D-Saccharic Acid	3.55	13.04	9.100E-04	3.087E-25
Adenine	1.08	12.61	7.278E-03	1.452E-20
N-Methyl-L-Glutamate	3.25	11.69	1.659E-13	2.051E-17
Creatine Phosphate	15.62	11.50	5.916E-06	5.037E-04
Ophthalmic Acid	0.88	11.28	7.957E-06	1.009E-07
5-Hydroxyindoleacetate	0.18	10.98	4.235E-01	3.821E-09
5-Oxo-L-Proline	2.99	10.21	2.490E-17	1.945E-11
N-Acetyl-Dl-Glutamic Acid	2.17	9.83	1.230E-14	1.728E-16
(S)-Dihydroorotate	2.78	9.48	7.688E-03	3.697E-11
Creatine	2.10	8.96	1.301E-12	1.032E-18
L-Glutamine	1.41	8.39	1.905E-03	8.740E-15
Kynurenine	0.15	8.39	2.998E-01	9.835E-11
5-Methylthioadenosine	1.23	8.25	1.212E-02	2.673E-21
D-Alanine	2.06	8.25	4.593E-09	1.859E-09
3-Ureidopropionate	0.79	7.55	1.682E-06	4.322E-08
O-Succinyl-L-Homoserine	2.28	7.44	2.281E-07	7.025E-17
S-(5-Adenosyl)-L-Homocysteine	3.35	6.54	2.589E-06	1.059E-13
D-Tryptophan	0.26	6.46	6.893E-02	1.043E-09
Maleamate	0.67	6.44	8.916E-04	4.409E-07
Phospho(Enol)Pyruvic Acid	4.46	6.42	6.349E-04	1.414E-08
L-Serine	0.77	6.00	1.408E-06	4.373E-09
Thymidine 5-Monophosphate	0.44	5.44	3.613E-01	8.334E-14
Adenosine	0.92	5.35	6.980E-02	3.253E-12
Glycine	0.64	4.72	3.202E-03	1.407E-11
L-Pipecolic Acid	2.40	4.40	4.626E-03	2.161E-06
Uridine-5-Monophosphate	0.03	4.36	9.301E-01	3.404E-13
Nicotinamide	2.07	4.16	2.385E-13	9.482E-16
L-Proline	1.00	4.00	3.602E-09	1.609E-13
2-Aminoethyl Dihydrogen Phosphate	-0.02	3.70	9.277E-01	4.795E-21
O-Acetyl-L-Carnitine	0.50	3.45	1.100E-03	3.595E-09
N-Alpha-Acetyl-L-Asparagine	0.09	3.43	3.050E-01	3.844E-04
Allantoin	1.10	3.19	1.496E-08	2.138E-15
N-Acetyl-Dl-Methionine	-0.51	2.92	7.572E-02	8.150E-08
Pyridoxal	-0.04	2.90	7.436E-01	2.138E-10
N-Acetyl-Dl-Serine	1.95	2.87	7.313E-16	2.505E-31
Isocitric Acid/Citric Acid	0.41	2.54	1.221E-02	4.995E-13
Leucine/Isoleucine/Norleucine	-0.06	2.46	5.881E-01	1.412E-07
Methionine	-0.07	2.42	6.211E-01	2.838E-07

Table II.1 continued

L-Threonine/L-Allothreonine	0.56	2.31	2.283E-04	1.855E-06
Glycerol 2-Phosphate	1.89	1.94	2.991E-06	1.607E-09
Itaconate	0.44	1.93	5.340E-02	7.674E-18
Fumarate	0.43	1.91	8.270E-03	2.136E-14
L-Phenylalanine	-0.33	1.60	2.025E-03	6.442E-06
Gluconic Acid	0.96	1.59	8.051E-10	6.398E-19
4-Acetamidobutanoate	0.34	1.50	2.162E-01	6.946E-06
2-Hydroxyglutaric Acid	0.72	1.48	5.224E-02	2.900E-08
N-Acetyl-L-Phenylalanine	-0.16	1.46	1.636E-01	5.612E-08
Alpha-D-Glucose 1-Phosphate	1.31	1.42	1.323E-02	4.915E-07
4-Aminobutanoate/Gamma-Aminobutyric Acid	0.43	1.25	1.377E-03	8.596E-04
N-Acetylneuraminate	0.50	1.23	1.550E-03	7.909E-14
Taurine	0.39	1.05	5.043E-05	1.850E-17
L-Tyrosine	-0.23	0.97	3.019E-02	2.083E-05
2,4-Dihydroxypyrimidine-5-Carboxylic Acid/Orotic Acid	1.73	0.96	1.710E-04	1.503E-03
D-Glucose	0.16	0.87	3.859E-01	1.628E-03
Mannitol	1.46	0.73	1.117E-03	3.081E-04
Citrulline	0.16	0.69	4.490E-01	2.423E-02
Guanine	0.28	0.56	3.741E-01	1.536E-03
N-Acetyl-L-Aspartic Acid	1.69	0.54	2.187E-11	2.460E-03
5-Deoxyadenosine	2.58	0.54	2.861E-03	1.571E-02
N-Acetyl-L-Leucine	1.22	0.45	2.716E-01	1.630E-01
O-Succinyl-L-Homoserine	1.35	0.25	8.517E-11	1.792E-01
Urocanate	0.49	0.22	3.286E-01	3.030E-01
N-Acetyl-D-Galactosamine	0.31	0.07	3.159E-01	6.184E-01
L-Aspartate	0.02	0.03	8.624E-01	8.090E-01
6-Carboxyhexanoate	0.10	0.02	6.520E-01	8.796E-01
S-Carboxymethyl-L-Cysteine	-0.33	-1.00	1.771E-01	4.607E-08
Inosine	0.14	-0.96	5.807E-01	8.005E-13
Diethyl 2-Methyl-3-Oxosuccinate	-0.49	-0.96	9.086E-06	7.572E-15
Suberic Acid	-0.65	-0.94	1.387E-07	7.827E-13
Azelaic Acid	-0.60	-0.94	4.699E-06	1.326E-12
Palatinose/Maltulose	-0.50	-0.90	1.647E-03	4.215E-09
Xanthine	0.67	-0.89	1.310E-01	1.721E-07
D-Glyceric Acid	-0.51	-0.84	5.216E-05	3.748E-11
Methyl Beta-D-Galactoside	-0.53	-0.80	2.886E-04	1.121E-07
3-Hydroxy-3-Methylglutarate	-0.32	-0.79	3.519E-02	1.849E-08

Table II.1 continued

2-Oxobutanoate	-0.52	-0.75	3.418E-05	2.615E-09
3-Sulfino-L-Alanine	0.18	-0.71	3.996E-01	8.398E-11
D-Glucuronic Acid	-0.22	-0.71	3.164E-01	5.859E-05
6-Deoxy-L-Galactose	-0.68	-0.70	5.863E-06	6.330E-07
Nalpha-Acetyl-L-Lysine	-0.81	-0.68	1.611E-04	9.104E-04
Urate	-0.61	-0.65	1.971E-03	3.634E-04
Uridine	0.14	-0.65	6.280E-01	2.974E-06
2-Oxoadipate	-0.14	-0.62	2.429E-01	1.277E-05
4-Methyl-2-Oxo-Pentanoic Acid	-0.70	-0.57	3.545E-07	1.708E-05
Thymidine	-0.01	-0.55	9.513E-01	7.241E-04
Hypoxanthine	0.65	-0.52	7.892E-02	5.637E-06
Butanoate	-0.33	-0.51	1.585E-04	1.354E-08
Ll-2,6-Diaminoheptanedioate	-0.54	-0.51	2.176E-03	2.373E-03
D-Ribose 5-Phosphate	-0.39	-0.48	8.676E-02	7.388E-04
L-Cystine	4.08	-0.39	3.286E-05	4.010E-01
Cytidine	0.43	-0.36	2.339E-01	1.357E-03
Uracil	0.02	-0.34	9.240E-01	1.086E-02
Oxaloacetate	-0.21	-0.31	2.387E-01	9.243E-02
Arginine	-0.53	-0.30	3.595E-03	6.172E-02
L-Arabitol	-0.60	-0.30	4.506E-04	5.180E-01
Adipic Acid	-0.19	-0.30	1.057E-01	2.051E-02
Guanosine	0.07	-0.27	8.039E-01	1.045E-01
Dethiobiotin	0.01	-0.26	9.562E-01	3.449E-02
4-Guanidinobutanoate	0.17	-0.19	1.545E-01	3.623E-02
Succinate	-0.11	-0.19	3.465E-01	7.704E-02
Alpha-Ketoglutaric Acid	-0.35	-0.17	1.367E-01	5.350E-01
'4-Hydroxy-2-Quinolinecarboxylic Acid/Kynurenic Acid'	-0.38	-0.12	2.633E-05	2.442E-01
Dehydroascorbate	-0.36	-0.12	5.409E-03	3.717E-01
4-Imidazoleacetic Acid	0.45	-0.06	5.239E-02	5.203E-01
Deoxyuridine	1.14	-0.04	4.702E-04	9.387E-01

APPENDIX III: METABOLITES OF SIGNIFICANTLY DIFFERENTIAL ABUNDANCE IN VPA-TREATED E8.5 EMBRYOS

Table III.1 Metabolites of Significantly Differential Abundance in VPA-treated E8.5 Embryos

Fold change (FC) and p values are relative to untreated E8.5 embryos.

Metabolite	FC	p value	FDR
2,4-Dihydroxypyrimidine-5-Carboxylic Acid/Orotic Acid	231315.2	0.000101	0.000625
S-Carboxymethyl-L-Cysteine	136441.8	5.96E-06	5.07E-05
Inosine	388.4198	6.48E-09	2.94E-07
S-(5-Adenosyl)-L-Homocysteine	90.66007	6.03E-05	0.00039
Uridine	83.8889	2.05E-07	4.64E-06
Cytidine	69.24708	1.28E-09	8.7E-08
Hypoxanthine	67.47478	4.89E-10	6.64E-08
Guanosine	26.94608	1.05E-06	1.3E-05
Xanthine	23.79456	4.65E-06	4.21E-05
Nalpha-Acetyl-L-Lysine	16.10791	0.000147	0.000798
D-Ribose 5-Phosphate	11.32494	7.91E-07	1.35E-05
5-Deoxyadenosine	7.836279	1.84E-06	1.92E-05
Guanine	7.528564	1.01E-06	1.38E-05
N-Acetyl-Dl-Methionine	7.497179	0.005959	0.01529
N-Acetyl-D-Galactosamine	4.262983	9.55E-08	2.6E-06
Maleamate	3.152688	7.61E-09	2.59E-07
D-Glucuronic Acid	2.843835	0.001308	0.004449
Uracil	2.503613	0.001081	0.004083
Leucine/Isoleucine/Norleucine	2.306053	1.18E-05	8.94E-05
L-Phenylalanine	2.255653	7.68E-06	6.15E-05
Methionine	2.254925	0.000703	0.002812
Arginine	2.087436	0.007051	0.017758
Ophthalmic Acid	2.084014	0.003763	0.010889
Dethiobiotin	2.048023	0.003993	0.011083
D-Tryptophan	1.910766	0.001182	0.004346
L-Aspartate	1.698815	0.000644	0.002653
L-Tyrosine	1.65908	0.001038	0.004033
L-Threonine/L-Allothreonine	1.29459	0.014442	0.030217
2-Deoxyadenosine 5-Triphosphate	0.782845	0.01706	0.03412
O-Acetyl-L-Carnitine	0.702552	0.007168	0.017724

Table III.1 continued

Urocanate	0.694534	0.012178	0.02629
O-Succinyl-L-Homoserine	0.646731	0.003187	0.009849
4-Acetamidobutanoate	0.643921	0.012161	0.026675
N-Acetyl-L-Aspartic Acid	0.635882	0.000459	0.002082
3-Hydroxy-3-Methylglutarate	0.634816	0.007195	0.017473
2-Aminoethyl Dihydrogen Phosphate	0.625163	0.003489	0.010315
Taurine	0.617704	3.4E-05	0.000231
Isocitric Acid/Citric Acid	0.574861	0.01367	0.029049
Suberic Acid	0.573524	0.000277	0.001394
Diethyl 2-Methyl-3-Oxosuccinate	0.556856	0.000549	0.002332
5-Oxo-L-Proline	0.551748	0.00325	0.009823
Oxidized glutathione	0.534635	0.015881	0.032237
Azelaic Acid	0.534056	0.001801	0.005975
Butanoate	0.532508	0.007509	0.017915
N-Acetyl-L-Leucine	0.518602	0.018483	0.034912
Hypotaurine	0.505195	0.005851	0.015302
L-Glutamine	0.502684	0.003764	0.010665
Palatinose/Maltulose	0.495823	0.000305	0.00148
Itaconate	0.489953	2.17E-05	0.000156
Glutamate	0.472907	0.002128	0.006889
2-Oxobutanoate	0.468162	0.004097	0.011143
Oxaloacetate	0.39163	0.010129	0.022959
Dehydroascorbate	0.38198	0.001215	0.004238
Glycerol 2-Phosphate	0.372708	0.002176	0.006883
N-Acetyl-Dl-Serine	0.357209	1.32E-06	1.49E-05
L-Carnitine	0.308258	0.01757	0.034137
Creatine Phosphate	0.282662	0.015735	0.032425
Uridine-5-Monophosphate	0.277163	0.000112	0.000661
Mannitol	0.271321	2.72E-07	5.28E-06
Deoxyuridine	0.243961	0.004713	0.012568
O-Phospho-Dl-Serine	0.215642	0.001186	0.004246
Cytidine 5-Diphosphate	0.112252	0.007949	0.018639
L-Cystine	0.069638	0.000528	0.002315
Adenosine 5-Diphosphoribose	0.033814	0.017072	0.033649
Uridine 5-Diphosphate	0.030696	0.000141	0.000799
Guanosine 5-Diphosphate	0.023678	0.026051	0.047877

Table III.1 continued

Adenosine 3,5-Diphosphate	0.021049	0.000186	0.000971
Adenosine 5-Triphosphate	0.007915	0.011116	0.024782
Uridine 5-Diphospho-N-Acetylglucosamine	0.004405	8E-07	1.21E-05
Uridine 5-Diphosphogalactose	0.001925	2.23E-06	2.17E-05
NAD	0.001332	0.000319	0.001498
Uridine 5-Diphosphoglucuronic Acid	7.5E-05	0.008186	0.01887
Uridine 5-Triphosphate	2.44E-05	0.02495	0.046482
Cytidine 5-Triphosphate	1.81E-05	0.017974	0.034429

APPENDIX IV: METABOLITES OF SIGNIFICANTLY DIFFERENTIAL ABUNDANCE IN *LIKELY AFFECTED* E8.5 EMBRYOS COMPARED TO *LIKELY UNAFFECTED* E8.5 EMBRYOS

Table IV.1 Metabolites of Significantly Differential Abundance in *Likely Affected* E8.5 Embryos Compared to *Likely Unaffected* E8.5 Embryos

Fold change (FC) and p values are relative to *likely unaffected* E8.5 embryos.

Metabolite	**FC**	**p value**	**FDR**
Arginine	3.127258	0.001488	0.01124
Methionine	2.375961	8.87E-05	0.001341
D-Tryptophan	2.203482	1.16E-07	1.58E-05
L-Glutamine	2.053384	1.05E-06	7.15E-05
L-Phenylalanine	1.829388	3E-05	0.00068
L-Tyrosine	1.812679	0.0001	0.001362
Leucine/Isoleucine/Norleucine	1.749528	2.26E-05	0.000614
L-Serine	1.62573	0.000123	0.001515
L-Threonine/L-Allothreonine	1.404364	0.000887	0.008042
D-Alanine	1.380234	0.002674	0.015809
N-Acetyl-L-Aspartic Acid	0.627777	0.000508	0.00532
Taurine	0.599058	0.004087	0.021381
Uridine 5-Diphosphoglucuronic Acid	0.575828	0.002211	0.01432
3-Sulfino-L-Alanine	0.569848	0.00186	0.012647
D-Glyceric Acid	0.542208	0.005035	0.025359
Dehydroascorbate	0.538348	0.001368	0.010947
Diethyl 2-Methyl-3-Oxosuccinate	0.537697	0.003392	0.018453
Uracil	0.530414	0.010665	0.04679
Oxaloacetate	0.523749	0.006177	0.028001
3-Hydroxy-3-Methylglutarate	0.515073	0.002894	0.016398
Succinate	0.505727	0.005184	0.02518
Gluconic Acid	0.488355	5.77E-06	0.000262
Fumarate	0.472373	0.001598	0.011435
Itaconate	0.464116	0.000325	0.003679
Suberic Acid	0.446541	3.54E-05	0.000687
Azelaic Acid	0.418427	1.58E-05	0.000536
Allantoin	0.412202	0.000513	0.004987
6-Deoxy-L-Galactose	0.392875	0.002356	0.014564
Isocitric Acid/Citric Acid	0.392359	3.79E-05	0.000644
S-Carboxymethyl-L-Cysteine	0.368204	0.006032	0.02829
Urate	0.269401	0.000997	0.008476

APPENDIX V: LIST OF ACRONYMS

1-C	one-carbon
AdoMet	S-adenosylmethionine
AED	antiepileptic drug
ALDH	aldehyde dehydrogenase
ALDH1L1	aldehyde dehydrogenase 1-like
ALDH1L2	aldehyde dehydrogenase 1-like 2
AMT	amino-methyl transferase
ANOVA	analysis of variance
AP	anterior-posterior
ART	antiretroviral therapy
ATIC	inosine monophosphate synthase
ATP	adenosine triphosphate
BCM	Baylor College of Medicine
Cd	*Crooked Tail* allele
cDNA	complimentary DNA
CFD	cerebral folate deficiency
CH^+-THF	5,10-methenyl- THF
CH2-THF	5,10-methylene-THF
CH3-THF	5-methyl-THF
CHO	chinese hamster ovary
CHO-THF	10-formyl-THF
CNS	central nervous system
CO_2	carbon dioxide
CRISPR	clustered regularly interspaced short palindromic repeats
CV	coefficient of variation
DHF	dihydrofolate
DHFR	dihydrofolate reductase
DLHP	dorsolateral hinge points
DMEM	Dulbecco's modified Eagle's medium
DMGDH	dimethylglycine dehydrogenase
DNA	deoxyribonucleic acid
DPBS	Dulbecco's phosphate buffered saline
DTG	dolutegravir
EdU	ethynyl deoxyuridine
ELISA	enzyme-linked immunosorbent assay
ES	embryonic stem

FA	folic acid
FAD^+	flavin adenine dinucleotide
FA-HRP	folic acid-horseradish peroxidase
FBP	folate binding protein
FBS	fetal bovine serum
FC	fold change
FDA	Food and Drug Administration
FDR	false discovery rate
Fhs	10-formyltetrahydrofolate synthetase (prokaryotic)
FOLR1	folate receptor 1
FPGS	folylpolyglutamate synthetase
FR	folate receptors
GABA	γ-aminobutyric acid
GART	phosphoribosylglycinamide formyltransferase
GCS	glycine cleavage system
GLDC	glycine decarboxylase
GMP	guanosine monophosphate
GSEA	gene set enrichment analysis
Hcy	homocysteine
HDAC	histone deacetylase
HFM	hereditary folate malabsorption
HIF1α	hypoxia-inducible factor 1α
HIV	human immunodeficiency virus
HRP	horseradish peroxidase
IACUC	Institutional Animal Care and Use Committee
IR	infrared
KO	knockout
LC-MS	liquid chromatrography-mass spectrometry
L-NAME	L-nitro-arginine methyl ester
LRP2	low-density lipoprotein receptor-related protein 2
LRP6	low-density lipoprotein receptor-related protein 6
MAT1A	methionine adenosyl transferase 1A
MEF	mouse embryonic fibroblast
MEM	minimal essential medium
MESDC2	mesoderm development candidate gene 2
MFT	mitochondrial folate transporter
MHP	mediolateral hinge point
ML	mediolateral

mLIF	mouse leukemia inhibitory factor
mOCM	mitochondrial one-carbon metabolism
mRNA	messenger RNA
MS	mass spectrometry
MTFMT	methionyl-tRNA formyltransferase
MTHFD	5,10-methylene-THF dehydrogenase
MTHFD1L	methylene-tetrahydrofolate dehydrogenase 1-like
MTHFR	methylene tetrahydrofolate reductase
MTR	methionine synthase
MTRR	methionine synthase reductase
NAD^+	nicotinamide adenine dinucleotide
$NADP^+$	nicotinamide adenine dinucleotide phosphate
NaOH	sodium hydroxide
NO	nitric oxide
NOS	nitric oxide synthase
Nrf2	nuclear factor erythroid 2-related factor 2
NTC	neural tube closure
NTD	neural tube defect
O_2	molecular oxygen
OCM	one-carbon metabolism
PBS	phosphate buffered saline
PC	principal component
PCA	principal component analysis
PCFT	proton-coupled folate transporter
PCR	polymerase chain reaction
p-HWE	p-value for Hardy-Weinberg Equilibrium
PORCN	porcupine O-acyltransferase
PQN	probabilistic quotient normalization
QC	quality control
qPCR	quantitative PCR
RFC	reduced folate carrier
RNA	ribonucleic acid
RPMI	Roswell Park Memorial Institute
SAH	S-adenosylhomocysteine
SAM	S-adenosylmethionine
SARDH	sarcosine dehydrogenase
SEM	standard error of the mean

SHMT	serine hydroxymethyl transferase
SV40	simian vacuolating virus 40
SWV	swiss-vancouver
TBS	tris buffered saline
TBS-T	tris buffered saline with 0.05% Tween-20
TCF/LEF	T-cell factor/lymphoid enhancer factor
THF	tetrahydrofolate
tRNA-fMET	N-formylmethionyl-tRNA
TYMS	thymidylate synthase
UDP	uridine diphosphate
UHPLC	ultra high performance liquid chromatography
VPA	valproic acid
WHO	World Health Organization

References

Adamska, M., B. T. MacDonald, Z. H. Sarmast, E. R. Oliver, and M. H. Meisler. 2004. 'En1 and Wnt7a interact with Dkk1 during limb development in the mouse', *Dev Biol*, 272: 134-44.

Agarwal, S., M. Behring, K. Hale, S. Al Diffalha, K. Wang, U. Manne, and S. Varambally. 2019. 'MTHFD1L, A Folate Cycle Enzyme, Is Involved in Progression of Colorectal Cancer', *Transl Oncol*, 12: 1461-67.

Aires, C. C., G. Soveral, P. B. Luis, H. J. ten Brink, I. T. de Almeida, M. Duran, R. J. Wanders, and M. F. Silva. 2008. 'Pyruvate uptake is inhibited by valproic acid and metabolites in mitochondrial membranes', *FEBS Lett*, 582: 3359-66.

Akimova, D., B. J. Wlodarczyk, Y. Lin, M. E. Ross, R. H. Finnell, Q. Chen, and S. S. Gross. 2017. 'Metabolite profiling of whole murine embryos reveals metabolic perturbations associated with maternal valproate-induced neural tube closure defects', *Birth Defects Res*, 109: 106-19.

Al Mamun Bhuyan, A., E. Signoretto, R. Bissinger, and F. Lang. 2016. 'Enhanced Eryptosis Following Exposure to Dolutegravir', *Cell Physiol Biochem*, 39: 639-50.

Albrecht, L. V., M. H. Bui, and E. M. De Robertis. 2019. 'Canonical Wnt is inhibited by targeting one-carbon metabolism through methotrexate or methionine deprivation', *Proc Natl Acad Sci U S A*, 116: 2987-95.

Allache, R., S. Lachance, M. C. Guyot, P. De Marco, E. Merello, M. J. Justice, V. Capra, and Z. Kibar. 2014. 'Novel mutations in Lrp6 orthologs in mouse and human neural tube defects affect a highly dosage-sensitive Wnt non-canonical planar cell polarity pathway', *Hum Mol Genet*, 23: 1687-99.

Alonso-Aperte, E., N. Ubeda, M. Achon, J. Perez-Miguelsanz, and G. Varela-Moreiras. 1999. 'Impaired methionine synthesis and hypomethylation in rats exposed to valproate during gestation', *Neurology*, 52: 750-6.

Alves dos Santos, M. T., and M. P. Smidt. 2011. 'En1 and Wnt signaling in midbrain dopaminergic neuronal development', *Neural Dev*, 6: 23.

Anderson, D. D., and P. J. Stover. 2009. 'SHMT1 and SHMT2 are functionally redundant in nuclear de novo thymidylate biosynthesis', *PLoS One*, 4: e5839.

Anderson, D. D., C. F. Woeller, and P. J. Stover. 2007. 'Small ubiquitin-like modifier-1 (SUMO-1) modification of thymidylate synthase and dihydrofolate reductase', *Clin Chem Lab Med*, 45: 1760-3.

Appling, D. R., E. Kastanos, L. B. Pasternack, and Y. Y. Woldman. 1997. 'Use of 13C nuclear magnetic resonance to evaluate metabolic flux through folate one-carbon pools in Saccharomyces cerevisiae', *Methods Enzymol*, 281: 218-31.

Araya, C., L. C. Ward, G. C. Girdler, and M. Miranda. 2016. 'Coordinating cell and tissue behavior during zebrafish neural tube morphogenesis', *Dev Dyn*, 245: 197-208.

Bachar-Dahan, L., J. Goltzmann, A. Yaniv, and A. Gazit. 2006. 'Engrailed-1 negatively regulates beta-catenin transcriptional activity by destabilizing beta-catenin via a glycogen synthase kinase-3beta-independent pathway', *Mol Biol Cell*, 17: 2572-80.

Bailey, J. D., M. Diotallevi, T. Nicol, E. McNeill, A. Shaw, S. Chuaiphichai, A. Hale, A. Starr, M. Nandi, E. Stylianou, H. McShane, S. Davis, R. Fischer, B. M. Kessler, J. McCullagh, K. M. Channon, and M. J. Crabtree. 2019. 'Nitric Oxide Modulates Metabolic Remodeling in Inflammatory Macrophages through TCA Cycle Regulation and Itaconate Accumulation', *Cell Rep*, 28: 218-30 e7.

Baillie, J. K., M. G. Bates, A. A. Thompson, W. S. Waring, R. W. Partridge, M. F. Schnopp, A. Simpson, F. Gulliver-Sloan, S. R. Maxwell, and D. J. Webb. 2007. 'Endogenous urate production augments plasma antioxidant capacity in healthy lowland subjects exposed to high altitude', *Chest*, 131: 1473-8.

Barlowe, C. K., and D. R. Appling. 1988. 'In vitro evidence for the involvement of mitochondrial folate metabolism in the supply of cytoplasmic one-carbon units', *Biofactors*, 1: 171-6.

Bates, M.K. 2012. 'Culturing Cells Under Hypoxic Conditions for Biologically Relevant Results', *American Laboratory*.

Baumholtz, A. I., A. Simard, E. Nikolopoulou, M. Oosenbrug, M. M. Collins, A. Piontek, G. Krause, J. Piontek, N. D. E. Greene, and A. K. Ryan. 2017. 'Claudins are essential for cell shape changes and convergent extension movements during neural tube closure', *Dev Biol*, 428: 25-38.

Beck, S.L. 1999. 'Contributions of dam and conceptus to differences in sensitivity to valproic acid among C57 black and SWV mice', *Reprod Toxicol*, 13: 353-60.

Beck, S.L. 2001. 'Does genomic imprinting contribute to valproic acid teratogenicity?', *Reprod Toxicol*, 15: 43-48.

Benjamini, Y., and Y. Hochberg. 1995. 'Controlling the False Discovery Rate: A Pracitical and Powerful Approach to Multiple Testing', *Journal of the Royal Statistical Society, Series B (Methodological)*, 57: 289-300.

Binkerd, P. E., J. M. Rowland, H. Nau, and A. G. Hendrickx. 1988. 'Evaluation of valproic acid (VPA) developmental toxicity and pharmacokinetics in Sprague-Dawley rats', *Fundam Appl Toxicol*, 11: 485-93.

'Birth defects due to topical adapalene and tretinoin'. 1998. *Prescrire Int*, 7: 148-9.

Blencowe, H., V. Kancherla, S. Moorthie, M. W. Darlison, and B. Modell. 2018. 'Estimates of global and regional prevalence of neural tube defects for 2015: a systematic analysis', *Ann N Y Acad Sci*, 1414: 31-46.

Bolusani, S., B. A. Young, N. A. Cole, A. S. Tibbetts, J. Momb, J. D. Bryant, A. Solmonson, and D. R. Appling. 2011. 'Mammalian MTHFD2L encodes a mitochondrial methylenetetrahydrofolate dehydrogenase isozyme expressed in adult tissues', *J Biol Chem*, 286: 5166-74.

Boshnjaku, V., K. W. Shim, T. Tsurubuchi, S. Ichi, E. V. Szany, G. Xi, B. Mania-Farnell, D. G. McLone, T. Tomita, and C. S. Mayanil. 2012. 'Nuclear localization of folate receptor alpha: a new role as a transcription factor', *Sci Rep*, 2: 980.

Boyle, E. A., Y. I. Li, and J. K. Pritchard. 2017. 'An Expanded View of Complex Traits: From Polygenic to Omnigenic', *Cell*, 169: 1177-86.

Bray, N. L., H. Pimentel, P. Melsted, and L. Pachter. 2016. 'Near-optimal probabilistic RNA-seq quantification', *Nat Biotechnol*, 34: 525-7.

Brown, S. D., R. C. Twells, P. J. Hey, R. D. Cox, E. R. Levy, A. R. Soderman, M. L. Metzker, C. T. Caskey, J. A. Todd, and J. F. Hess. 1998. 'Isolation and characterization of LRP6, a novel member of the low density lipoprotein receptor gene family', *Biochem Biophys Res Commun*, 248: 879-88.

Bryant, J. D. 2017. 'Characterization of MTHFD2L Expression and Alternative Splicing and Loss of MTHFD1L Activity in Murine Emrbyos and Adults', *University of Texas Libraries Repository: Electronic Theses and Dissertations*.

Bryant, J. D., S. R. Sweeney, E. Sentandreu, M. Shin, H. Ipas, B. Xhemalce, J. Momb, S. Tiziani, and D. R. Appling. 2018. 'Deletion of the neural tube defect-associated gene Mthfd1l disrupts one-carbon and central energy metabolism in mouse embryos', *J Biol Chem*, 293: 5821-33.

Burton, G. J., and E. Jaunaiux. 2001. 'Maternal vascularisation of the human placenta: does the embryo develop in a hypoxic environment?', *Gynecol Obstet Fertil*, 29: 503-8.

Butler, M. T., and J. B. Wallingford. 2017. 'Planar cell polarity in development and disease', *Nat Rev Mol Cell Biol*, 18: 375-88.

Cabrera, R. M., G. M. Shaw, J. L. Ballard, S. L. Carmichael, W. Yang, E. J. Lammer, and R. H. Finnell. 2008. 'Autoantibodies to folate receptor during pregnancy and neural tube defect risk', *J Reprod Immunol*, 79: 85-92.

Cabrera, R. M., J. P. Souder, J. W. Steele, G. Tukeman, D. A. Gorelick, and R. H. Finnell. 2019. 'The antagonism of folate receptor by dolutegravir: developmental toxicity reduction by supplemental folic acid', *AIDS*, 33: 1967-76.

Cabrera, R. M.; Wlodarczyk, B.; Finnell, R.H. 2018. 'Elucidation of folate-mediated cascades in the developing neural tube: congenital malformations induced by methyltransferase inhibition', *J Mol Clin Med*, 1: 119-26.

Cai, C. Q., Y. L. Fang, J. B. Shu, L. S. Zhao, R. P. Zhang, L. R. Cao, Y. Z. Wang, X. F. Zhi, H. L. Cui, O. Y. Shi, and W. Liu. 2019. 'Association of neural tube defects with maternal alterations and genetic polymorphisms in one-carbon metabolic pathway', *Ital J Pediatr*, 45: 37.

Cao, L., C. Tan, F. Meng, P. Liu, E. A. Reece, and Z. Zhao. 2016. 'Amelioration of intracellular stress and reduction of neural tube defects in embryos of diabetic mice by phytochemical quercetin', *Sci Rep*, 6: 21491.

Carter, M., X. Chen, B. Slowinska, S. Minnerath, S. Glickstein, L. Shi, F. Campagne, H. Weinstein, and M. E. Ross. 2005. 'Crooked tail (Cd) model of human folate-responsive neural tube defects is mutated in Wnt coreceptor lipoprotein receptor-related protein 6', *Proc Natl Acad Sci U S A*, 102: 12843-8.

Carter, M., S. Ulrich, Y. Oofuji, D. A. Williams, and M. E. Ross. 1999. 'Crooked tail (Cd) models human folate-responsive neural tube defects', *Hum Mol Genet*, 8: 2199-204.

Centers for Disease, Control. 2016. 'Spina bifida'.

Chen, C., J. Ke, X. E. Zhou, W. Yi, J. S. Brunzelle, J. Li, E. L. Yong, H. E. Xu, and K. Melcher. 2013. 'Structural basis for molecular recognition of folic acid by folate receptors', *Nature*, 500: 486-9.

Chen, E. Y., M. Fujinaga, and A. J. Giaccia. 1999. 'Hypoxic microenvironment within an embryo induces apoptosis and is essential for proper morphological development', *Teratology*, 60: 215-25.

Chen, Z., Y. Lei, Y. Zheng, V. Aguiar-Pulido, M. E. Ross, R. Peng, L. Jin, T. Zhang, R. H. Finnell, and H. Wang. 2018. 'Threshold for neural tube defect risk by accumulated singleton loss-of-function variants', *Cell Res*, 28: 1039-41.

Colman, N., N. Hettiarachchy, and V. Herbert. 1981. 'Detection of a milk factor that facilitates folate uptake by intestinal cells', *Science*, 211: 1427-9.

Copp, A. J., and N. D. Greene. 2010. 'Genetics and development of neural tube defects', *J Pathol*, 220: 217-30.

Cordes, T., A. Lucas, A. S. Divakaruni, A. N. Murphy, P. Cabrales, and C. M. Metallo. 2020. 'Itaconate modulates tricarboxylic acid and redox metabolism to mitigate reperfusion injury', *Mol Metab*, 32: 122-35.

de Bakker, B. S., S. Driessen, B. J. D. Boukens, M. J. B. van den Hoff, and R. J. Oostra. 2017. 'Single-site neural tube closure in human embryos revisited', *Clin Anat*, 30: 988-99.

de la Cruz, J. M., R. N. Bamford, R. D. Burdine, E. Roessler, A. J. Barkovich, D. Donnai, A. F. Schier, and M. Muenke. 2002. 'A loss-of-function mutation in the CFC domain of TDGF1 is associated with human forebrain defects', *Hum Genet*, 110: 422-8.

De Marco, P., M. G. Calevo, A. Moroni, E. Merello, A. Raso, R. H. Finnell, H. Zhu, L. Andreussi, A. Cama, and V. Capra. 2003. 'Reduced folate carrier polymorphism (80A-->G) and neural tube defects', *Eur J Hum Genet*, 11: 245-52.

Dieterle, F., A. Ross, G. Schlotterbeck, and H. Senn. 2006. 'Probabilistic quotient normalization as robust method to account for dilution of complex biological mixtures. Application in 1H NMR metabonomics', *Analytical chemistry*, 78: 4281-90.

Dong, D., E. A. Reece, and P. Yang. 2016. 'The Nrf2 Activator Vinylsulfone Reduces High Glucose-Induced Neural Tube Defects by Suppressing Cellular Stress and Apoptosis', *Reprod Sci*, 23: 993-1000.

Dorokhov, Y. L., A. V. Shindyapina, E. V. Sheshukova, and T. V. Komarova. 2015. 'Metabolic methanol: molecular pathways and physiological roles', *Physiol Rev*, 95: 603-44.

Ducker, G. S., L. Chen, R. J. Morscher, J. M. Ghergurovich, M. Esposito, X. Teng, Y. Kang, and J. D. Rabinowitz. 2016. 'Reversal of Cytosolic One-Carbon Flux Compensates for Loss of the Mitochondrial Folate Pathway', *Cell Metab*, 23: 1140-53.

Ducker, G. S., and J. D. Rabinowitz. 2017. 'One-Carbon Metabolism in Health and Disease', *Cell Metab*, 25: 27-42.

Dunwoodie, S. L. 2009. 'The role of hypoxia in development of the Mammalian embryo', *Dev Cell*, 17: 755-73.

Ebrahimi, K. B., M. Cano, J. Rhee, S. Datta, L. Wang, and J. T. Handa. 2018. 'Oxidative Stress Induces an Interactive Decline in Wnt and Nrf2 Signaling in Degenerating Retinal Pigment Epithelium', *Antioxid Redox Signal*, 29: 389-407.

Eich, M. L., M. D. C. Rodriguez Pena, D. S. Chandrashekar, A. Chaux, S. Agarwal, J. B. Gordetsky, J. E. Ferguson, G. P. Sonpavde, G. J. Netto, and S. Varambally. 2019. 'Expression and Role of Methylenetetrahydrofolate Dehydrogenase 1 Like (MTHFD1L) in Bladder Cancer', *Transl Oncol*, 12: 1416-24.

Eom, D. S., S. Amarnath, and S. Agarwala. 2013. 'Apicobasal polarity and neural tube closure', *Dev Growth Differ*, 55: 164-72.

Ernest, S., M. Carter, H. Shao, A. Hosack, N. Lerner, C. Colmenares, D. S. Rosenblatt, Y. H. Pao, M. E. Ross, and J. H. Nadeau. 2006. 'Parallel changes in metabolite and expression profiles in crooked-tail mutant and folate-reduced wild-type mice', *Hum Mol Genet*, 15: 3387-93.

Escuin, S., B. Vernay, D. Savery, C. B. Gurniak, W. Witke, N. D. Greene, and A. J. Copp. 2015. 'Rho-kinase-dependent actin turnover and actomyosin disassembly are necessary for mouse spinal neural tube closure', *J Cell Sci*, 128: 2468-81.

Eszlari, N., D. Kovacs, P. Petschner, D. Pap, X. Gonda, R. Elliott, I. M. Anderson, J. F. Deakin, G. Bagdy, and G. Juhasz. 2016. 'Distinct effects of folate pathway genes MTHFR and MTHFD1L on ruminative response style: a potential risk mechanism for depression', *Transl Psychiatry*, 6: e745.

Etheredge, A. J., R. H. Finnell, S. L. Carmichael, E. J. Lammer, H. Zhu, L. E. Mitchell, and G. M. Shaw. 2012. 'Maternal and infant gene-folate interactions and the risk of neural tube defects', *Am J Med Genet A*, 158A: 2439-46.

Fathe, K. 2014. 'Dietary and Genetic Influences on Neural Tube Defects', *University of Texas Libraries Repository: Electronic Theses and Dissertations*.

Fathe, K., A. Palacios, and R. H. Finnell. 2014. 'Brief report novel mechanism for valproate-induced teratogenicity', *Birth Defects Res A Clin Mol Teratol*, 100: 592-7.

Ferreira, A. V., M. G. Netea, and J. Dominguez-Andres. 2019. 'Itaconate as an immune modulator', *Aging (Albany NY)*, 11: 3898-99.

Field, M. S., E. Kamynina, O. C. Agunloye, R. P. Liebenthal, S. G. Lamarre, M. E. Brosnan, J. T. Brosnan, and P. J. Stover. 2014. 'Nuclear enrichment of folate cofactors and methylenetetrahydrofolate dehydrogenase 1 (MTHFD1) protect de novo thymidylate biosynthesis during folate deficiency', *J Biol Chem*, 289: 29642-50.

Findley, T. O., J. C. Tenpenny, M. R. O'Byrne, A. C. Morrison, J. E. Hixson, H. Northrup, and K. S. Au. 2017. 'Mutations in folate transporter genes and risk for human myelomeningocele', *Am J Med Genet A*, 173: 2973-84.

Finnell, R. H., G. D. Bennett, S. B. Karras, and V. K. Mohl. 1988. 'Common hierarchies of susceptibility to the induction of neural tube defects in mouse embryos by valproic acid and its 4-propyl-4-pentenoic acid metabolite', *Teratology*, 38: 313-20.

Finnell, R. H., J. Gelineau-van Waes, G. D. Bennett, R. C. Barber, B. Wlodarczyk, G. M. Shaw, E. J. Lammer, J. A. Piedrahita, and J. H. Eberwine. 2000. 'Genetic basis of susceptibility to environmentally induced neural tube defects', *Ann N Y Acad Sci*, 919: 261-77.

Finnell, R. H., S. P. Moon, L. C. Abbott, J. A. Golden, and G. F. Chernoff. 1986. 'Strain differences in heat-induced neural tube defects in mice', *Teratology*, 33: 247-52.

Finnell, R. H., B. C. Wlodarczyk, J. C. Craig, J. A. Piedrahita, and G. D. Bennett. 1997. 'Strain-dependent alterations in the expression of folate pathway genes following teratogenic exposure to valproic acid in a mouse model', *Am J Med Genet*, 70: 303-11.

'Folic acid to prevent neural tube defects'. 1991. *Lancet*, 338: 379-80.

Franke, B., S. H. Vermeulen, R. P. Steegers-Theunissen, M. J. Coenen, M. M. Schijvenaars, H. Scheffer, M. den Heijer, and H. J. Blom. 2009. 'An association study of 45 folate-related genes in spina bifida: Involvement of cubilin (CUBN) and tRNA aspartic acid methyltransferase 1 (TRDMT1)', *Birth Defects Res A Clin Mol Teratol*, 85: 216-26.

Frey, B. N., S. S. Valvassori, G. Z. Reus, M. R. Martins, F. C. Petronilho, K. Bardini, F. Dal-Pizzol, F. Kapczinski, and J. Quevedo. 2006. 'Effects of lithium and valproate on amphetamine-induced oxidative stress generation in an animal model of mania', *J Psychiatry Neurosci*, 31: 326-32.

Garcia-Martinez, L. F., and D. R. Appling. 1993. 'Characterization of the folate-dependent mitochondrial oxidation of carbon 3 of serine', *Biochemistry*, 32: 4671-6.

Gelineau-van Waes, J., S. Heller, L. K. Bauer, J. Wilberding, J. R. Maddox, F. Aleman, T. H. Rosenquist, and R. H. Finnell. 2008. 'Embryonic development in the reduced folate carrier knockout mouse is modulated by maternal folate supplementation', *Birth Defects Res A Clin Mol Teratol*, 82: 494-507.

Graham, C. H., T. S. Hawley, R. G. Hawley, J. R. MacDougall, R. S. Kerbel, N. Khoo, and P. K. Lala. 1993. 'Establishment and characterization of first trimester human trophoblast cells with extended lifespan', *Exp Cell Res*, 206: 204-11.

Gray, J. D., S. Kholmanskikh, B. S. Castaldo, A. Hansler, H. Chung, B. Klotz, S. Singh, A. M. Brown, and M. E. Ross. 2013. 'LRP6 exerts non-canonical effects on Wnt signaling during neural tube closure', *Hum Mol Genet*, 22: 4267-81.

Gray, J. D., G. Nakouzi, B. Slowinska-Castaldo, J. E. Dazard, J. S. Rao, J. H. Nadeau, and M. E. Ross. 2010. 'Functional interactions between the LRP6 WNT co-receptor and folate supplementation', *Hum Mol Genet*, 19: 4560-72.

Gray, J. D., and M. E. Ross. 2009. 'Mechanistic insights into folate supplementation from Crooked tail and other NTD-prone mutant mice', *Birth Defects Res A Clin Mol Teratol*, 85: 314-21.

Greene, N. D., and A. J. Copp. 2009. 'Development of the vertebrate central nervous system: formation of the neural tube', *Prenat Diagn*, 29: 303-11.

Greene, N. D., and A. J. Copp. 2014. 'Neural tube defects', *Annu Rev Neurosci*, 37: 221-42.

Greene, N. D., K. Y. Leung, and A. J. Copp. 2017. 'Inositol, neural tube closure and the prevention of neural tube defects', *Birth Defects Res*, 109: 68-80.

Greene, N. D., K. Y. Leung, V. Gay, K. Burren, K. Mills, L. S. Chitty, and A. J. Copp. 2016. 'Inositol for the prevention of neural tube defects: a pilot randomised controlled trial', *Br J Nutr*, 115: 974-83.

Grootveld, M., and B. Halliwell. 1987. 'Measurement of allantoin and uric acid in human body fluids. A potential index of free-radical reactions in vivo?', *Biochem J*, 243: 803-8.

Groves, J. T., and C. C. Wang. 2000. 'Nitric oxide synthase: models and mechanisms', *Curr Opin Chem Biol*, 4: 687-95.

Haigo, S. L., J. D. Hildebrand, R. M. Harland, and J. B. Wallingford. 2003. 'Shroom induces apical constriction and is required for hingepoint formation during neural tube closure', *Curr Biol*, 13: 2125-37.

Hansler, A., Q. Chen, J. D. Gray, M. E. Ross, R. H. Finnell, and S. S. Gross. 2014. 'Untargeted metabolite profiling of murine embryos to reveal metabolic perturbations associated with neural tube closure defects', *Birth Defects Res A Clin Mol Teratol*, 100: 623-32.

Harris, M. J., and D. M. Juriloff. 2007. 'Mouse mutants with neural tube closure defects and their role in understanding human neural tube defects', *Birth Defects Res A Clin Mol Teratol*, 79: 187-210.

Harris, M. J., and D. M. Juriloff. 2010. 'An update to the list of mouse mutants with neural tube closure defects and advances toward a complete genetic perspective of neural tube closure', *Birth Defects Res A Clin Mol Teratol*, 88: 653-69.

Hendrickx, A. G., H. Nau, P. Binkerd, J. M. Rowland, J. R. Rowland, M. J. Cukierski, and M. A. Cukierski. 1988. 'Valproic acid developmental toxicity and pharmacokinetics in the rhesus monkey: an interspecies comparison', *Teratology*, 38: 329-45.

Heseker, H. B., J. B. Mason, J. Selhub, I. H. Rosenberg, and P. F. Jacques. 2009. 'Not all cases of neural-tube defect can be prevented by increasing the intake of folic acid', *Br J Nutr*, 102: 173-80.

Hsieh, C. L., H. E. Wang, W. J. Tsai, C. C. Peng, and R. Y. Peng. 2012. 'Multiple point action mechanism of valproic acid-teratogenicity alleviated by folic acid, vitamin C, and N-acetylcysteine in chicken embryo model', *Toxicology*, 291: 32-42.

Hubacek, J. A., V. Stanek, M. Gebauerova, R. Poledne, M. Aschermann, H. Skalicka, J. Matouskova, A. Kruger, M. Penicka, H. Hrabakova, J. Veselka, P. Hajek, V. Lanska, V. Adamkova, and J. Pit ha. 2015. 'Rs6922269 marker at the MTHFD1L gene predict cardiovascular mortality in males after acute coronary syndrome', *Mol Biol Rep*, 42: 1289-93.

Huebner, R. J., and J. B. Wallingford. 2018. 'Coming to Consensus: A Unifying Model Emerges for Convergent Extension', *Dev Cell*, 46: 389-96.

Jiang, J., Y. Zhang, L. Wei, Z. Sun, and Z. Liu. 2014. 'Association between MTHFD1 G1958A polymorphism and neural tube defects susceptibility: a meta-analysis', *PLoS One*, 9: e101169.

Johannessen, C. U., and S. I. Johannessen. 2003. 'Valproate: past, present, and future', *CNS Drug Rev*, 9: 199-216.

Johannessen, C. U., D. Petersen, F. Fonnum, and B. Hassel. 2001. 'The acute effect of valproate on cerebral energy metabolism in mice', *Epilepsy Res*, 47: 247-56.

Kancherla, V., K. Wagh, Q. Johnson, and G. P. Oakley, Jr. 2018. 'A 2017 global update on folic acid-preventable spina bifida and anencephaly', *Birth Defects Res*, 110: 1139-47.

Kang, Y., S. Tiziani, G. Park, M. Kaul, and G. Paternostro. 2014. 'Cellular protection using Flt3 and PI3K alpha inhibitors demonstrates multiple mechanisms of oxidative glutamate toxicity', *Nature Communications*, 5.

Kao, F., L. Chasin, and T. T. Puck. 1969. 'Genetics of somatic mammalian cells. X. Complementation analysis of glycine-requiring mutants', *Proc Natl Acad Sci U S A*, 64: 1284-91.

Kastanos, E. K., Y. Y. Woldman, and D. R. Appling. 1997. 'Role of mitochondrial and cytoplasmic serine hydroxymethyltransferase isozymes in de novo purine synthesis in Saccharomyces cerevisiae', *Biochemistry*, 36: 14956-64.

Khaksary Mahabady, M., M. R. Gholami, H. Najafzadeh Varzi, A. Zendedel, and M. Doostizadeh. 2016. 'Protective effect of quercetin on skeletal and neural tube teratogenicity induced by cyclophosphamide in rat fetuses', *Vet Res Forum*, 7: 133-8.

Khan, S., T. Ahmad, C. V. Parekh, P. P. Trivedi, S. Kushwaha, and G. Jena. 2011. 'Investigation on sodium valproate induced germ cell damage, oxidative stress and genotoxicity in male Swiss mice', *Reprod Toxicol*, 32: 385-94.

Kikuchi, G., Y. Motokawa, T. Yoshida, and K. Hiraga. 2008. 'Glycine cleavage system: reaction mechanism, physiological significance, and hyperglycinemia', *Proc Jpn Acad Ser B Phys Biol Sci*, 84: 246-63.

Kim, D. W., T. Huang, D. Schirch, and V. Schirch. 1996. 'Properties of tetrahydropteroylpentaglutamate bound to 10-formyltetrahydrofolate dehydrogenase', *Biochemistry*, 35: 15772-83.

Kim, J., Y. Lei, J. Guo, S. E. Kim, B. J. Wlodarczyk, R. M. Cabrera, Y. L. Lin, T. K. Nilsson, T. Zhang, A. Ren, L. Wang, Z. Yuan, Y. F. Zheng, H. Y. Wang, and R. H. Finnell. 2018. 'Formate rescues neural tube defects caused by mutations in Slc25a32', *Proc Natl Acad Sci U S A*, 115: 4690-95.

Kokubu, C., U. Heinzmann, T. Kokubu, N. Sakai, T. Kubota, M. Kawai, M. B. Wahl, J. Galceran, R. Grosschedl, K. Ozono, and K. Imai. 2004. 'Skeletal defects in ringelschwanz mutant mice reveal that Lrp6 is required for proper somitogenesis and osteogenesis', *Development*, 131: 5469-80.

Krupenko, N. I., M. E. Dubard, K. C. Strickland, K. M. Moxley, N. V. Oleinik, and S. A. Krupenko. 2010. 'ALDH1L2 is the mitochondrial homolog of 10-formyltetrahydrofolate dehydrogenase', *J Biol Chem*, 285: 23056-63.

Kur, E., N. Mecklenburg, R. M. Cabrera, T. E. Willnow, and A. Hammes. 2014. 'LRP2 mediates folate uptake in the developing neural tube', *J Cell Sci*, 127: 2261-8.

Labuschagne, C. F., N. J. van den Broek, G. M. Mackay, K. H. Vousden, and O. D. Maddocks. 2014. 'Serine, but not glycine, supports one-carbon metabolism and proliferation of cancer cells', *Cell Rep*, 7: 1248-58.

Large, C. H., M. Kalinichev, A. Lucas, C. Carignani, A. Bradford, N. Garbati, I. Sartori, N. E. Austin, A. Ruffo, D. N. Jones, G. Alvaro, and K. D. Read. 2009. 'The relationship between sodium channel inhibition and anticonvulsant activity in a model of generalised seizure in the rat', *Epilepsy Res*, 85: 96-106.

Lawrence, S. A., J. C. Hackett, and R. G. Moran. 2011. 'Tetrahydrofolate recognition by the mitochondrial folate transporter', *J Biol Chem*, 286: 31480-9.

Lawrence, S. A., S. A. Titus, J. Ferguson, A. L. Heineman, S. M. Taylor, and R. G. Moran. 2014. 'Mammalian mitochondrial and cytosolic folylpolyglutamate synthetase maintain the subcellular compartmentalization of folates', *J Biol Chem*, 289: 29386-96.

Lee, D., I. M. Xu, D. K. Chiu, R. K. Lai, A. P. Tse, L. Lan Li, C. T. Law, F. H. Tsang, L. L. Wei, C. Y. Chan, C. M. Wong, I. O. Ng, and C. C. Wong. 2017. 'Folate cycle enzyme MTHFD1L confers metabolic advantages in hepatocellular carcinoma', *J Clin Invest*, 127: 1856-72.

Lehninger, A. L., D. L. Nelson, and M. M. Cox. 2013. *Lehninger principles of biochemistry* (W.H. Freeman: New York).

Lei, Y., K. Fathe, D. McCartney, H. Zhu, W. Yang, M. E. Ross, G. M. Shaw, and R. H. Finnell. 2015. 'Rare LRP6 variants identified in spina bifida patients', *Hum Mutat*, 36: 342-9.

Leung, K. Y., S. C. De Castro, D. Savery, A. J. Copp, and N. D. Greene. 2013. 'Nucleotide precursors prevent folic acid-resistant neural tube defects in the mouse', *Brain*, 136: 2836-41.

Leung, K. Y., Y. J. Pai, Q. Chen, C. Santos, E. Calvani, S. Sudiwala, D. Savery, M. Ralser, S. S. Gross, A. J. Copp, and N. D. E. Greene. 2017. 'Partitioning of One-Carbon Units in Folate and Methionine Metabolism Is Essential for Neural Tube Closure', *Cell Rep*, 21: 1795-808.

Li, H., X. Fu, F. Yao, T. Tian, C. Wang, and A. Yang. 2019. 'MTHFD1L-Mediated Redox Homeostasis Promotes Tumor Progression in Tongue Squamous Cell Carcinoma', *Front Oncol*, 9: 1278.

Li, R., M. Chase, S. K. Jung, P. J. Smith, and M. R. Loeken. 2005. 'Hypoxic stress in diabetic pregnancy contributes to impaired embryo gene expression and defective development by inducing oxidative stress', *Am J Physiol Endocrinol Metab*, 289: E591-9.

Lipson, A. H., F. Collins, and W. S. Webster. 1993. 'Multiple congenital defects associated with maternal use of topical tretinoin', *Lancet*, 341: 1352-3.

Liu, D., J. Xue, Y. Liu, H. Gu, X. Wei, W. Ma, W. Luo, L. Ma, S. Jia, N. Dong, J. Huang, Y. Wang, and Z. Yuan. 2018. 'Inhibition of NRF2 signaling and increased reactive oxygen species during embryogenesis in a rat model of retinoic acid-induced neural tube defects', *Neurotoxicology*, 69: 84-92.

Liu, H., R. Y. Fu, Q. K. Liao, F. Y. Li, Y. P. Zhu, J. Gao, and Y. Q. Mao. 2009. '[Valproic acid induced intracellular GSH-redox imbalance and apoptosis of leukemic cells resistant to dexamethasone and doxorubicin]', *Sichuan Da Xue Xue Bao Yi Xue Ban*, 40: 133-7.

Lloyd, K.A. 2013. 'A scientific review: mechanisms of valproate-mediated teratogenesis', *BioscienceHorizons*, 6: 1-10.

Lodi, A. , A. Saha, X. Lu, B Wang, E. Sentandreu, M. Collins, M.G. Kolonin, J. DiGiovanni, and S. Tiziani. 2017. 'Combinatorial treatment with natural

compounds inhibits prostate tumor growth and leads to key modulations of cancer cell metabolism', *NPJ Precision Oncology*.

Lodi, A., S. Tiziani, F. L. Khanim, M. T. Drayson, U. L. Guenther, C. M. Bunce, and M. R. Viant. 2011. 'Hypoxia Triggers Major Metabolic Changes in AML Cells without Altering Indomethacin-Induced TCA Cycle Deregulation', *Acs Chemical Biology*, 6: 169-75.

Lodi, A., S. Tiziani, F. L. Khanim, U. L. Guenther, M. R. Viant, G. J. Morgan, C. M. Bunce, and M. T. Drayson. 2013. 'Proton NMR-Based Metabolite Analyses of Archived Serial Paired Serum and Urine Samples from Myeloma Patients at Different Stages of Disease Activity Identifies Acetylcarnitine as a Novel Marker of Active Disease', *Plos One*, 8.

Loges, N. T., H. Olbrich, L. Fenske, H. Mussaffi, J. Horvath, M. Fliegauf, H. Kuhl, G. Baktai, E. Peterffy, R. Chodhari, E. M. Chung, A. Rutman, C. O'Callaghan, H. Blau, L. Tiszlavicz, K. Voelkel, M. Witt, E. Zietkiewicz, J. Neesen, R. Reinhardt, H. M. Mitchison, and H. Omran. 2008. 'DNAI2 mutations cause primary ciliary dyskinesia with defects in the outer dynein arm', *Am J Hum Genet*, 83: 547-58.

Lopez-Escobar, B., B. J. Wlodarczyk, J. Caro-Vega, Y. Lin, R. H. Finnell, and P. Ybot-Gonzalez. 2019. 'The interaction of maternal diabetes with mutations that affect folate metabolism and how they affect the development of neural tube defects in mice', *Dev Dyn*, 248: 900-17.

Lu, X., A. Salmoson, A. Lodi, S. Nowinsky, E. Sentandreu, C. Riley, E. Mills, and S. Tiziani. 2017. 'The early metabolomic response of adipose tissue during acute cold exposure in mice', *Scientific Reports*, 7: 3455.

Lu, X., A. Solmonson, A. Lodi, S. M. Nowinski, E. Sentandreu, C. L. Riley, E. M. Mills, and S. Tiziani. 2017. 'The early metabolomic response of adipose tissue during acute cold exposure in mice', *Scientific Reports*, 7: 3455.

Lundberg, Y. W., R. M. Cabrera, K. A. Greer, J. Zhao, R. Garg, and R. H. Finnell. 2004. 'Mapping a chromosomal locus for valproic acid-induced exencephaly in mice', *Mamm Genome*, 15: 361-9.

Ma, X. Y., J. T. Yu, Z. C. Wu, Q. Zhang, Q. Y. Liu, H. F. Wang, W. Wang, and L. Tan. 2012. 'Replication of the MTHFD1L gene association with late-onset Alzheimer's disease in a Northern Han Chinese population', *J Alzheimers Dis*, 29: 521-5.

Mairuae, N., and P. Cheepsunthorn. 2018. 'Valproic acid attenuates nitric oxide and interleukin-1beta production in lipopolysaccharide-stimulated iron-rich microglia', *Biomed Rep*, 8: 359-64.

Marson, A.G., Sills, G.J. 2015. ' Chapter 51: Valproate. In: Shorvon S, Perucca E, Engel J, editors. The Treatment of Epilepsy 4th ed.', *John Wiley & Sons, Ltd*: 652-66.

Martinez-Reyes, I., and N. S. Chandel. 2014. 'Mitochondrial one-carbon metabolism maintains redox balance during hypoxia', *Cancer Discov*, 4: 1371-3.

Massa, V., R. M. Cabrera, E. Menegola, E. Giavini, and R. H. Finnell. 2005. 'Valproic acid-induced skeletal malformations: associated gene expression cascades', *Pharmacogenet Genomics*, 15: 787-800.

McBurney, M. W., and G. F. Whitmore. 1974. 'Characterization of a Chinese hamster cell with a temperature-sensitive mutation in folate metabolism', *Cell*, 2: 183-8.

McCarthy, E. A., S. A. Titus, S. M. Taylor, C. Jackson-Cook, and R. G. Moran. 2004. 'A mutation inactivating the mitochondrial inner membrane folate transporter creates a glycine requirement for survival of chinese hamster cells', *J Biol Chem*, 279: 33829-36.

McComb, J. G. 1997. 'Spinal and cranial neural tube defects', *Semin Pediatr Neurol*, 4: 156-66.

McDowell, M. M., J. E. Blatt, C. P. Deibert, N. T. Zwagerman, Z. J. Tempel, and S. Greene. 2018. 'Predictors of mortality in children with myelomeningocele and symptomatic Chiari type II malformation', *J Neurosurg Pediatr*, 21: 587-96.

McFarlane, A.J., Anderson, D.D., Flodby, P., Perry, C.A., Allen, R.H., Stabler, S.P., and Stover, P.J. 2011. 'Nuclear localization of de novo thymidylate biosynthesis pathway is required to prevent uracil accumulation in DNA', *J Biol Chem*, 286: 44015-22.

McKenzie, P, Lei, Y, Momb, J, Appling, D, Finnell, RH. 2018. 'A Common Variant in MTHFD1L is Associated with Increased Risk for Spina Bifida', *J Mol Clin Med*, 1: 19-22.

Meador, K. J., G. A. Baker, R. H. Finnell, L. A. Kalayjian, J. D. Liporace, D. W. Loring, G. Mawer, P. B. Pennell, J. C. Smith, M. C. Wolff, and Nead Study Group. 2006. 'In utero antiepileptic drug exposure: fetal death and malformations', *Neurology*, 67: 407-12.

Meador, K., M. W. Reynolds, S. Crean, K. Fahrbach, and C. Probst. 2008. 'Pregnancy outcomes in women with epilepsy: a systematic review and meta-analysis of published pregnancy registries and cohorts', *Epilepsy Res*, 81: 1-13.

Minguzzi, S., S. D. Selcuklu, C. Spillane, and A. Parle-McDermott. 2014. 'An NTD-associated polymorphism in the 3' UTR of MTHFD1L can affect disease risk by altering miRNA binding', *Hum Mutat*, 35: 96-104.

Minton, D. R., M. Nam, D. J. McLaughlin, J. Shin, E. C. Bayraktar, S. W. Alvarez, V. O. Sviderskiy, T. Papagiannakopoulos, D. M. Sabatini, K. Birsoy, and R. Possemato. 2018. 'Serine Catabolism by SHMT2 Is Required for Proper Mitochondrial Translation Initiation and Maintenance of Formylmethionyl-tRNAs', *Mol Cell*, 69: 610-21 e5.

Miyata, T., S. Takizawa, and C. van Ypersele de Strihou. 2011. 'Hypoxia. 1. Intracellular sensors for oxygen and oxidative stress: novel therapeutic targets', *Am J Physiol Cell Physiol*, 300: C226-31.

Mohanty, V., A. Shah, E. Allender, M. R. Siddiqui, S. Monick, S. Ichi, B. Mania-Farnell, G. McLone D, T. Tomita, and C. S. Mayanil. 2016. 'Folate Receptor Alpha Upregulates Oct4, Sox2 and Klf4 and Downregulates miR-138 and miR-let-7 in Cranial Neural Crest Cells', *Stem Cells*, 34: 2721-32.

Momb, J., and D. R. Appling. 2014. 'Mitochondrial one-carbon metabolism and neural tube defects', *Birth Defects Res A Clin Mol Teratol*, 100: 576-83.

Momb, J., J. P. Lewandowski, J. D. Bryant, R. Fitch, D. R. Surman, S. A. Vokes, and D. R. Appling. 2013. 'Deletion of Mthfd1l causes embryonic lethality and neural tube and craniofacial defects in mice', *Proc Natl Acad Sci U S A*, 110: 549-54.

Morland, C., K. Nordengen, and V. Gundersen. 2012. 'Valproate causes reduction of the excitatory amino acid aspartate in nerve terminals', *Neurosci Lett*, 527: 100-4.

Morrow, G. P., L. MacMillan, S. G. Lamarre, S. K. Young, A. J. MacFarlane, M. E. Brosnan, and J. T. Brosnan. 2015. 'In vivo kinetics of formate metabolism in folate-deficient and folate-replete rats', *J Biol Chem*, 290: 2244-50.

Morscher, R. J., G. S. Ducker, S. H. Li, J. A. Mayer, Z. Gitai, W. Sperl, and J. D. Rabinowitz. 2018. 'Mitochondrial translation requires folate-dependent tRNA methylation', *Nature*, 554: 128-32.

Nachmany, A., V. Gold, A. Tsur, D. Arad, and M. Weil. 2006. 'Neural tube closure depends on nitric oxide synthase activity', *J Neurochem*, 96: 247-53.

Nakatsu, T., C. Uwabe, and K. Shiota. 2000. 'Neural tube closure in humans initiates at multiple sites: evidence from human embryos and implications for the pathogenesis of neural tube defects', *Anat Embryol (Berl)*, 201: 455-66.

Narisawa, A., S. Komatsuzaki, A. Kikuchi, T. Niihori, Y. Aoki, K. Fujiwara, M. Tanemura, A. Hata, Y. Suzuki, C. L. Relton, J. Grinham, K. Y. Leung, D. Partridge, A. Robinson, V. Stone, P. Gustavsson, P. Stanier, A. J. Copp, N. D. Greene, T. Tominaga, Y. Matsubara, and S. Kure. 2012. 'Mutations in genes encoding the glycine cleavage system predispose to neural tube defects in mice and humans', *Hum Mol Genet*, 21: 1496-503.

Nau, H. 1985. 'Teratogenic valproic acid concentrations: infusion by implanted minipumps vs conventional injection regimen in the mouse', *Toxicol Appl Pharmacol*, 80: 243-50.

Nau, H., and R. Zierer. 1982. 'Pharmacokinetics of valproic acid and metabolites in mouse plasma and brain following constant-rate application of the drug and its unsaturated metabolite with an osmotic delivery system', *Biopharm Drug Dispos*, 3: 317-28.

Nicholls, P. 1975. 'Formate as an inhibitor of cytochrome c oxidase', *Biochem Biophys Res Commun*, 67: 610-6.

Nichols, J., K. Jones, J. M. Phillips, S. A. Newland, M. Roode, W. Mansfield, A. Smith, and A. Cooke. 2009. 'Validated germline-competent embryonic stem cell lines from nonobese diabetic mice', *Nat Med*, 15: 814-8.

Nieto-Patlan, E., J. Serafin-Lopez, I. Wong-Baeza, S. M. Perez-Tapia, L. Cobos-Marin, S. Estrada-Parra, I. Estrada-Garcia, A. D. Chavez-Blanco, and R. Chacon-Salinas. 2019. 'Valproic acid promotes a decrease in mycobacterial survival by enhancing nitric oxide production in macrophages stimulated with IFN-gamma', *Tuberculosis (Edinb)*, 114: 123-26.

Nikolopoulou, E., G. L. Galea, A. Rolo, N. D. Greene, and A. J. Copp. 2017. 'Neural tube closure: cellular, molecular and biomechanical mechanisms', *Development*, 144: 552-66.

Nikolopoulou, E., C. S. Hirst, G. Galea, C. Venturini, D. Moulding, A. R. Marshall, A. Rolo, S. C. P. De Castro, A. J. Copp, and N. D. E. Greene. 2019. 'Spinal neural tube closure depends on regulation of surface ectoderm identity and biomechanics by Grhl2', *Nat Commun*, 10: 2487.

O'Neill, L. A. J., and M. N. Artyomov. 2019. 'Itaconate: the poster child of metabolic reprogramming in macrophage function', *Nat Rev Immunol*, 19: 273-81.

O'Rahilly, R., and F. Muller. 2002. 'The two sites of fusion of the neural folds and the two neuropores in the human embryo', *Teratology*, 65: 162-70.

Okubo, T., S. Fujimoto, D. Hayashi, T. Suzuki, M. Sakaue, Y. Miyazaki, K. Tanaka, M. Usami, and T. Takizawa. 2019. 'Valproic acid promotes mature neuronal differentiation of adipose tissue-derived stem cells through iNOS-NO-sGC signaling pathway', *Nitric Oxide*, 93: 1-5.

Pai, Y. J., N. L. Abdullah, S. W. Mohd-Zin, R. S. Mohammed, A. Rolo, N. D. Greene, N. M. Abdul-Aziz, and A. J. Copp. 2012. 'Epithelial fusion during neural tube morphogenesis', *Birth Defects Res A Clin Mol Teratol*, 94: 817-23.

Pai, Y. J., K. Y. Leung, D. Savery, T. Hutchin, H. Prunty, S. Heales, M. E. Brosnan, J. T. Brosnan, A. J. Copp, and N. D. Greene. 2015. 'Glycine decarboxylase deficiency causes neural tube defects and features of non-ketotic hyperglycinemia in mice', *Nat Commun*, 6: 6388.

Palmer, B. R., S. Slow, K. L. Ellis, A. P. Pilbrow, L. Skelton, C. M. Frampton, S. C. Palmer, R. W. Troughton, T. G. Yandle, R. N. Doughty, G. A. Whalley, M. Lever, P. M. George, S. T. Chambers, C. Ellis, A. M. Richards, and V. A. Cameron. 2014. 'Genetic polymorphism rs6922269 in the MTHFD1L gene is associated with survival and baseline active vitamin B12 levels in post-acute coronary syndromes patients', *PLoS One*, 9: e89029.

Pangilinan, F., A. M. Molloy, J. L. Mills, J. F. Troendle, A. Parle-McDermott, C. Signore, V. B. O'Leary, P. Chines, J. M. Seay, K. Geiler-Samerotte, A. Mitchell, J. E. VanderMeer, K. M. Krebs, A. Sanchez, J. Cornman-Homonoff, N. Stone, M. Conley, P. N. Kirke, B. Shane, J. M. Scott, and L. C. Brody. 2012. 'Evaluation of common genetic variants in 82 candidate genes as risk factors for neural tube defects', *BMC Med Genet*, 13: 62.

Parchure, A., N. Vyas, and S. Mayor. 2018. 'Wnt and Hedgehog: Secretion of Lipid-Modified Morphogens', *Trends Cell Biol*, 28: 157-70.

Parle-McDermott, A., F. Pangilinan, K. K. O'Brien, J. L. Mills, A. M. Magee, J. Troendle, M. Sutton, J. M. Scott, P. N. Kirke, A. M. Molloy, and L. C. Brody. 2009. 'A common variant in MTHFD1L is associated with neural tube defects and mRNA splicing efficiency', *Hum Mutat*, 30: 1650-6.

Pasternack, L. B., D. A. Laude, Jr., and D. R. Appling. 1992. '13C NMR detection of folate-mediated serine and glycine synthesis in vivo in Saccharomyces cerevisiae', *Biochemistry*, 31: 8713-9.

Pasternack, L. B., D. A. Laude, Jr., and D. R. Appling. 1994. '13C NMR analysis of intercompartmental flow of one-carbon units into choline and purines in Saccharomyces cerevisiae', *Biochemistry*, 33: 74-82.

Pasternack, L. B., L. E. Littlepage, D. A. Laude, Jr., and D. R. Appling. 1996. '13C NMR analysis of the use of alternative donors to the tetrahydrofolate-dependent one-carbon pools in Saccharomyces cerevisiae', *Arch Biochem Biophys*, 326: 158-65.

Pennarun, G., C. Chapelin, E. Escudier, A. M. Bridoux, F. Dastot, V. Cacheux, M. Goossens, S. Amselem, and B. Duriez. 2000. 'The human dynein intermediate chain 2 gene (DNAI2): cloning, mapping, expression pattern, and evaluation as a candidate for primary ciliary dyskinesia', *Hum Genet*, 107: 642-9.

Perchiniak, E., S. A. Lawrence, S. Kasten, B. A. Woodard, S. M. Taylor, and R. G. Moran. 2007. 'Probing the mechanism of the hamster mitochondrial folate transporter by mutagenesis and homology modeling', *Biochemistry*, 46: 1557-67.

Petrere, J. A., J. A. Anderson, R. Sakowski, J. E. Fitzgerald, and F. A. de la Iglesia. 1986. 'Teratogenesis of calcium valproate in rabbits', *Teratology*, 34: 263-9.

Piao, W., J. Guo, Y. Bao, F. Wang, T. Zhang, J. Huo, and K. Zhang. 2016. 'Analysis of polymorphisms of genes associated with folate-mediated one-carbon metabolism and neural tube defects in Chinese Han Population', *Birth Defects Res A Clin Mol Teratol*, 106: 232-9.

Piedrahita, J. A., B. Oetama, G. D. Bennett, J. van Waes, B. A. Kamen, J. Richardson, S. W. Lacey, R. G. Anderson, and R. H. Finnell. 1999. 'Mice lacking the folic acid-binding protein Folbp1 are defective in early embryonic development', *Nat Genet*, 23: 228-32.

Pietzke, M., J. Meiser, and A. Vazquez. 2020. 'Formate metabolism in health and disease', *Mol Metab*, 33: 23-37.

Pike, S. T., R. Rajendra, K. Artzt, and D. R. Appling. 2010. 'Mitochondrial C1-tetrahydrofolate synthase (MTHFD1L) supports the flow of mitochondrial one-carbon units into the methyl cycle in embryos', *J Biol Chem*, 285: 4612-20.

Pinson, K. I., J. Brennan, S. Monkley, B. J. Avery, and W. C. Skarnes. 2000. 'An LDL-receptor-related protein mediates Wnt signalling in mice', *Nature*, 407: 535-8.

'Prevention of neural tube defects: results of the Medical Research Council Vitamin Study. MRC Vitamin Study Research Group'. 1991. *Lancet*, 338: 131-7.

Pugsley, M. K., E. J. Yu, T. H. McLean, and A. L. Goldin. 1999. 'Blockade of neuronal sodium channels by the antiepileptic drugs phenytoin, carbamazepine and sodium valproate', *Proc West Pharmacol Soc*, 42: 105-8.

Qiu, A., M. Jansen, A. Sakaris, S. H. Min, S. Chattopadhyay, E. Tsai, C. Sandoval, R. Zhao, M. H. Akabas, and I. D. Goldman. 2006. 'Identification of an intestinal folate transporter and the molecular basis for hereditary folate malabsorption', *Cell*, 127: 917-28.

Ray, H. J., and L. Niswander. 2012. 'Mechanisms of tissue fusion during development', *Development*, 139: 1701-11.

Reece, E. A., M. Khandelwal, Y. K. Wu, and M. Borenstein. 1997. 'Dietary intake of myo-inositol and neural tube defects in offspring of diabetic rats', *Am J Obstet Gynecol*, 176: 536-9.

Ren, R. J., L. L. Wang, R. Fang, L. H. Liu, Y. Wang, H. D. Tang, Y. L. Deng, W. Xu, G. Wang, and S. D. Chen. 2011. 'The MTHFD1L gene rs11754661 marker is associated with susceptibility to Alzheimer's disease in the Chinese Han population', *J Neurol Sci*, 308: 32-4.

Rhinn, M., and P. Dolle. 2012. 'Retinoic acid signalling during development', *Development*, 139: 843-58.

Rogers, L. M., A. M. Cordero, C. M. Pfeiffer, D. B. Hausman, B. L. Tsang, L. M. De-Regil, J. Rosenthal, H. Razzaghi, E. C. Wong, A. P. Weakland, and L. B. Bailey. 2018. 'Global folate status in women of reproductive age: a systematic review with emphasis on methodological issues', *Ann N Y Acad Sci*, 1431: 35-57.

Rolo, A., D. Savery, S. Escuin, S. C. de Castro, H. E. Armer, P. M. Munro, M. A. Mole, N. D. Greene, and A. J. Copp. 2016. 'Regulation of cell protrusions by small GTPases during fusion of the neural folds', *Elife*, 5: e13273.

Roscoe B. Jackson Memorial Laboratory., and E. L. Green. 1966. *Biology of the laboratory mouse* (Blakiston Division: New York,).

Rothenberg, S. P., M. P. da Costa, J. M. Sequeira, J. Cracco, J. L. Roberts, J. Weedon, and E. V. Quadros. 2004. 'Autoantibodies against folate receptors in women with a pregnancy complicated by a neural-tube defect', *N Engl J Med*, 350: 134-42.

Sabers, A., and T. Tomson. 2009. 'Managing antiepileptic drugs during pregnancy and lactation', *Curr Opin Neurol*, 22: 157-61.

Sah, S., S. Aluri, K. Rex, and U. Varshney. 2015. 'One-carbon metabolic pathway rewiring in Escherichia coli reveals an evolutionary advantage of 10-formyltetrahydrofolate synthetase (Fhs) in survival under hypoxia', *J Bacteriol*, 197: 717-26.

Salojin, K. V., R. M. Cabrera, W. Sun, W. C. Chang, C. Lin, L. Duncan, K. A. Platt, R. Read, P. Vogel, Q. Liu, R. H. Finnell, and T. Oravecz. 2011. 'A mouse model of hereditary folate malabsorption: deletion of the PCFT gene leads to systemic folate deficiency', *Blood*, 117: 4895-904.

Sanghvi, T. G., P. W. Harvey, and E. Wainwright. 2010. 'Maternal iron-folic acid supplementation programs: evidence of impact and implementation', *Food Nutr Bull*, 31: S100-7.

Sankar, R. 2007. 'Teratogenicity of antiepileptic drugs: role of drug metabolism and pharmacogenomics', *Acta Neurol Scand*, 116: 65-71.

Santoro, V., I. Kovalenko, K. Vriens, S. Christen, A. Bernthaler, A. Haegebarth, S. M. Fendt, and S. Christian. 2020. 'SLC25A32 sustains cancer cell proliferation by regulating flavin adenine nucleotide (FAD) metabolism', *Oncotarget*, 11: 801-12.

Santos, C., Y. J. Pai, M. R. Mahmood, K. Y. Leung, D. Savery, S. N. Waddington, A. J. Copp, and N. Greene. 2020. 'Impaired folate 1-carbon metabolism causes formate-preventable hydrocephalus in glycine decarboxylase-deficient mice', *J Clin Invest*, 130: 1446-52.

Schiff, M., A. Veauville-Merllie, C. H. Su, A. Tzagoloff, M. Rak, H. Ogier de Baulny, A. Boutron, H. Smedts-Walters, N. B. Romero, O. Rigal, P. Rustin, C. Vianey-Saban, and C. Acquaviva-Bourdain. 2016. 'SLC25A32 Mutations and Riboflavin-Responsive Exercise Intolerance', *N Engl J Med*, 374: 795-7.

Schweizer, L., and H. Varmus. 2003. 'Wnt/Wingless signaling through beta-catenin requires the function of both LRP/Arrow and frizzled classes of receptors', *BMC Cell Biol*, 4: 4.

Scott, D.F. 1993. 'The History of Epileptic Therapy: An Account of How Medication was Developed', *CRC Press*.

Semmler, A., C. Frisch, C. Bleul, D. Smith, L. Bigler, J. C. Prost, H. Blom, and M. Linnebank. 2017. 'Intrauterine valproate exposure is associated with alterations in

hippocampal cell numbers and folate metabolism in a rat model of valproate teratogenicity', *Seizure*, 46: 7-12.

Shah, R. H., H. Northrup, J. E. Hixson, A. C. Morrison, and K. S. Au. 2016. 'Genetic association of the glycine cleavage system genes and myelomeningocele', *Birth Defects Res A Clin Mol Teratol*, 106: 847-53.

Shane, B. 1989. 'Folylpolyglutamate synthesis and role in the regulation of one-carbon metabolism', *Vitam Horm*, 45: 263-335.

Shi, Z., X. Yang, B. B. Li, S. Chen, L. Yang, L. Cheng, T. Zhang, H. Wang, and Y. Zheng. 2018. 'Novel Mutation of LRP6 Identified in Chinese Han Population Links Canonical WNT Signaling to Neural Tube Defects', *Birth Defects Res*, 110: 63-71.

Shin, M., J. D. Bryant, J. Momb, and D. R. Appling. 2014. 'Mitochondrial MTHFD2L is a dual redox cofactor-specific methylenetetrahydrofolate dehydrogenase/ methenyltetrahydrofolate cyclohydrolase expressed in both adult and embryonic tissues', *J Biol Chem*, 289: 15507-17.

Shin, M., J. Momb, and D. R. Appling. 2017. 'Human mitochondrial MTHFD2 is a dual redox cofactor-specific methylenetetrahydrofolate dehydrogenase/ methenyltetrahydrofolate cyclohydrolase', *Cancer Metab*, 5: 11.

Shin, M., A. Vaughn, J. Momb, and D. R. Appling. 2019. 'Deletion of neural tube defect-associated gene Mthfd1l causes reduced cranial mesenchyme density', *Birth Defects Res*, 111: 1520-34.

Shum, A. S., and A. J. Copp. 1996. 'Regional differences in morphogenesis of the neuroepithelium suggest multiple mechanisms of spinal neurulation in the mouse', *Anat Embryol (Berl)*, 194: 65-73.

Simic, P., J. Willuhn, H. Sahm, and L. Eggeling. 2002. 'Identification of glyA (encoding serine hydroxymethyltransferase) and its use together with the exporter ThrE to increase L-threonine accumulation by Corynebacterium glutamicum', *Appl Environ Microbiol*, 68: 3321-7.

Song, I., J. Borland, N. Arya, B. Wynne, and S. Piscitelli. 2015. 'Pharmacokinetics of dolutegravir when administered with mineral supplements in healthy adult subjects', *J Clin Pharmacol*, 55: 490-6.

Spaan, A. N., L. Ijlst, C. W. van Roermund, F. A. Wijburg, R. J. Wanders, and H. R. Waterham. 2005. 'Identification of the human mitochondrial FAD transporter and

its potential role in multiple acyl-CoA dehydrogenase deficiency', *Mol Genet Metab*, 86: 441-7.

Steegers-Theunissen, R. P., G. H. Boers, F. J. Trijbels, J. D. Finkelstein, H. J. Blom, C. M. Thomas, G. F. Borm, M. G. Wouters, and T. K. Eskes. 1994. 'Maternal hyperhomocysteinemia: a risk factor for neural-tube defects?', *Metabolism*, 43: 1475-80.

Steele, J. W., S. Bayliss, J. Bayliss, Y. L. Lin, B. J. Wlodarczyk, R. M. Cabrera, Y. G. Asfaw, T. J. Cummings, R. H. Finnell, and T. M. George. 2020. 'Heritable spina bifida in sheep: A potential model for fetal repair of myelomeningocele', *J Pediatr Surg*, 55: 475-81.

Steele, J. W., S. E. Kim, and R. H. Finnell. 2020. 'One-carbon metabolism and folate transporter genes: Do they factor prominently in the genetic etiology of neural tube defects?', *Biochimie*.

Steinfeld, R., M. Grapp, R. Kraetzner, S. Dreha-Kulaczewski, G. Helms, P. Dechent, R. Wevers, S. Grosso, and J. Gartner. 2009. 'Folate receptor alpha defect causes cerebral folate transport deficiency: a treatable neurodegenerative disorder associated with disturbed myelin metabolism', *Am J Hum Genet*, 85: 354-63.

Strickland, K. C., N. I. Krupenko, M. E. Dubard, C. J. Hu, Y. Tsybovsky, and S. A. Krupenko. 2011. 'Enzymatic properties of ALDH1L2, a mitochondrial 10-formyltetrahydrofolate dehydrogenase', *Chem Biol Interact*, 191: 129-36.

Subramanian, A., P. Tamayo, V. K. Mootha, S. Mukherjee, B. L. Ebert, M. A. Gillette, A. Paulovich, S. L. Pomeroy, T. R. Golub, E. S. Lander, and J. P. Mesirov. 2005. 'Gene set enrichment analysis: a knowledge-based approach for interpreting genome-wide expression profiles', *Proc Natl Acad Sci U S A*, 102: 15545-50.

Sweeney, S. R, A. Kavanaugh, A. Lodi, B. Wang, D. Boyle, S. Tiziani, and M. Guma. 2016. 'Metabolomic profiling predicts outcome of rituximab therapy in rheumatoid arthritis', *RMD open*, 2: e000289.

Takada, S., S. Fujimori, T. Shinozuka, R. Takada, and Y. Mii. 2017. 'Differences in the secretion and transport of Wnt proteins', *J Biochem*, 161: 1-7.

Tamai, K., X. Zeng, C. Liu, X. Zhang, Y. Harada, Z. Chang, and X. He. 2004. 'A mechanism for Wnt coreceptor activation', *Mol Cell*, 13: 149-56.

Tan, C., F. Meng, E. A. Reece, and Z. Zhao. 2018. 'Modulation of nuclear factor-kappaB signaling and reduction of neural tube defects by quercetin-3-glucoside in embryos of diabetic mice', *Am J Obstet Gynecol*, 219: 197 e1-97 e8.

Tani, H., S. Ohnishi, H. Shitara, T. Mito, M. Yamaguchi, H. Yonekawa, O. Hashizume, K. Ishikawa, K. Nakada, and J. I. Hayashi. 2018. 'Mice deficient in the Shmt2 gene have mitochondrial respiration defects and are embryonic lethal', *Sci Rep*, 8: 425.

Taylor, R. T., and M. L. Hanna. 1977. 'Folate-dependent enzymes in cultured Chinese hamster cells: folypolyglutamate synthetase and its absence in mutants auxotrophic for glycine + adenosine + thymidine', *Arch Biochem Biophys*, 181: 331-4.

Taylor, R. T., and M. L. Hanna. 1982. 'Folate-dependent enzymes in cultured Chinese hamster ovary cells: impaired mitochondrial serine hydroxymethyltransferase activity in two additional glycine--auxotroph complementation classes', *Arch Biochem Biophys*, 217: 609-23.

Tibbetts, A. S., and D. R. Appling. 2010. 'Compartmentalization of Mammalian folate-mediated one-carbon metabolism', *Annu Rev Nutr*, 30: 57-81.

Tiboni, G. M., F. Chiarelli, and A. Verrotti. 2013. 'Inhibition of nitric oxide synthesis enhances teratogenic effects induced by valproic Acid', *In Vivo*, 27: 513-8.

Titus, S. A., and R. G. Moran. 2000. 'Retrovirally mediated complementation of the glyB phenotype. Cloning of a human gene encoding the carrier for entry of folates into mitochondria', *J Biol Chem*, 275: 36811-7.

Titus, S. A., Moran, R.G. 2000. 'Retrovirally mediated complementation of the glyB phenotype. Cloning of a human gene encoding the carrier for entry of folates into mitochondria', *Journal of Biological Chemistry*, 275: 36811-17.

Tiziani, S., Y. Kang, J. S. Choi, W. Roberts, and G. Paternostro. 2011. 'Metabolomic high-content nuclear magnetic resonance-based drug screening of a kinase inhibitor library', *Nature Communications*, 2.

Tiziani, S., Y. Kang, R. Harjanto, J. Axelrod, C. Piermarocchi, W. Roberts, and G. Paternostro. 2013. 'Metabolomics of the Tumor Microenvironment in Pediatric Acute Lymphoblastic Leukemia', *Plos One*, 8.

Tomson, T., and D. Battino. 2009. 'Teratogenic effects of antiepileptic medications', *Neurol Clin*, 27: 993-1002.

Tone, S., K. Sugimoto, K. Tanda, T. Suda, K. Uehira, H. Kanouchi, K. Samejima, Y. Minatogawa, and W. C. Earnshaw. 2007. 'Three distinct stages of apoptotic nuclear condensation revealed by time-lapse imaging, biochemical and electron microscopy analysis of cell-free apoptosis', *Exp Cell Res*, 313: 3635-44.

Tremolizzo, L., V. Rodriguez-Menendez, G. Sala, J. C. Di Francesco, and C. Ferrarese. 2005. 'Valproate and HDAC inhibition: a new epigenetic strategy to mitigate phenotypic severity in ALS?', *Amyotroph Lateral Scler Other Motor Neuron Disord*, 6: 185-6.

Tung, E. W., and L. M. Winn. 2011. 'Valproic acid increases formation of reactive oxygen species and induces apoptosis in postimplantation embryos: a role for oxidative stress in valproic acid-induced neural tube defects', *Mol Pharmacol*, 80: 979-87.

Vajda, F. 2012. 'Dose issues in antiepileptic therapy', *J Clin Neurosci*, 19: 1475-7.

Van Allen, M. I., D. K. Kalousek, G. F. Chernoff, D. Juriloff, M. Harris, B. C. McGillivray, S. L. Yong, S. Langlois, P. M. MacLeod, D. Chitayat, and et al. 1993. 'Evidence for multi-site closure of the neural tube in humans', *Am J Med Genet*, 47: 723-43.

Van Straaten, H. W., H. C. Janssen, M. C. Peeters, A. J. Copp, and J. W. Hekking. 1996. 'Neural tube closure in the chick embryo is multiphasic', *Dev Dyn*, 207: 309-18.

Wallingford, J. B. 2006. 'Planar cell polarity, ciliogenesis and neural tube defects', *Hum Mol Genet*, 15 Spec No 2: R227-34.

Wallingford, J. B. 2012. 'Planar cell polarity and the developmental control of cell behavior in vertebrate embryos', *Annu Rev Cell Dev Biol*, 28: 627-53.

Wallingford, J. B., S. E. Fraser, and R. M. Harland. 2002. 'Convergent extension: the molecular control of polarized cell movement during embryonic development', *Dev Cell*, 2: 695-706.

Wallingford, J. B., L. A. Niswander, G. M. Shaw, and R. H. Finnell. 2013. 'The continuing challenge of understanding, preventing, and treating neural tube defects', *Science*, 339: 1222002.

Walls, J. R., L. Coultas, J. Rossant, and R. M. Henkelman. 2008. 'Three-dimensional analysis of vascular development in the mouse embryo', *PLoS One*, 3: e2853.

Wang, L., Y. Xiao, T. Tian, L. Jin, Y. Lei, R. H. Finnell, and A. Ren. 2018. 'Digenic variants of planar cell polarity genes in human neural tube defect patients', *Mol Genet Metab*, 124: 94-100.

Weil, M., R. Abeles, A. Nachmany, V. Gold, and E. Michael. 2004. 'Folic acid rescues nitric oxide-induced neural tube closure defects', *Cell Death Differ*, 11: 361-3.

West, M. G., D. W. Horne, and D. R. Appling. 1996. 'Metabolic role of cytoplasmic isozymes of 5,10-methylenetetrahydrofolate dehydrogenase in Saccharomyces cerevisiae', *Biochemistry*, 35: 3122-32.

WHO. 2018. 'Updated recommendations on first-line and second-line antiretroviral regimens and postexposure prophylaxis and recommendations on early infant diagnosis of HIV. Supplement to the 2016 consolidated guidelines on the use of antiretroviral drugs for treating and preventing HIV infection.', *Geneva: World Health Organization*: 82.

Wilde, J. J., J. R. Petersen, and L. Niswander. 2014. 'Genetic, epigenetic, and environmental contributions to neural tube closure', *Annu Rev Genet*, 48: 583-611.

Williams, J., C. T. Mai, J. Mulinare, J. Isenburg, T. J. Flood, M. Ethen, B. Frohnert, R. S. Kirby, Control Centers for Disease, and Prevention. 2015. 'Updated estimates of neural tube defects prevented by mandatory folic Acid fortification - United States, 1995-2011', *MMWR Morb Mortal Wkly Rep*, 64: 1-5.

Williams, L. J., C. T. Mai, L. D. Edmonds, G. M. Shaw, R. S. Kirby, C. A. Hobbs, L. E. Sever, L. A. Miller, F. J. Meaney, and M. Levitt. 2002. 'Prevalence of spina bifida and anencephaly during the transition to mandatory folic acid fortification in the United States', *Teratology*, 66: 33-9.

Wittwer, A. J., and C. Wagner. 1980. 'Identification of folate binding protein of mitochondria as dimethylglycine dehydrogenase', *Proc Natl Acad Sci U S A*, 77: 4484-8.

Wlodarczyk, B. J., A. M. Palacios, T. M. George, and R. H. Finnell. 2012. 'Antiepileptic drugs and pregnancy outcomes', *Am J Med Genet A*, 158A: 2071-90.

Woeller, C. F., D. D. Anderson, D. M. Szebenyi, and P. J. Stover. 2007. 'Evidence for small ubiquitin-like modifier-dependent nuclear import of the thymidylate biosynthesis pathway', *J Biol Chem*, 282: 17623-31.

Yaliwal, L. V., and R. M. Desai. 2012. 'Methylenetetrahydrofolate reductase mutations, a genetic cause for familial recurrent neural tube defects', *Indian J Hum Genet*, 18: 122-4.

Yang, C. H., F. M. Sirotnak, and M. Dembo. 1984. 'Interaction between anions and the reduced folate/methotrexate transport system in L1210 cell plasma membrane

vesicles: directional symmetry and anion specificity for differential mobility of loaded and unloaded carrier', *J Membr Biol*, 79: 285-92.

Yang, X. M., and R. E. MacKenzie. 1993. 'NAD-dependent methylenetetrahydrofolate dehydrogenase-methenyltetrahydrofolate cyclohydrolase is the mammalian homolog of the mitochondrial enzyme encoded by the yeast MIS1 gene', *Biochemistry*, 32: 11118-23.

Yang, Y. S., Y. Yuan, W. P. Hu, Q. X. Shang, and L. Q. Chen. 2018. 'The role of mitochondrial folate enzyme MTHFD1L in esophageal squamous cell carcinoma', *Scand J Gastroenterol*, 53: 533-40.

Ye, J., J. Fan, S. Venneti, Y. W. Wan, B. R. Pawel, J. Zhang, L. W. Finley, C. Lu, T. Lindsten, J. R. Cross, G. Qing, Z. Liu, M. C. Simon, J. D. Rabinowitz, and C. B. Thompson. 2014. 'Serine catabolism regulates mitochondrial redox control during hypoxia', *Cancer Discov*, 4: 1406-17.

Yi, Z., M. Deng, M. J. Scott, G. Fu, P. A. Loughran, Z. Lei, S. Li, P. Sun, C. Yang, W. Li, H. Xu, F. Huang, and T. R. Billiar. 2020. 'IRG1/Itaconate Activates Nrf2 in Hepatocytes to Protect Against Liver Ischemia-Reperfusion Injury', *Hepatology*.

Young, N. L., K. Sheridan, T. A. Burke, S. Mukherjee, and A. McCormick. 2013. 'Health outcomes among youths and adults with spina bifida', *J Pediatr*, 162: 993-8.

Zash, R., J. Makhema, and R. L. Shapiro. 2018. 'Neural-Tube Defects with Dolutegravir Treatment from the Time of Conception', *N Engl J Med*, 379: 979-81.

Zash, R.; Makhema, J.; Diseko, M.; Jacobson, D.L.; Mayondi, G., et al. 2018. 'Surveillance for neural tube defects following antiretroviral exposure from conception.', *22nd International AIDS Conference.*: NATAP.

Zhang, C., E. Tannous, and J. J. Zheng. 2019. 'Oxidative stress upregulates Wnt signaling in human retinal microvascular endothelial cells through activation of disheveled', *J Cell Biochem*, 120: 14044-54.

Zhang, T., J. Lou, R. Zhong, J. Wu, L. Zou, Y. Sun, X. Lu, L. Liu, X. Miao, and G. Xiong. 2013. 'Genetic variants in the folate pathway and the risk of neural tube defects: a meta-analysis of the published literature', *PLoS One*, 8: e59570.

Zhao, R., S. H. Min, Y. Wang, E. Campanella, P. S. Low, and I. D. Goldman. 2009. 'A role for the proton-coupled folate transporter (PCFT-SLC46A1) in folate receptor-mediated endocytosis', *J Biol Chem*, 284: 4267-74.

Vita

John William Steele was born in 1992 at Travis Air Force Base in Fairfield, California. He was raised in Pensacola, Florida and attended the University of West Florida. In 2014, he graduated with a Bachelor of Science in biology and matriculated at the University of Texas at Austin for graduate studies in the Institute for Cellular and Molecular Biology. He joined the Finnell/Cabrera Birth Defects Research Laboratory and moved with the lab to Houston, Texas in 2017 to finish his graduate research at Baylor College of Medicine.

Permanent email address: john.steele@bcm.edu

This dissertation was typed by the author.